Johns Hopkins APL

TECHNICAL DIGEST

July-September 1980, Vol. 1, No. 3

The Magsat issue

The *Johns Hopkins APL Technical Digest* (ISSN 0001-2211), established in 1961 as the *APL Technical Digest*, is published quarterly under the auspices of The Johns Hopkins University Applied Physics Laboratory (JHU/APL), Johns Hopkins Road, Laurel, Md. 20810. The objective of the publication is to provide a summary of unclassified individual programs under way at JHU/APL. Requests for free individual copies, free subscriptions, or permission to reprint the text should be submitted to the Managing Editor.

Postmaster: Send address changes to that address. Second-class postage paid at Laurel, Md.

Johns Hopkins APL
TECHNICAL DIGEST

July-September 1980, Volume 1, Number 3

The Magsat issue

Front Cover:
Conceptual painting by S. G. Smith of the *Digest* staff. The earth, showing the magnetic anomalies measured by Magsat and earlier satellite vehicles, is silhouetted against the frontispiece of Gilbert's seminal treatise on geomagnetism (*De Magnete*, second edition, 1628). A line drawing of Magsat is in the foreground.

THOMAS A. POTEMRA, FREDERICK F. MOBLEY, and LEWIS D. ECKARD

THE GEOMAGNETIC FIELD AND ITS MEASUREMENT: INTRODUCTION AND MAGNETIC FIELD SATELLITE (MAGSAT) GLOSSARY

The earth's magnetic field, its measurement by conventional methods, and the specific objectives and functions of the Magsat system to obtain precise absolute and directional values of the earth's magnetic field on a global scale are briefly described.

EARLY HISTORY

The directional property of the earth's magnetic field has been appreciated by the Chinese for more than 4500 years. Records indicate[1] that in 2634 B.C. the Chinese emperor Hoang-Ti was at war with a local prince named Tchi-Yeou and that they fought a great battle in the plain of Tcho-luo. Tchi-Yeou raised a dense fog that produced disorder in the imperial army — a forerunner of the modern smokescreen. As a countermeasure, Hoang-Ti constructed a chariot on which stood the small figure of a man with his arm outstretched. This figure, apparently free to revolve on its vertical axis, always pointed to the south, allowing the emperor to locate the direction of his enemy's retreat. Tchi-Yeou was captured and put to death.

The first systematic and scientific study of the earth's magnetic field was conducted by William Gilbert, physician (later promoted to electrician) to Queen Elizabeth, who published in 1600 his proclamation "*Magnus magnes ipse est globus terrestrius*" (the earth globe itself is a great magnet) in his *De Magnete.*[2] This treatise was published nearly a century before Newton's *Philosophiae Naturalis Principia Mathematica* (1687), and it has been suggested that Gilbert invented the whole process of modern science rather than merely having discovered the basic laws of magnetism and of static electricity.[3] Gilbert's efforts may have been inspired by the need for Her Majesty's Navy to improve (if not understand) the principal means of navigation — the magnetic compass. This fact is evident from the frontispiece of the second Latin edition of *De Magnete*, (Fig. 1) published in 1628.

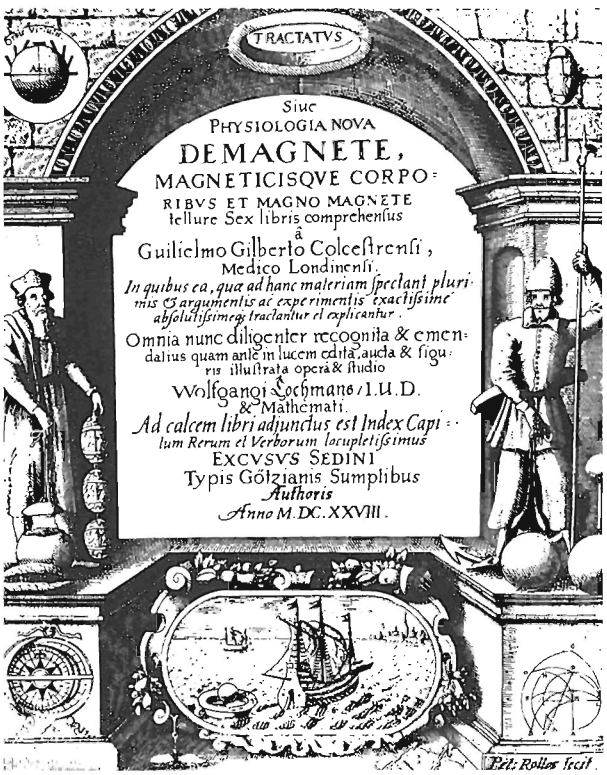

Fig. 1—The engraved title page from the second Latin edition of Gilbert's *De Magnete.* It shows lodestones, compasses, and a terrella (a small spherical magnet simulating the earth, in the upper left corner). In a vignette at the bottom is a ship sailing away from a floating bowl compass with a terrella at the center. The first edition of *De Magnete* was published in 1600, and copies have become extremely rare.

An understanding of the earth's magnetic field and its variations is still of great importance to navigators. (More recently the U.S. Navy has "inspired" APL to develop and improve a more advanced satellite system for navigation.) The geomagnetic field also plays an important practical role in searching for possible resources beneath the earth's crust and in stabilizing artificial satellites. Major disturbances to the geomagnetic field — called "magnetic storms" — induce large, un-

wanted effects in long-distance telephone circuits and sometimes cause widespread power blackouts. The geomagnetic field and its interaction with the continuous flow of ionized gas (plasma) from the sun (the solar wind) provide the basic framework for the complicated space environment of the earth, including the Van Allen radiation belts and auroral zones. The distorted configuration of its geomagnetic field is called the "magnetosphere." Many APL-built spacecraft have made major contributions to an understanding of the geomagnetic field and associated magnetospheric phenomena during the past 15 years. Magsat is the latest one to do so.

GEOMAGNETIC FIELD DESCRIPTION

The geomagnetic field can be thought of as being produced by a huge bar magnet imbedded in the earth, with the axis of the magnet tilted away slightly from the earth's rotational axis. The poles of this magnet are located near Thule, Greenland, and Vostok, Antarctica (a U.S.S.R. research station). To a good approximation, the geomagnetic field can be represented by a simple dipole, but there is a significant contribution from nondipole components and from a system of complicated currents that flow in the magnetospheric regions surrounding the earth. The most accurate representation of the geomagnetic field is provided by a series of spherical harmonic functions.[4] The coefficients of such a series representation are evaluated from an international set of spacecraft and surface observations of the geomagnetic field and are published for a variety of practical uses in navigation and resource surveys. A principal goal of Magsat is to provide the most accurate evaluation of the geomagnetic field model in this manner (see the article by Langel in this issue).

MAGNETIC UNITS AND TERMINOLOGY

A wide variety of units and symbols are currently in use in the many scientific and engineering fields involved with magnetism. The following definitions are offered in hope of clarifying some of these for a better understanding of the following discussions.

Classic experiments have shown that the force acting on a charged particle moving in a magnetic field is proportional to the magnitude of the charge. A vector quantity known as the "magnitude induction" is usually denoted by $\vec{\mathbf{B}}$ which characterizes the magnetic field in a manner similar to that done for electric fields by $\vec{\mathbf{E}}$, for example. This unit of induction, $\vec{\mathbf{B}}$, is 1 weber per square meter (1 Wb/m^2); it is the magnetic induction of a field in which 1 coulomb of charge, moving with a component of velocity of 1 m/s perpendicular to the field, is acted on by a force of 1 newton. In SI units, 1 Wb/m^2 = 1 tesla.

In studies of planetary fields, where very small fields are involved, the nanotesla (nT), formerly the "gamma" (γ), is used where 1 nT = 10^{-9} tesla = 10^{-9} Wb/m^2 = 1 γ. (The cgs unit of magnetic intensity is the gauss, where 1 tesla = 10^4 gauss.) The intensity of the surface geomagnetic field varies from about 30,000 nT at the equator to more than 50,000 nT at high latitudes near the magnetic poles.

SECULAR VARIATION

It has been known for over 400 years that the main geomagnetic field is not steady but experiences global secular variations. In fact, from a study of the paleomagnetic properties of igneous rocks, it has been determined that the geomagnetic field has reversed polarity several times over the past 4.5 million years (Fig. 2).[5]

The behavior of the geomagnetic field over a shorter time scale is shown in Fig. 3. That figure shows the positions of the virtual geomagnetic pole since 1000 A.D. based on the assumption that the geomagnetic field is a centered dipole.[6]

The following five features of the secular variation have been determined:[7]

1. A decrease in the moment of the dipole field by 0.05% per year, indicating that the present geomagnetic field may reverse polarity 2000 years from now. Preliminary analysis of Magsat data has revealed that this variation may be more rapid than was suspected from previous observations, and that the field may reverse polarity in only 1400 years;
2. A westward precessional rotation of the dipole of 0.05° of longitude per year;
3. A rotation of the dipole toward the geographic axis of 0.02° of latitude per year;
4. A westward drift of the nondipole field of 0.2° of longitude per year;
5. Growth and decay of features of the nondipole field with average changes of about 10 nT per year.

Although these secular variations necessitate continual corrections to magnetic compasses they pro-

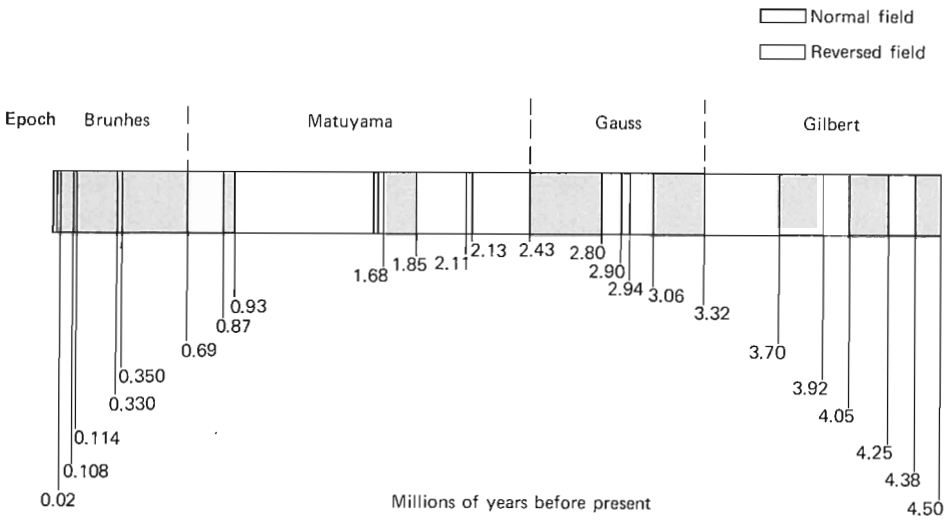

Fig. 2—The polarity of the geomagnetic field for the past 4.5 million years deduced from measurements on igneous rocks dated by the potassium- argon method and from measurements on cores from ocean sediments (from Ref. 5).

vide some clues to the internal source of the geomagnetic field.

GEOMAGNETIC FIELD SOURCES

If the average westward drift of the dipole field in item 2 above is representative of the rate of motion of the field, then the corresponding surface velocity is about 20 km per year. This is a million times faster than the large-scale motions of the solid part of the earth deduced from geological observations and considerations. Seismological evidence reveals a fluid core for the earth that can easily experience large-scale motions, and it is presumed that the geomagnetic secular variation — and indeed the main field itself — is related to this fluid core. Furthermore, geochemical and density considerations are consistent with a core composed mainly of iron — a good electric and magnetic conductor. Therefore, the study of the earth's internal magnetic field draws in another discipline — magnetohydrodynamics, which involves moving fluid conductors and magnetic fields.

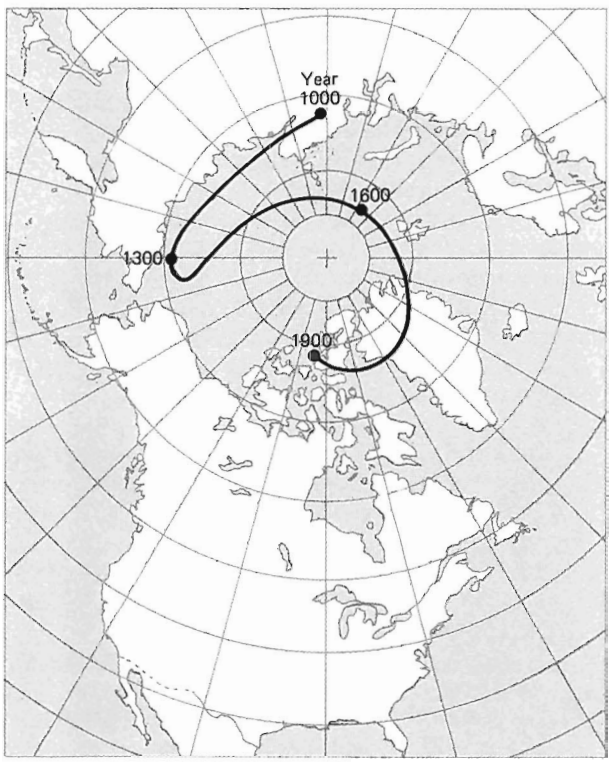

Fig. 3—The virtual geomagnetic pole positions since 1000 A.D., which correspond to the secular variations at London if one ascribes the geomagnetic field entirely to a centered dipole. The London variations were deduced from magnetic field orientations of samples obtained from archeological kilns, ovens, and hearths in the southern half of Britain (from Ref. 6). The present virtual pole is located near Thule, Greenland.

Modern theories of the geomagnetic field are based on the original suggestion of Larmor that the appropriate internal motion of a conducting fluid could cause it to act as a self-exciting dynamo.[8] To visualize this, assume the moving core to be an infinitely good conductor. Any primordial magnetic field lines, outside the core, for example, will be dragged around by the currents within the core as if they were "frozen" into the core. If the core rotates nonuniformly with depth, the field lines will become twisted around the axis of rotation in a way that opposes the initial field. The twisting action packs the magnetic field lines more closely, causing the field intensity to grow. This growth can neutralize the original field and produce an even larger reversal field. The concept of magnetic field amplification by the differential rotation of conductors has been used by astrophysicists to explain the magnetic fields of stars (including the sun), Jupiter, and Saturn. Many theories exist, but the precise generation mechanisms for the internal geomagnetic field are still unknown.[8]

MAGNETOSPHERIC CURRENTS

When viewed from outer space, the earth's magnetic field does not resemble a simple dipole

but is severely distorted into a comet-shaped configuration by the continuous flow of plasma (the solar wind) from the sun (depicted in Fig. 4). This distortion demands the existence of a complicated set of currents flowing within the distorted magnetic field configuration called the "magnetosphere." For example, the compression of the geomagnetic field by the solar wind plasma on the day side of the earth must give rise to a large-scale current flowing across the geomagnetic field lines, called the Chapman-Ferraro or magnetopause current (see Fig. 4).

The magnetospheric system includes large-scale currents that flow in the "tail"; "Birkeland" currents that flow along geomagnetic field lines (see the article by Potemra in this issue) into and away from the two auroral regions; the ring current that flows at high altitudes around the equator of the earth; and a complex system of currents that flow completely within the layers of the ionosphere, the earth's ionized atmosphere. The intensities of these various currents reach millions of amperes and are closely related to solar activity. They produce magnetic fields that vary with time scales ranging from a few seconds (micropulsations) to 11 years (corresponding to the solar cycle).

Widespread magnetic disturbances sometimes observed over the entire surface of the earth are known as magnetic storms. These storms are associated with major solar eruptions that emit X rays, ultraviolet and extreme ultraviolet radiations, and particles with energies from 1 keV to sometimes over 100 MeV. The solar plasma accompanying solar eruptions causes a magnetic storm when it collides with the earth's magnetosphere. Minor magnetic storms can occur every few weeks during the peak of the 11-year solar cycle (the peak of the present cycle is thought to have occurred in 1980), whereas "super" magnetic storms that so severely distort the geomagnetic field as to move the entire auroral zone to lower latitudes are a much rarer event (the last super storm occurred on August 2, 1972, when an aurora was observed in Kentucky). Besides the evaluation of models for the internal geomagnetic field, Magsat, launched in October 1979, provided the most sensitive measurements yet of the magnetospheric current system.

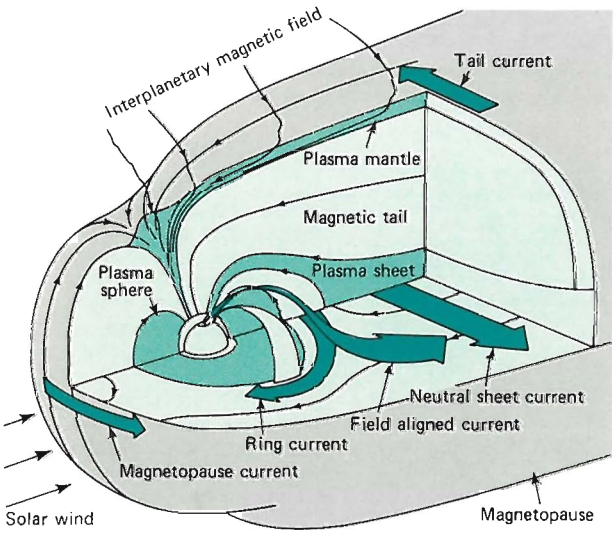

Fig. 4—The configuration of the earth's dipole magnetic field distorted into the comet-like shape called the magnetosphere. The various current systems that flow in this complicated plasma laboratory are labeled. The interplanetary magnetic field is the magnetic field of the sun, which has a modulating effect on the processes that occur within the magnetosphere.

MAGNETIC FIELD MEASUREMENTS

The technique of using airplanes for magnetic field surveys for geological prospecting became well established in the 1950's. Airplanes make their surveys at altitudes of 1 to 5 km, whereas satellites orbit the earth at 200 km or higher. Thus it was somewhat of a surprise when scientists discovered from the data of the Orbiting Geophysical Observatory satellites in 1972 that useful information about the structure of the earth's crust could be derived from satellite data — information that would be very difficult to detect in airplane survey data. Ideas for a satellite devoted to this objective were discussed for a number of years, finally leading to the Magsat program, which had the additional objective of measuring the "main" field for making new magnetic charts.

MAGSAT SPACECRAFT

Preliminary discussions among APL, NASA, and the U.S. Geological Survey (USGS), commencing in the mid-1970's, culminated in conceptual studies of a spacecraft dedicated to the task of completing a global survey of the earth's geomagnetic field. NASA and the USGS subsequently entered into an agreement to conduct such a program on a cooperative basis. The Goddard Space Flight Center (GSFC) was selected by NASA as the lead laboratory for this endeavor. Numerous trade-off design studies were undertaken, with emphasis on flying an adaptation of an available spacecraft design, launched from an early Space Shuttle, as against flying a small spacecraft on a NASA/DoD Scout launch vehicle. However, in view of the uncertainties surrounding the availability of the Shuttle, and in light of the desire of USGS to incorporate satellite magnetic field data into their 1980 map updates, the decision was made by early 1977 to proceed with a Scout-launched spacecraft.

In April 1977, after a successful preliminary design review, APL was funded to proceed with the Magsat design and development effort with the goal of launching the spacecraft by September 21, 1979, at a projected cost of about ten million dollars.

The Small Astronomical Satellite (SAS-3) had been designed and built by APL and launched in

1975. Many of the features of SAS-3 seemed ideally suited to the magnetic field satellite mission. It was a small spacecraft capable of being launched by the inexpensive Scout rocket, it had the world's most precise tracking system (i.e., position determination) in its Doppler tracking system (a derivative of the APL Transit system), it had two star trackers that could provide attitude determination to 10 arc-s (1 arc-s = 0.00028) accuracy, and its attitude control system used an infrared earth-horizon scanner/momentum wheel assembly that was ideally suited for Magsat. A critical problem, which was quickly identified, was the excessive weight of Magsat. Tape recorders with a larger capacity for data storage were needed, and new S-band transmitters were required for the high data rate during tape recorder playback. Compromises in the solar cell array were necessary to keep the weight down to 182 kg, the maximum that the Scout rocket could launch into a 350 by 500 km orbit.

MAGSAT ORBIT

An orbit was needed that would give full earth coverage and as little shadowing by the earth as possible. A polar orbit would be ideal for earth coverage, but because the orbit plane would remain fixed in space, the motion of the earth about the sun would cause shadowing of the satellite within 30 to 60 days after launch. Also, it would be difficult to find star camera orientations that would not present problems with direct sunlight. However, for an orbit inclination of 97°, the orbit plane precesses at the rate of 1°/day, just the right amount to make the orbit plane follow the sun. (This precession is due to the bulge in the earth's gravity field at the equator.) This sun-synchronous orbit (Fig. 5) gives nearly 100% earth coverage and many months of full sunlit orbits. The star cameras could be placed on the dark side of the satellite to avoid direct sunlight.

Even in this case, as the sun approaches the highest latitudes of +23° on June 21, the orbit would be shadowed in the south polar region. Shadowing was expected to begin in April so a launch date of September 1979 was chosen, which would allow six months of fully sunlit orbits. Launch actually occurred at the end of October 1979, so 5½ months of fully sunlit orbits were obtained.

THE SPACECRAFT

Magsat was intended to measure the vector components of the earth's field to an accuracy of 0.01%; this meant that the orientation of the vector sensors must be known to 15 arc-s accuracy. The star cameras were good to an accuracy of 10 arc-s, but they had 2 kg of essential magnetic shielding that would distort the magnetic field. An extendable boom was needed to put the vector sensors 6 meters away from the magnetic disturbance caused by the star cameras. But it was not possible for the boom to be mechanically stable to 5 arc-s. A system was needed to measure the orientation of the vector sensors relative to the star cameras. This system, the Attitude Transfer System (ATS), used an optical technique involving mirrors attached to the vector sensor to make the necessary measurement (see the article by Fountain *et al.* in this issue).

The elements of the ATS and the two star cameras had to be tied together mechanically in some permanent and extremely stable fashion. The structure to achieve this was the optical bench, a built-up assembly of graphite fiber and epoxy resin that provided a near-zero coefficient of thermal expansion. The bench was attached to the satellite at five points, two of which were released by pyrotechnic devices after the satellite was in orbit. The

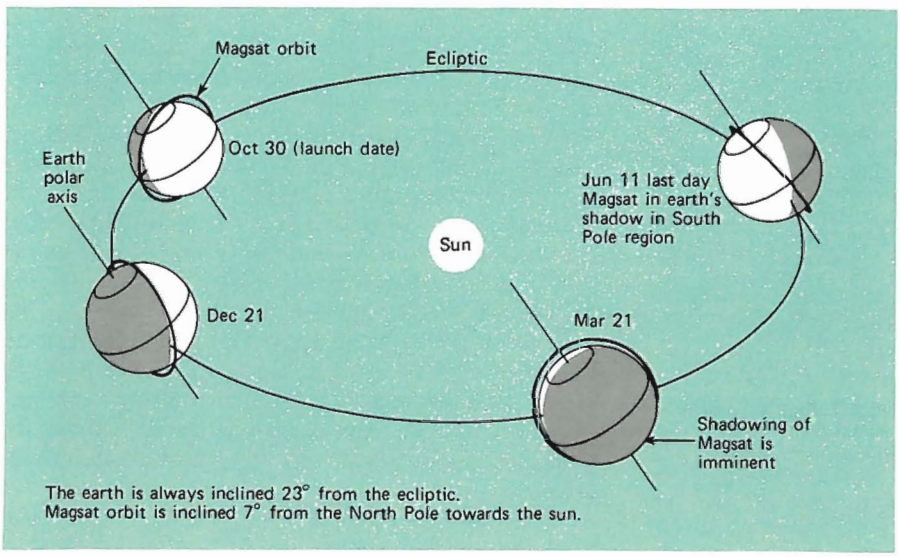

Fig. 5—The precession of the Magsat orbit plane with time. The Magsat orbit plane makes an angle of 97° with the earth's equatorial plane. At this inclination (and at the altitude of Magsat), the equatorial bulge of the earth causes the orbit plane to rotate above the polar axis at 1°/day, just the right amount to turn the orbit plane toward the sun as the earth proceeds in its orbit about the sun. Unfortunately, the 23° tilt of the earth polar axis adds to the 7° tilt of the orbit plane in June, causing shadowing of the southern portion of the orbit by the earth. This shadowing began in mid-April for Magsat.

three remaining support points did not apply stress to the bench. Heaters and temperature sensors at eight places stabilized the bench temperature at 25°C.

At the end of the 6 meter extendable boom were the vector magnetometer sensor and a scalar magnetometer sensor (see the articles by Acuna and Farthing). The vector sensor consisted of three small toroidal cores of highly permeable magnetic material with platinum wire windings used to sense the components of the field. They were mounted on a very stable ceramic block, and the temperature was controlled at 25°C. The scalar magnetometer measured the field magnitude very accurately, but not its direction. It used Zeeman splitting of energy levels in cesium-133 gas as a technique for measuring the field. The scalar data provided redundancy and an independent check on the calibration of the vector magnetometer.

Magsat was the latest and most complex of the satellites built by APL. The command system featured its own dual computers, which permitted storage of 164 commands, to be implemented at desired times (see the article by Lew *et al.*). This was very helpful because the low altitude of Magsat meant that a ground station had only 9 to 10 minutes in which to send commands, receive the data played back by the tape recorders, and make decisions about managing the satellite's health. The command system was also designed to accept commands from another on-board system, *viz.*, the attitude control system. The attitude control system also used a small computer to manage the satellite attitude. When it decided that commands were needed, a request was sent to the command system, which then implemented the command.

TESTING

Fabrication and test of components and subassemblies commenced during the winter of 1977-78 and were completed in 1979. The instrument module was assembled in December 1978 and exposed to a thermal balance test in vacuum. The base module was assembled in January and February 1979, and a critical test of the attitude control system was performed to verify various design and performance parameters. Development difficulties delayed availability of the magnetometer boom assembly until May 1979. The base module and instrument module were assembled without the boom and taken to GSFC for the star camera and ATS alignments.

The alignment and calibration of all the optical elements mounted on the optical bench was an especially difficult task. It was done with the fully assembled satellite mounted inside an aluminum cage, using the optical test laboratory at GSFC. Since the calibration was done in the gravity field of the earth (i.e., 1 g), the weight of the star camera and ATS components would distort the optical bench. But in orbit, the satellite continuously experiences zero g, these distortions would disappear, and our ground calibrations would be invalidated. To solve the problem, we made a second calibration with the satellite upside down, thereby reversing the direction of the weight force (i.e., −1 g) and producing distortions equal and opposite to those of the initial calibration. We then presumed that the zero-g calibration must be exactly midway between the two results. This technique has been confirmed with our flight results.

The spacecraft was returned to APL where the two modules were separated so that the magnetometer boom assembly could be installed. A series of boom extension tests was performed to verify ATS performance and alignment and to calibrate the boom deployment telemetry channels. In June 1979, the spacecraft was reassembled and, after a preliminary weight and balance determination, was returned to GSFC for initial magnetics tests and radio frequency interference tests aimed at verifying that all subsystems could operate in the orbital configuration without interfering with one another. Upon its return to APL, there followed detailed electrical performance tests, establishing the baseline for future reference.

During August 1979, the spacecraft was exposed to launch phase vibration and shock excitation tests followed by two weeks of combined thermal vacuum and thermal balance testing. In September the spacecraft was once again taken to GSFC for final weight, center-of-gravity location, and moment-of-inertia determinations; final magnetic tests; and post-environmental verification of the optical alignment of the star cameras and ATS. Upon its return to APL, a final vibration exposure (single axis) was performed to ensure that all components were secure. This was followed by a short electrical test.

LAUNCH AND POST-LAUNCH EXPERIENCES

The spacecraft, ground station, and supporting equipment were trucked from APL to Vandenberg Air Force Base, arriving on the morning of October 8, 1979. Intensive field operations followed, including electrical tests, assembly to the fourth stage rocket, and final spin balance. The spacecraft fourth stage rocket assembly was then mounted on the main rocket assembly, the heat shield was installed, and all-systems tests were performed. On October 27, 1979, a dress rehearsal was conducted, leaving all in readiness for launch, planned for October 29 at dawn. The countdown began on the evening of October 28 but had to be suspended just prior to terminal countdown because of extremely high winds at about 10,000 ft altitude. The launch operation was resumed on the evening of October 29 and culminated in a successful launch at 6:16 A.M. PST, October 30, 1979. All stages fired cor-

rectly and the spacecraft was injected into a 352 by 578 km sun-synchronous orbit.

Data were recorded until the satellite burned up at low altitude on June 11, 1980. A large amount of vector and scalar magnetometer data was collected, and scientific results are beginning to become available. We experienced some operational problems because of earth shadowing in the latter portion of Magsat's life, primarily caused by an unexpected loss of battery capacity that forced some compromises in data collection. The sunshades of the star cameras showed light leaks, which caused the loss of some data. On the whole, however, the Magsat satellite has been very successful, and all mission objectives should be accomplished when the data are fully processed.

The articles that follow describe the developments that led to the Magsat program, and the mission objectives, and summarize early flight events. Subsequently, details of the spacecraft components are discussed. The concluding articles describe the scientific results and on-going studies.

REFERENCES

[1]S. Chapman and J. Bartels, *Geomagnetism*, Oxford Press, p. 888 (1940).

[2]W. Gilbert, *On the Magnet; The Collector's Series in Science* (D. J. Price, ed.) Basic Books, Inc., New York (1958).

[3]*Ibid*, pp. v-xi.

[4]A. J. Zmuda (ed.), *World Magnetic Survey, 1957-1969*, International Association of Geomagnetism and Aeronomy Bulletin No. 28, Paris (1971).

[5]F. D. Stacey, *Physics of the Earth*, John Wiley and Sons, New York (1969).

[6]M. J. Aitken and G. H. Weaver, "Recent Archeomagnetic Results in England," *J. Geomag. Geoelect.* **17**, p. 391 (1965).

[7]T. Nagata, "Main Characteristics of Recent Geomagnetic Secular Variation," *J. Geomag. Geoelect.* **17**, p. 263 (1965).

[8]See reviews of W. M. Elsasser, "Hydromagnetic Dynamo Theory," *Revs. Mod. Phys.* **28**, p. 135 (1956); D. R. Inglis, "Theories of the Earth's Magnetism," *Revs. Mod. Phys.* **27**, p. 212 (1955); and T. Rikitake, *Electromagnetism and the Earth's Interior*, Elsevier, Amsterdam (1966).

A GLOSSARY OF MAGSAT COMPONENTS

Aerotrim Boom — A motorized extendable boom consisting of a pair of silver-plated beryllium-copper tapes, 0.002 inch thick, rolled on a pair of spools. When extended the tapes formed a tube 0.5 inch in diameter up to 12 meters long. The air drag on the boom was used to balance the aerodynamic torques in yaw.

Attitude Control System — The system that controlled the satellite attitude; in Magsat it held the satellite properly oriented with respect to the earth and the orbit plane. It consisted primarily of a momentum wheel with an integral infrared earth horizon scanner, magnetic torque coils, gyro system, and associated electronics.

Attitude Transfer System (ATS) — An electronic and optical system for measuring the orientation of the vector magnetometer sensor relative to the star cameras. Two optical heads of the ATS were mounted on the optical bench near the star cameras. One of the heads transmitted a beam of light to a plane mirror on the back of the vector magnetometer. The beam was reflected back into the same head where its angular deviation was measured and two angles of the plane mirror were determined. The second head sent a beam of light to a dihedral mirror also on the back of the vector magnetometer. The light was reflected to a dihedral mirror on the optical bench, and then via the first dihedral mirror back to the optical head. The position of the reflected beam was used to measure the twist angle of the vector sensor.

Command System — The apparatus aboard the satellite that accepted the digital bit stream from the receiver portion of the transponders, decoded it to recover the command words transmitted from the ground, and routed the words to the destinations designated by the address codes contained in each word. At destination, the word was further decoded and the specific element of the satellite addressed was placed in the mode designated by the word.

Data Formatter — The portion of the telemetry system that took the various science and housekeeping digital data bits and arranged them in a predetermined sequence for modulation onto the carrier frequency of the transmitter as well as for recording by the tape recorders. The predetermined sequence permitted decoding of the signals by ground-based computers.

Despin/Separation Timer — One of a pair of devices mounted on the head cap of the fourth-stage rocket motor. It was intended to initiate despin followed by spacecraft separation at predetermined times following the completion of firing of the fourth-stage rocket motor.

Horizon Scanner — The momentum wheel had within its structure an optical system capable of detecting radiation from the earth in the infrared (IR) at 15 micrometers. The field-of-view was a narrow beam rotated to form a 90° cone as the wheel spun. When the beam intersected the earth, the IR radiation was detected; an electronic system derived the pitch and roll angles of the satellite from this information.

Magnetic Coils — Magsat had X-, Y-, and Z-axis coils for torquing by interaction with the earth's magnetic field. A coil consisted of many turns of aluminum wire mounted on the outer skin of the satellite. When energized with a steady electric current, the coils experienced torques from the earth's magnetic field that were used for attitude control.

Magnetometer Boom — A collapsible structural element composed of seven pairs of links in a scissors or "lazy-tongs"-type arrangement intended to move the sensor platform from its caged, launch-phase position to a position 6 meters away from the instrument module.

Magnetometers — The scientific in-

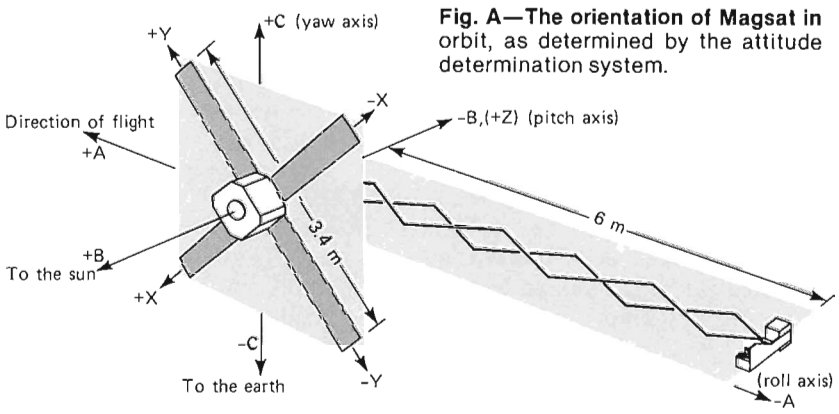

Fig. A—The orientation of Magsat in orbit, as determined by the attitude determination system.

Fig. B—The configuration of Magsat.

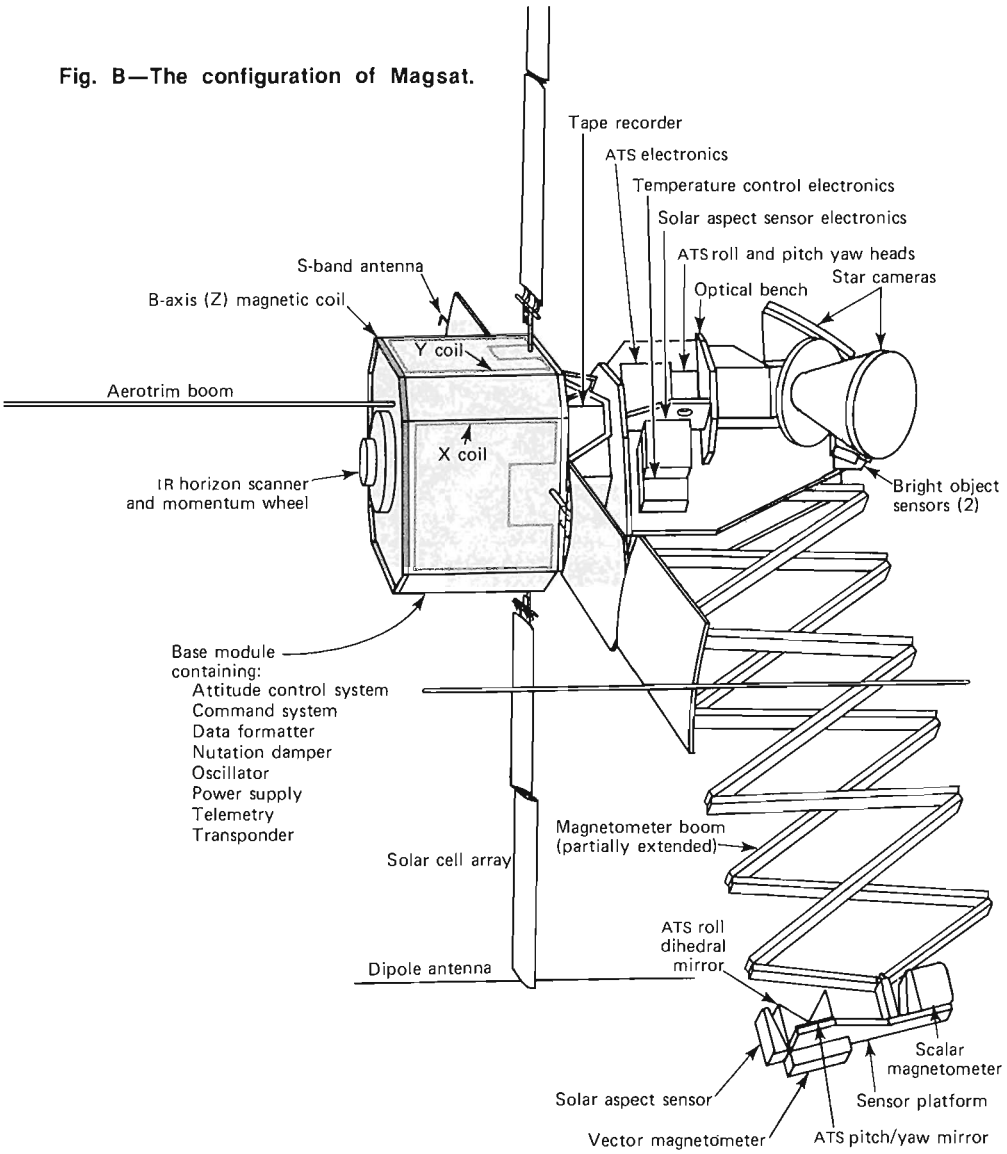

struments of Magsat consisted of a three-axis vector magnetometer and a scalar magnetometer for measuring the magnetic field of the earth. The vector magnetometer sensor had three small magnetic elements, each sensitive to one component of the earth's field. The scalar magnetometer measured only the magnitude of the field by optical pumping of atomic excitation states in cesium-133 gas.

Momentum Wheel — Magsat had an internal tungsten wheel that spun at about 1500 rpm. This rotation provided angular momentum that gave the satellite a form of gyroscopic attitude stability. This was a key feature of the attitude control system.

Nutation Damper — When a disturbance torque is applied to a gyro-stabilized satellite such as Magsat, the attitude motion includes nodding or wobbling. After the torque is removed, this nodding ("nutation") persists unless damped. In Magsat, damping was accomplished in two ways: by a pendulous mechanical damper that used magnetic eddy currents for damping, and by the closed-loop attitude control that modulated the momentum wheel speed to damp nutation.

Optical Bench — A structural platform constructed of a graphite fiber-epoxy-laminate honeycomb that was designed to provide a very stable surface for mounting the star cameras and ATS components. The properties of the material were used to ensure that the exact angular relationship was maintained between the star cameras and ATS components irrespective of instrument-module temperature fluctuations.

Oscillator — An ultrastable quartz crystal oscillator producing a 5 MHz output used as the source for the 162 and 324 MHz Doppler signals. The 5-MHz signal was also used to synchronize the various DC-DC converters aboard the spacecraft to avoid developing spurious beat frequencies that could be a source of interference to the various electronic devices. The stability of the oscillator was achieved by placing the crystal inside a double-oven arrangement, providing a high degree of thermal isolation from the fluctuations experienced by the base module, and by using a cut quartz crystal selected so that its turnover temperature and the oven temperature were precisely matched. This permitted operation with virtually no temperature effect on the oscillation frequency.

Power Supply — The system consisted of the following elements: solar cell arrays to generate electricity; a battery mounted in the base module to store the electrical energy for use during any shadowed portions of the orbits and to meet peak power demands; battery voltage limiter devices to control battery charging; and DC-DC converter regulators to condition power to the voltages needed by each user.

Solar Aspect Sensors — Several types were included in Magsat. Of special interest was the "precision" solar aspect sensor, mounted near the vector magnetometer sensor, which measured the angles to the sun with an accuracy of 5 to 10 arc-seconds.

Star Cameras — Two star cameras were mounted rigidly on the optical bench. Each camera had a 4-inch-diameter lens that focused the stars on the front end of an "image-dissector" electronic tube. Inside the tube, in the vacuum, was a very sensitive surface that emitted electrons wherever starlight fell upon it. These electrons were directed by magnetic coils to pass through a small hole into an electron multiplier where a cascade of electrons was generated, finally accumulating enough effect to be a measurable electric current. With magnetic coils driven in a predetermined manner, the surface of the tube was searched for sources of electrons (i.e., starlight). When a source was found, the magnetic coils "locked" onto it for a few seconds and the position was recorded.

Tape Recorder — A device used to store telemetry data until the satellite was over or near a ground station. The signals were recorded magnetically on iron-oxide-coated Mylar tape running between a pair of coaxially mounted reels. Two tape recorders were mounted on the deck between the base module and instrument module.

Telemetry — The process by which the scientific (magnetometer) data and information concerning the satellite attitude, load currents, bus voltages, temperatures, and other "housekeeping" data were transmitted to the NASA STDN ground stations.

Transponder — A combined radio receiver and transmitter operating at S-band, used for receiving command signals transmitted from the NASA STDN ground stations and for transmitting the telemetry signals from Magsat to the same ground stations. This NASA Standard Near-Earth Transponder could also be used as a range/range rate transponder for satellite tracking and orbit determination. Magsat, however, used the much more precise Doppler beacons in conjunction with the DMA tracking network.

Vehicle Adapter — The conically-shaped transition section bolted to the fourth-stage rocket to which the spacecraft was clamped. The two halves of the clamp were fastened together at each end by bolts passing through pyrotechnically operated cutters. Separation of the spacecraft from the launch vehicle was achieved by actuating the bolt cutters by a stimulus from the spacecraft battery initiated by the despin/separation timers. When the bolts were cut, the two clamp halves moved apart, allowing small springs to force the spacecraft away from the adapter/fourth-stage assembly.

GILBERT W. OUSLEY

OVERVIEW OF THE MAGSAT PROGRAM

The Magsat project, the background leading to its inception, and its mission objectives are briefly described, followed by summaries of plans for studies of regional geology and geophysics, geomagnetic field modeling, and the inner earth.

PROJECT DESCRIPTION

The purpose of the Magsat project was to design, develop, and launch a satellite to measure the near-earth geomagnetic field as part of NASA's Resource Observation Program. It was intended to provide precise magnetic field measurements for geoscientific investigations by:

- Accurately describing the earth's main magnetic field for charting and mapping applications and for investigating the nature of the field source. This will provide more accurate magnetic navigation information for small craft, will trace more accurately the magnetic field lines for the near-earth magnetosphere, will separate the magnetic field into crustal and external field contributions, and will permit study of the earth's core and core-mantle boundary; and
- Mapping, on a global basis, the fields caused by sources in the earth's crust. This will contribute to our understanding of large-scale variations in the geologic and geophysical characteristics of the crust, and will in turn affect the future planning of resource exploration strategy.

BACKGROUND

Magsat is one of several integrated elements of the NASA Resource Observation Program that use satellites to study the earth's nonrenewable resources. One facet of this program is the use of space techniques to improve our understanding of the dynamic processes that formed the present geologic features of the earth and how these processes relate to phenomena such as earthquakes and to the location of resources.

One part of the Resource Observation Program is the measurement of the near-earth geomagnetic field. Before the satellite era, magnetic data from many geographic regions were acquired over periods of years by a variety of measurement techniques. However, for many regions such as the oceans and poles, data were either sparse or nonexistent.

Satellite measurements of the geomagnetic field began with the launch of Sputnik 3 in May 1958 and have continued sporadically in the intervening years. To date only the OGO-2, -4, and -6 satellites, which are the Polar Orbiting Geophysical Observatories (Pogo's), have provided a truly accurate global geomagnetic survey. These satellites operated between October 1965 and June 1971, and their alkali-vapor magnetometers provided global measurements of the field magnitude approximately every half second over an altitude range of 400 to 1500 km.

The satellite geomagnetic field measurements were intended for mapping the main geopotential field originating in the earth's core, for determining the long-term temporal or secular variations in that field, and for investigating short-term field perturbations caused by ionospheric currents. Analysis of data from the Pogo satellites disclosed that the lower altitude contains separable fields related to anomalies in the earth's crust, thus opening the door to a new class of investigations. Several geomagnetic field models and crustal anomaly maps based on the Pogo data have been published.

NASA established the Magsat program to provide the United States Geological Survey (USGS) of the Department of the Interior with data to be used in making magnetic field maps for the 1980 epoch. The program is managed by the Goddard Space Flight Center (GSFC) in cooperation with the USGS. Responsibility for spacecraft design, development, and testing was assigned to APL.

The Magsat data are expected to resolve directional ambiguities in both field modeling and magnetic anomaly mapping. Increased resolution, coupled with higher signal levels from anomalous fields, will overcome some of the shortcomings of the Pogo data and provide improved anomaly maps.

Magsat data will be correlated with other geophysical measurements. For example, the highly accurate determination of the earth's gravity field and geoid accomplished by both laser tracking of satellites and altimetry studies with geodetic satellites provides information about the density distribution within the earth's crust.

MISSION OBJECTIVES

The USGS, principal user agency for this mission, and other users from both U.S. and foreign governments, universities, and industry will pursue the following objectives:

- Obtain an accurate, up-to-date, quantitative description of the earth's main magnetic field. Accuracy goals are 6 nanoteslas (1 nT = 10^{-9} weber per square meter) root sum squares (rss) in each direction at the satellite altitude and 20 nT rss at the earth's surface in its representation of the field from the earth's core at the time of the measurement;
- Provide data and a worldwide magnetic field model suitable for USGS use in updating and refining world and regional magnetic charts;
- Compile a global scalar and vector map of crustal magnetic anomalies. Accuracy goals are 3 nT rss in magnitude and 6 nT rss in each component. The spatial resolution goal of the anomaly map is 300 km; and
- Interpret the crustal anomaly map in terms of geologic and geophysical models of the earth's crust for assessing natural resources and determining future exploration strategy.

MISSION PARAMETERS

The altitude of the Magsat measurements was dictated by a trade-off between two requirements: the lowest possible altitude is necessary for increasing the anomaly signals and their spatial resolution; a minimum satellite lifetime is necessary for obtaining adequate data distribution. On the basis of these requirements, the nominal perigee was about 350 km. The apogee was selected to provide the required lifetime. Although higher altitude data are less useful, data up to 500 km could be used in anomaly studies. Accuracy goals are determined by the fact that, based on experience with Pogo, the anomaly amplitudes at 300 km are expected to be in the range of 0 to 50 nT. To obtain the maximum anomaly resolution and signal strength, data were acquired as the orbit decayed below 300 km during the reentry phase.

The main field and anomaly measurements must be made in the presence of the perturbing fields from ionospheric and magnetospheric sources. Since the mission was conducted during a period of very intense solar activity, only approximately 20% of the data obtained at latitudes below 50° will be sufficiently free of these perturbations to yield the required accuracy. At latitudes higher than 50° even fewer data are usable. To achieve a 300 km global anomaly resolution, coverage is needed along grid lines that are no more than 150 km apart. The time required for achieving this anomaly resolution is estimated to be 10 days for perfectly quiet data or 50 days during periods of maximum solar activity. This time represents minimal coverage with no capability of averaging or statistical analysis. To provide a workable sample, data that are three times as dense are needed.

Before launch the desired lifetime of the mission was established as approximately 150 days. The actual lifetime was 225 days. This additional time provided a more than adequate statistical sample and increased the probability of obtaining "quiet day" coverage.

Data at all local times except for those between 0900 and 1500 are useful for anomaly studies. A dawn launch was chosen to obtain useful anomaly data on all portions of the orbit and to maximize power.

Originally, a 325 by 550 km orbit was proposed to provide an orbital lifetime of between 4 and 8 months. Because of the very high solar flux that was subsequently predicted during late 1979 and early 1980 (this flux increases the height of the atmosphere and leads to higher drag forces), the final selected orbit was 350 by 550 km. A four-stage Scout vehicle injected Magsat into a sunlit (dawn to dusk) sun-synchronous orbit. It was launched from the Kennedy Space Center Western Test Range, Vandenberg AFB, Calif., on October 30, 1979.

INVESTIGATION PLANS

To achieve the Magsat mission objectives, investigations are being carried out at GSFC and the USGS and by competitively selected principal investigators.

The GSFC investigations are those required for rapidly producing the principal mission products — spherical harmonic models of the main geopotential field and magnetic anomaly maps, analytic tools needed by other investigators (e.g., equivalent source models of the anomaly field), and development of preliminary crustal models of selected areas not being studied by other investigators.

The USGS will produce charts of both the United States and the entire earth; will develop sophisticated models of the main geopotential field using Magsat data along with appropriate correlation data, with particular emphasis on secular variation studies; and will develop crustal models of selected regions.

REGIONAL GEOLOGIC AND GEOPHYSICAL STUDIES

Magnetic anomaly data are useful for regional studies of crustal structure and composition, the usefulness including possible correlation with the emplacement of natural resources and guidance for future resource exploration. Magnetic anomaly maps based on aeromagnetic surveys are standard tools for oil and mineral exploration. A magnetic anomaly, as the term is used in this overview, is the residual field remaining after the broader-scale earth's field is removed. The removed field is usually computed from a spherical harmonic

model. The primary purpose of the regional studies is to identify subsurface geologic structures that may extend over distances and depths of a few kilometers and to help target specific areas for drilling or mining. Because of incomplete coverage and because of large temporal changes in background fields between the times when adjacent local surveys were made and when large local variations occurred, available aeromagnetic anomaly maps cannot effectively probe broad regional geological features. With the advent of the theory of plate tectonics, interest in identifying and mapping these broad regional features is increasing.

The anomalies measured by Magsat will reflect such important geologic features as composition, temperature of rock formation, remanent magnetism, and geologic structure (faulting, subsidence, etc.) on a regional scale. Magsat is therefore providing information on the broad structure of the earth's crust, with near global coverage.

Continental coverage will be most important for immediate economic applications. Magsat data will help to delineate the fundamental structure of the very old crystalline basement that underlies most continental areas. This structure will not necessarily parallel known younger trends.

Interpretation of the basic scalar anomaly map begins with the construction of a model of regional susceptibility contrasts. The inclusion of vector data will improve model accuracy. Vector data are then used to infer the magnetic-moment direction for each anomaly, permitting the presence of large-scale remanent magnetism to be distinguished from susceptibility contrasts. Correlative data, such as gravity anomalies and known geology, are used in interpretation so that the resulting geological and geophysical models closely resemble reality. These models will contribute substantially to our knowledge of the unexposed fundamental geology of the continents. Models yield information for both the shallow crustal features that are important to resource assessment and the deep features that relate to faulting and earthquake mechanisms.

One application of Magsat anomaly maps will be the long-range planning of mineral and hydrocarbon exploration programs. Such planning is concerned with delineating entire regions (frequently of subcontinental extent) that should be explored rather than with discovery of specific oil or mineral deposits. For example, in Australia serious exploration for oil began in areas that were known to have thick accumulations of sedimentary rock (i.e., sedimentary basins). Regional studies eventually narrowed the broad target areas to a few promising structures, which were then explored in detail.

Some idea of the relationship between the regional geology and mineralogy can be seen by noting that metallic mineral deposits are usually associated, either directly or indirectly, with igneous rocks. From a broader viewpoint, the distribution of such deposits is closely interrelated with regional geology, such as structure, lithology, and depth of exposure. For example, copper deposits such as those of the southwestern United States are associated with a class of young granite intrusion that is, in turn, related to the Basin and Range Province, a large zone of block-faulting. In contrast, chromium occurs in large intrusions of iron-rich igneous rock of much greater age and completely different tectonic setting. A general factor that strongly affects both the formation of mineral deposits and the eventual discovery of their location is the crustal level at which they occur.

Because of these relationships, a sound knowledge of regional geology and geophysics is essential to the planning of mineral exploration and, generally, to the assessment of the mineral reserves of a region or country. Magsat is providing new information on crustal structure and composition over very large areas, including those in which bedrock is poorly exposed. Therefore, the data will be helpful in selecting the most promising areas for future mineral exploration and in determining the exploration strategy to be used. The full potential of the crustal anomaly measurements will not be realized for some time, but the near-term application of the initial results is obviously promising.

GEOMAGNETIC FIELD MODELING

One of the principal contributions of satellite magnetic field measurements to geomagnetism has been to make available a rapidly obtained global survey instead of conventional surface measurements that present the problem of the long-term, or secular, variation in the main geomagnetic field (which can amount to as much as 1% per year in some localities). In order to represent the global geomagnetic field accurately at any given instant, measurements must be made worldwide at nearly the same time. This can be achieved only by satellite observations and, even then, only by spacecraft that are in polar orbits and that are equipped with on-board tape recorders. In addition, accurate global respresentation of the secular variation requires periodic worldwide surveys. Magsat will furnish one such survey and, together with existing surface data, will permit accurate global representation of secular variation for the period beginning with OGO-2 to the demise of Magsat (October 1965 to June 1980).

Although Pogo data were global and taken over a short time, the limitation of measuring only the field magnitude resulted in some ambiguity in the field direction in spherical harmonic analyses. Magsat is eliminating this ambiguity by providing global vector data.

INNER-EARTH STUDIES

The radius of the earth is about 6378 km. Direct measurements in mines, drill holes, etc. are available only in the upper few kilometers of the crust. In particular, for information regarding the core

and mantle, the only sources of data are extruded geologic structures (upper mantle only), the gravity field of the earth, the rotation rate and polar motion, seismic measurements, and the magnetic field of the earth. Therefore, we must depend on only a few indirect measurements for information on more than 96% of the earth's volume.

To understand the tectonic processes that contribute to the dynamics of the earth's crust (i.e., plate motions, earthquakes, volcanism, and mineral formation), it is necessary to investigate the mantle and core in which these processes originate.

Characteristics of magnetic fields at and near the earth's surface (e.g., secular change, field reversals, and power spectra of magnetic-field models) have heretofore been used to infer properties internal to the earth. Combining Magsat data with earlier satellite surveys and with surface data from intervening times will permit more accurate determination of secular variation. This information can be used to investigate changes of the fluid motions in the core that give rise to the field, properties of the core-mantle boundary that greatly affect fluid motions of the core, and the transmission of this temporarily varying field through the lower mantle.

When magnetospheric fields are time varying, they result in induced fields within the earth because of the finite conductivity of the earth. The characteristics of these induced fields are determined by the composition and temperature of the materials in the earth's mantle. At present the limiting factor in determining a precise conductivity profile within the earth with adequate spatial resolution is the accuracy possible in determining the external and induced fields. Although the ultimate usefulness of satellite vector measurements in these studies is not completely clear, preliminary results are encouraging, suggesting that Magsat vector measurements will enable a much more accurate analysis to be made.

FREDERICK F. MOBLEY

MAGSAT PERFORMANCE HIGHLIGHTS

This article describes the commands given to the spacecraft during the first week after launch to prepare for collection of scientific data. It also discusses the performance of systems and instruments during the data-gathering phase.

POST-LAUNCH ACTIVITY OCTOBER 30 — NOVEMBER 3, 1979

Attitude Control

It was critically important for Magsat to obtain the proper attitude relative to the sun very soon after launch. Most satellites are designed to generate adequate electrical power regardless of their solar orientation; in such cases the post-launch attitude control adjustments can proceed gradually. However, Magsat had many electrical load requirements that could not be dispensed with, and the solar array could not meet those loads except when the B axis of the satellite was within 60° of the sun (see Glossary, Fig. A). At the moment of satellite release in orbit, this angle (β) would be near 90°, and the solar array output would be zero. Therefore, an immediate attitude control maneuver was required to move the B axis toward the sun before the battery became dangerously discharged.

Figure 1 shows the attitude control maneuvers that were programmed to occur in the first two orbits of Magsat. These maneuvers were accomplished by commanding a B-axis coil to be energized with a current of 0.9 A, producing a magnetic dipole parallel to the satellite B axis. This dipole interacted with the earth's magnetic field and produced a torque on the satellite. Since the satellite had substantial angular momentum (due to an internal wheel spinning at 1500 rpm as well as to the rotation of the satellite itself) and the torque is applied perpendicular to the momentum vector, the effect is to shift slowly the *direction* of the momentum vector in space.

To move the vector in a desired direction requires knowledge of the magnetic field strength and direction at the satellite position and the proper choice of command timing to take advantage of the field direction. This led to a particular command sequence and timing; the result is the predicted track of the B axis shown in Fig. 1. The commands for these maneuvers consisted of a series of B-coil commands, e.g., + SENSE, COIL ON, OFF, −SENSE, ON, OFF, etc., each at a particular time.

The Magsat command system could accommodate 82 stored commands in each of its two redundant systems. Almost all of this capability was used

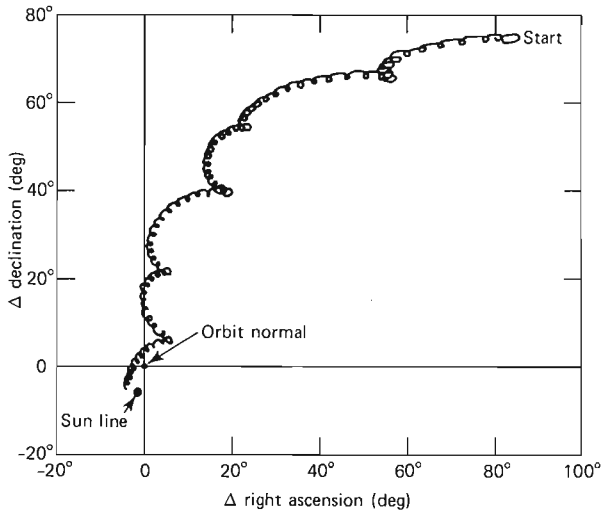

Fig. 1—Predicted track of +B-axis maneuver in initial orbits of Magsat. Initial spin rate: 0.67 rpm.

to carry out the following commands in the first orbit:

1. Turn off a tape recorder a few minutes after injection into orbit to save power;
2. Fire pyrotechnics to release two of the five mounting points for the optical bench and to release the mechanical retention of the boom links (but not the magnetometer platform — that would come later);
3. Turn the Doppler transmitter on for the benefit of a receiving station in Winkfield, England;
4. Turn the B coil on and off at the right times and with the correct polarity in order to maneuver the B axis toward the sun; and
5. Extend the aerotrim boom to balance aerodynamic yaw torques.

Figure I shows the predicted track of the +B axis with an assumed satellite spin rate of 0.67 rpm. Figure 2 compares the predicted variation of the angle β versus time with the actual result in orbit. Since the actual spin rate was 1.22 rpm, the angular momentum was greater than expected and the B axis failed to reach the sun line. Nevertheless, the final angle of 20° was more than adequate to provide the power requirements of the satellite.

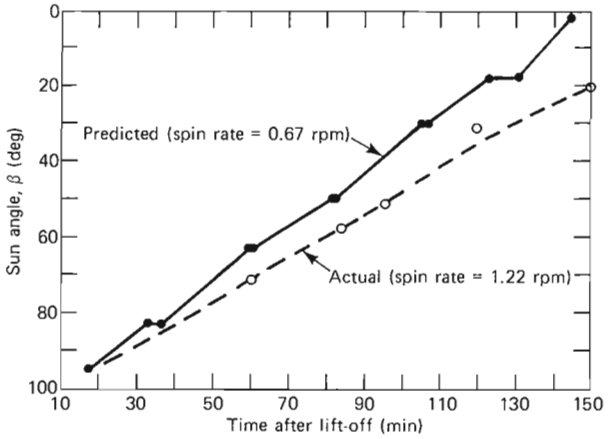

Fig. 2—Sun angle versus time for initial attitude maneuver of Magsat. A B-axis coil is turned on to interact with the earth's magnetic field to precess the satellite spin axis toward the sun in a programmed maneuver. The predicted motion was not fully achieved because the satellite spin rate was higher than expected. The solar array generated 135 W at the final orientation.

Two additional manually controlled magnetic maneuvers were carried out in the next 48 hours to bring the B axis within 5° of the sun line.

The magnetic spin/despin system was used to reduce the spin rate from 1.22 to 0.05 rpm in the first day. This system used X- and Y-axis coils that were energized proportionally to Y and X magnetometers, respectively, making the satellite behave like the armature of a DC electric motor and changing its spin rate slowly.

On October 31, 1979, the scalar and precision vector magnetometers were turned on to help absorb some of the excess solar-array power (even though the magnetometer boom was not yet extended and the data would be useless for scientific purposes). Very little drift in B-axis attitude was observed during this time period. The aerotrim boom had been extended to 4.63 m as part of the initial stored command sequence. Even though this was shorter than the planned length of 5.30 m, the yaw aerodynamic torques were well trimmed.

Until this time the attitude of the satellite was not under any form of continuous active control. The momentum wheel was running at a constant speed of 1500 rpm, and the associated angular momentum provided a form of "gyro" stability. Now the orientation of the satellite allowed the IR scanner to see the earth, and closed-loop pitch control was possible. At 1644 UT (Universal Time) on October 31, the attitude control was changed by command from the constant wheel-speed mode into the active pitch-control mode. In the latter mode the pitch angle of the satellite is detected by the IR scanner and if the pitch angle differs from the desired value, the wheel speed is increased or decreased to produce a reaction torque on the satellite in pitch, driving the pitch angle to the desired value. At 1730 UT on November 1, the automatic system for active roll-and yaw-angle control was activated. Full control of pitch, roll, and yaw angles was maintained thereafter.

Boom Extension and ATS Capture

Late on November 1, 1979, the magnetometer boom was deployed by command. Figure 3 shows the observed extension process versus time. The entire extension took 20 minutes, and was followed immediately by a further extension of the aerotrim boom to 6.99 m.

At this point the "moment of truth" came for one of the most challenging engineering tasks of the Magsat program. The pitch/yaw head of the attitude transfer system (ATS) sent a narrow beam of collimated light from the satellite to a small mirror (9 by 9 cm) mounted at the end of the boom, 6 m away. The mirror reflected the light back into the lens of the sending unit in order to measure the mirror angles of pitch and yaw. The ATS measures the mirror angles accurately over a range of ±3 arc-min (0.01667°) and is able to detect a signal out to ±6 arc-min (but cannot measure the angle accurately). Beyond that angle there is no signal. The critical question was, would the boom position and angle be correct for an ATS signal to be received? We had simulated the zero-gravity condition of space in a flow-tank test setup, but the pitch and yaw angles had to be simulated separately. Were our ground calibrations correct? Had some last minute changes disturbed our final alignments? Had the vibration of launch changed some critical angle? We were relieved and happy to discover after the boom extension that ATS signals in pitch,

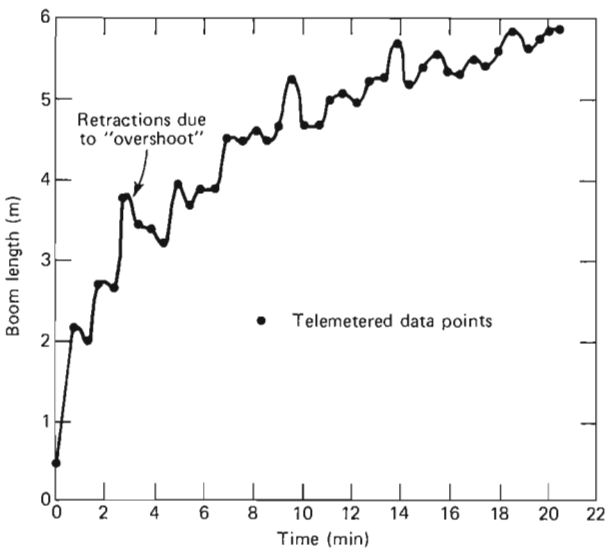

Fig. 3—Magnetometer boom extension on November 1, 1979. The boom is extended by a screw drive at the base of the boom. Static friction is overcome and the boom extends rapidly, overshoots, and partially retracts – then the process repeats. This accounts for the irregular extension process.

yaw, and roll were immediately received! On November 2 the three-axis gimbals at the base of the boom were commanded to adjust the boom angles to bring all three ATS outputs into the linear range of the system. Subsequent boom deflections due to temperature changes are discussed on p. 203. It is important to note that the ATS signals were in their nominal range continuously, a credit to the design of the boom.

Star Camera Operation

With attitude control fully established and the magnetometer boom extended, the star cameras were turned on during the morning of November 2 and functioned normally. Figure 4 shows typical outputs of a star camera. The position of a star in the field of view of the camera is recorded in terms of its X′ and Y′ coordinates. While tracking a star, the Y′ voltage stays relatively constant and the X′ voltage increases steadily, which is expected because the satellite rotates slowly about its B axis. At a rate of ≈4°/min, a star would seem to move across the field of the star camera in ≈2 min because the star camera field of view is 8 by 8°. However, the star camera was programmed to break lock on a star after a shorter time (e.g., 30 s). The camera then began a raster scan to find another star and to track it for 30 s. Occasionally a star passed out of the field of view before the 30 s had elapsed; in such cases the camera started searching again.

Thermal Problems

During the first few days in orbit, the internal temperatures of the base module rose about 10°C higher than predicted. This caused concern because the tape recorder lifetime could be shortened at elevated temperature and the battery as well as the IR detector could be damaged by high temperatures. The temperature of the IR detector stabilized at 43°C, about 3°C higher than the recommended maximum operating temperature. Battery temperature was reduced by operating the battery in a mode in which it was not charged from the solar cells but was used to supply power during peak demand. The battery was recharged about once every 5 days. The tape recorder temperature reached 38°C after a period of continuous recording. This temperature was higher than desired but was tolerable for the short mission lifetime of Magsat. No satisfactory explanation for the higher temperatures has been found.

SUBSEQUENT PERFORMANCE

By November 3, 1979, the satellite was fully operational and collection of scientific data began. In the normal operating mode, tape recorder data playbacks were scheduled four times per day. Each playback proceeded at a data rate of 320,000 bits/s for telemetering to the ground data that were accumulated at ≈2000 bits/s during the previous 6 to 7 hours. Before a playback was initiated the second tape recorder was started so that no scientific data were missed during the playback itself. Doppler transmitters were on continuously and Doppler data at 162 and 324 MHz were received by the worldwide Tranet stations of the Defense Mapping Agency. These data were forwarded to APL where the definitive satellite position versus time was produced by B. Holland. Position accuracy of better than 70 m root mean square was achieved in spite of the high drag condition of the Magsat orbit.

Observation of attitude drift indicated that we had overcompensated for yaw aerodynamic torque with an aerotrim boom length of 6.99 m. A series of retractions brought the boom back to 4.48 m where a very good trim condition was established. Figure 5 shows the drift track of the satellite B axis from November 22 to December 3. The B axis drifts in a small clockwise circle about 1.5° in

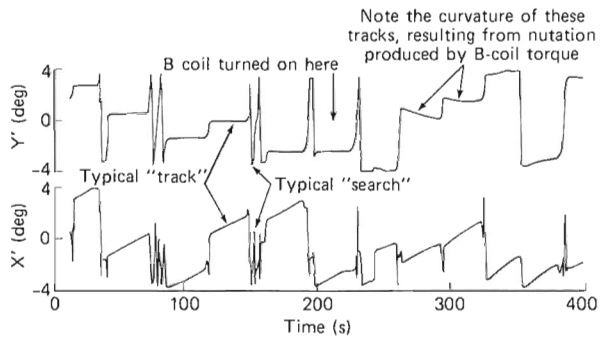

Fig. 4—Typical X′ and Y′ coordinates from star camera No. 2 versus time (Day 311, 1835 UT), showing "tracking" of stars and the effect of nutation produced by the B-coil torque with the earth's magnetic field.

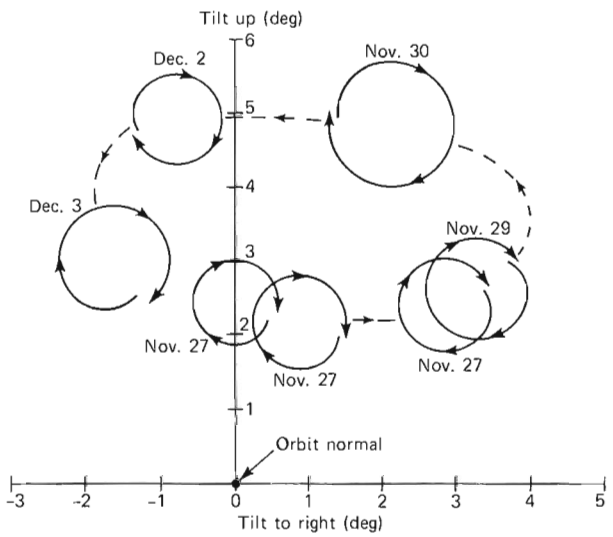

Fig. 5—Drift of B axis in space. The direction of the B axis drifts in a small circle during each orbit, and the center of this circle drifts in a larger elliptical path.

diameter in each orbit. The circle gradually drifted about in a large counterclockwise elliptical path whose center was displaced about 4° above the orbit normal. We believe this apparent tendency to circle about an orientation offset from the orbit normal was due to the rotation of the earth's atmosphere — a predicted effect. However, subsequent drift tracks have not been as simple and the cause is uncertain. It is important to note that hardly any magnetic torquing was necessary to maintain the satellite attitude except when the satellite came into lower altitudes and encountered higher aerodynamic forces.

Orbit Decay

Figure 6 shows the actual decay of the apogee and perigee of the Magsat orbit versus time as compared with an initial prediction made shortly after launch. Magsat remained in orbit longer than predicted, allowing more data collection when the magnetic field was quiet. However, there was a disadvantage because the low altitude data were delayed, to the extent that eclipsing of the satellite by the earth in April 1980 had deleterious effects on power, so that duty cycling of subsystems was necessary.

Vector and Scalar Magnetometers

The scalar magnetometer data were noisy from the start, probably because of lamp instability problems similar to those encountered before launch. However, the 20 to 40% of the data points that were valid have been used to make final adjustments in the calibration of the vector magnetometer to achieve a correlation of 1.2 nT rms in the total field as measured by the two instruments. (More detail on these devices may be found in the Farthing and Acuna articles in this issue.)

Star Camera Operation

Loss of star camera data for time periods of 30 to 40 minutes was observed beginning in early November. It occurred only in the southern hemisphere and is believed to be caused by sunlight falling directly on the sides of the sunshades and penetrating the black plastic skin of the sunshade. As expected, this phenomenon shifted from the southern to the northern hemisphere in March and April as the sun moved north.

FINAL EVENTS

On April 12, 1980, eclipsing of Magsat by the earth began, as predicted. The loss of solar array power during the eclipse meant that the satellite systems were entirely dependent on the stored energy in the nickel-cadmium battery. The battery voltage dropped much more rapidly than we expected during the eclipse. After the data were analyzed it became apparent that the battery capacity had dropped to about 12% of its nominal capacity of 8 ampere-hours. This loss in capacity has been ascribed to the "memory" effect associated with shallow discharging of nickel-cadmium batteries (which occurred prior to the eclipsing period) and also to simultaneous exposure to elevated temperatures.

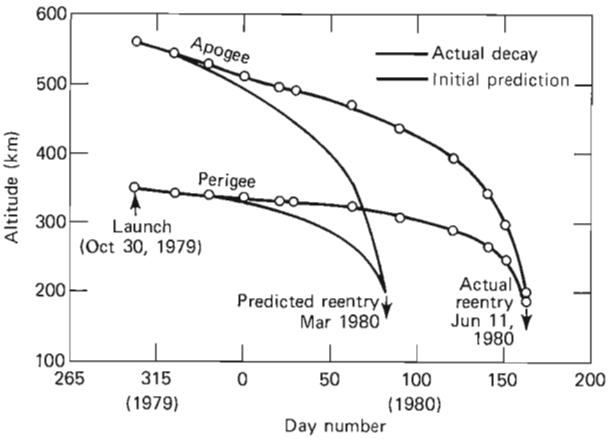

Fig. 6—Magsat orbit decay. The decay was slower than predicted because the density of the atmosphere was less than expected. The satellite reentered on June 11, 1980.

The reduced battery capacity caused operational problems. During each orbit various subsystems were commanded OFF prior to eclipse and ON after eclipse. In spite of this effort, a low battery voltage condition occurred on April 17. The battery voltage dipped below 13.2 V and the satellite automatically went into a self-protective mode, which included turning off the gyro. The attitude control system responded by going automatically into another pitch control mode that does not require gyro input. Several hours later, the satellite was restored to normal operation by commands from the ground. A similar event occurred in May.

In early June, the satellite altitude decayed to ≈240 km and eclipse times of 35 minutes were experienced. It was necessary to turn off the scalar magnetometer, the star cameras, and the ATS to save power. The vector magnetometer data were acquired until a few hours before reentry. Since the star cameras were off, the vector data cannot be used to determine the field direction. However, the three components will be combined to form the magnitude of the field, and those data will be analyzed for evidence of geomagnetic anomalies.

Reentry of the satellite occurred at 0720 UT on June 11, 1980, in the Atlantic Ocean. The satellite probably vaporized from the heat of aerodynamic friction. However, the momentum wheel (made of tungsten) may have survived. Some mariners of future civilizations may be puzzled at the strange "anchors" we used.

WALTER E. ALLEN

THE MAGSAT POWER SYSTEM

The Magsat power system was required to generate, store, and condition energy for use by all spacecraft systems. It consisted of a solar cell array, a rechargeable battery, redundant battery charge regulators, and several converters, inverters, and regulators to condition power for use by Magsat loads.

SOLAR CELL ARRAY

An array of silicon solar cells mounted on four deployable panels generated electrical power for the Magsat spacecraft. Each panel consisted of two interhinged, curved segments that were designed to be folded inside the rocket heat shield and restrained against the side of the base module during launch by a thin-wire despin cable. After the spin-stabilized last rocket stage was fired, a special purpose timer activated pyrotechnic devices that released the despin weights and cables. This action caused the spacecraft to despin while simultaneously allowing deployment of the spring-loaded panels. The deployed panels formed a planar cruciform array, with the long axis of each panel perpendicular to the spacecraft B axis.

Each of the eight array segments was a curved, lightweight, aluminum-honeycomb structure approximately 64 cm long by 36 cm wide. Two of the eight segments flown were from another spacecraft program and had 2 by 2 cm silicon solar cells on both sides. The remaining six segments were of more recent manufacture and had 2 by 4 cm, high-efficiency silicon solar cells on one side only. All segments were configured with two circuits of 57 series-connected cells in order to permit effective recharge of the spacecraft battery.

Opposing panel pairs in the array could be independently rotated about their common axis, if desired, by ground command. Rotation to any angle from 0° (the normal value at deployment) to 90° could be effected. A separate synchronous motor drive was employed aboard the spacecraft to perform this function for each axis. The feature could have been used to optimize power generation by the array if the spacecraft had assumed some anomalous attitude.

The Magsat attitude control system was designed to maintain the B axis of the spacecraft nearly perpendicular to the sun-synchronous orbit plane. This resulted in relatively close alignment of the sun-earth line and the B axis of the spacecraft, and full orbit sunlight illumination throughout most of the mission lifetime. Therefore, the power generated by the solar array was largely a function of the angle ψ between the +B axis of the spacecraft and the sun-earth line. Figure 1 illustrates the prelaunch predicted power available at the battery as a function of this angle.

BATTERY

The spacecraft battery consisted of 12 series-connected 8 A-h (ampere-hours) nickel-cadmium cells operating at a nominal voltage of 16.7 V. The battery supplied energy to meet brief demands in excess of the generating capability of the solar array and operated the spacecraft during transient phases of orbit acquisition and attitude adjustment. It also sustained operation of the spacecraft during periods of solar eclipse that occurred late in the mission lifetime.

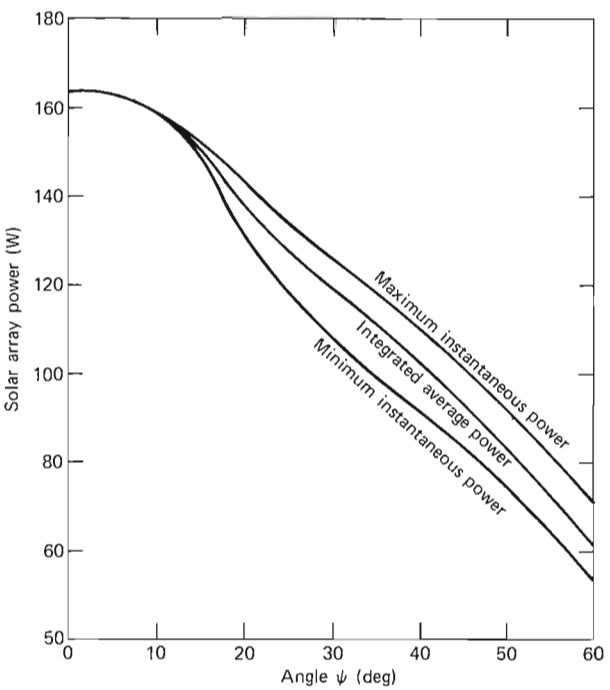

Fig. 1—Power output of the Magsat solar array as a function of angle ψ between the +B spacecraft axis and the sun-earth line. Variations in instantaneous array power output illustrated here result from array shadowing by both the base and instrument modules. These losses were evaluated with the assistance of a 3/8-scale model of the spacecraft.

BATTERY CHARGE CONTROL

Since the Magsat battery was to be exposed to extended periods of continuous overcharge, considerable design effort was expended to provide a charge control system that would permit rapid recharge of a depleted battery and would limit overcharge to levels that were electrically and thermally acceptable. The power system therefore incorporated a lightweight shunt regulator of special design to dissipate excessive solar array power as heat (up to a maximum of approximately 120 W) on three externally mounted radiator panels.

The dissipative shunt regulator and its control element were fully redundant. The inputs to the control element were bus voltage, battery temperature, and a voltage proportional to battery current. Depending on the operating mode selected (either fixed-rate trickle charge or voltage-limited charge), the controller exercised active elements in the regulator to shunt unwanted battery current. The electronic elements (shunt drivers) were mounted on an external panel on the +B axis of the spacecraft. The resistive elements were distributed on external radiators mounted on the sides of the base module. The selectable voltage limit charge control characteristics are shown in Fig. 2.

We anticipated that ground controllers would primarily employ shunt regulator No. 1 in the voltage-limited mode to permit rapid recharge of a depleted battery while limiting maximum battery voltage to a conservative value. The trickle charge mode, a viable one for noneclipsed orbits, was considered a secondary operating mode. The trickle charge limit for both shunt regulators was 250 mA.

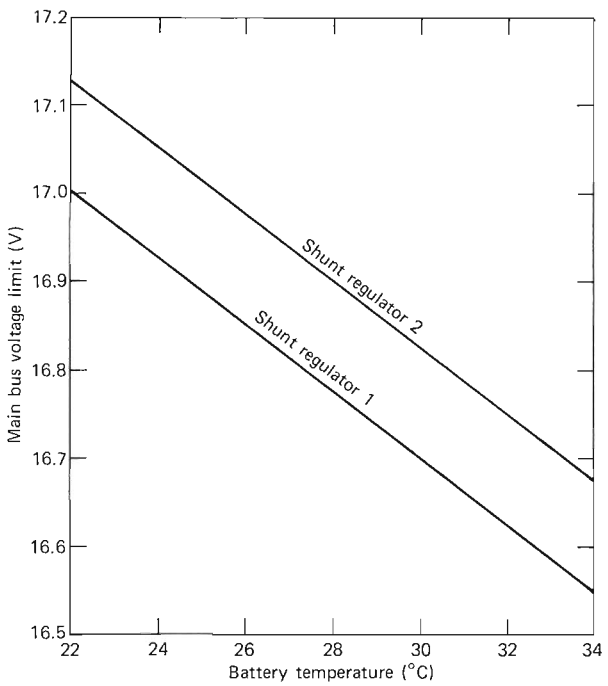

Fig. 2—Voltage limit of the Magsat main bus as a function of battery temperature.

A block diagram of the subsystem is shown in Fig. 3, and its salient characteristics are provided in Table I.

Table 1

POWER SYSTEM CHARACTERISTICS

Power available	120 to 163 W, average
Main regulator capacity	4.0 A, maximum
Unregulated bus voltage	18.6 V, maximum 16.7 V, nominal 15.0 V, minimum expected (circuit breaker actuates at 13.2 V)
Regulated bus voltage	13.5 V ± 2%
Charge control system	Redundant shunt regulator provides trickle charge and/or temperature compensated voltage limit. Shunt capacity: 120 W
Battery	12 series-connected 8 A-h cells. Battery cell manufacturer: SAFT America, Inc.
Solar cell array type	Four panels in rotatable coplanar pairs. Each panel consists of two interhinged segments.
Number of cells	1824, 2 × 2 cm 1368, 2 × 4 cm
Solar cell type	Centralab 10 Ω-cm, Si, N/P cells, 2 × 2 cm, and Spectrolab 10 Ω-cm, Si, N/P cells, 2 × 4 cm
Number of cells in series	57
Coverglass type	6 mil microsheet with antireflective filter applied by Optical Coating Laboratories

SYSTEM OPERATION UNDER ABNORMAL CONDITIONS

The Magsat power system was designed to accommodate malfunctions within the spacecraft automatically. A low-voltage sensing system, acting as a circuit breaker, controlled all commandable relays that supplied power to noncritical loads. If the main bus voltage fell below 13.2 V (which indicates a depleted battery), the system automatically took remedial action as indicated in the box on the next page. Ground controllers were required to reset the desired spacecraft power system configuration and to reenable the system to function by command, upon recovery from an undervoltage fault.

ORBITAL PERFORMANCE

The Magsat power system performed satisfactorily. The output power of the solar array exceeded

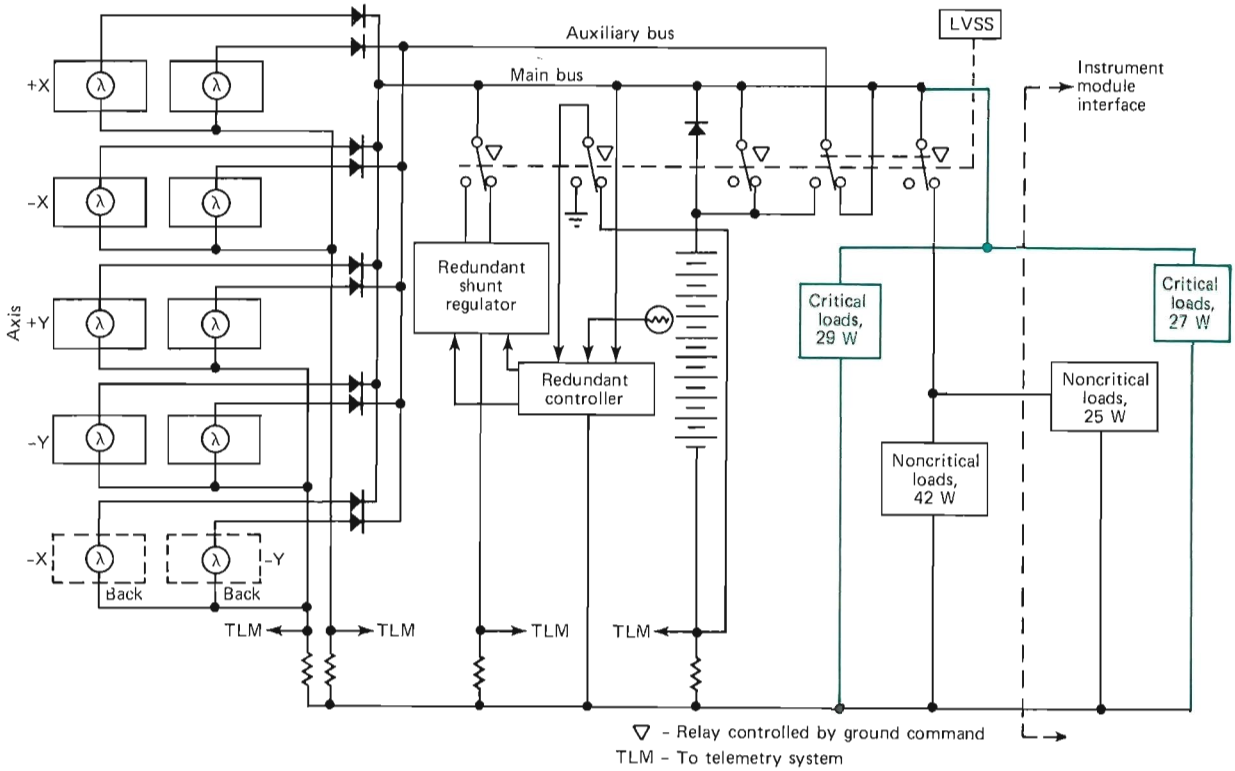

Fig. 3—Block diagram of the Magsat power subsystem. The loads are divided into critical and noncritical categories. Critical loads are defined as those that are essential to mission success and that must be powered continuously. The critical power system loads are the command system, selected attitude control system elements, and instrument module thermal control. All loads derive power from the main power bus. The solar array is equally divided between the main bus and an auxiliary bus that is normally connected to the main bus when the noncritical loads are powered.

the predicted value by approximately 10%. This was attributable to the seasonal increase in solar illumination intensity at the time of observation, panel illumination enhancement from earth albedo, and sunlight reflections from the highly reflective thermal control surfaces of the base and instrument modules onto the solar panels. We believe that reflections are the principal contributor to array power enhancement.

The orbital operating temperatures of elements in the Magsat base module were somewhat higher than anticipated. In an attempt to minimize temperatures in the base module, the battery had been primarily operated in the OR mode with the battery diode not bypassed. OR mode operation, as the term suggests, permitted either the solar array or the battery (or both) to supply power to the main bus through their respective "one-way" blocking diodes. System operation in the OR mode prevented the battery from being charged but had the positive effect of reducing internal power dissipation in the base module by approximately 5 W, thereby lowering temperatures. The battery was discharged briefly during recovery of tape-recorded data, and continuously by internal self-discharge mechanisms. As a result the battery required periodic recharge in order to maintain the necessary reserve capacity to meet anticipated storage demands and to cover contingencies.

In order to recharge the battery in orbit while operating in the OR mode, the battery diode was typically bypassed for one orbital revolution every

Actuation of the Low-Voltage Sensing System

Main bus voltage drops below 13.2 V:

Cause 1—Insufficient solar array generating capability (most probably attitude related).
Cause 2—System electrical overload.
Cause 3—Shunt regulator overload.
Cause 4—Battery failure.

System Response:

Action 1—Noncritical loads are turned off to conserve power.
Action 2—The auxiliary solar array is connected directly to the battery to effect a rapid battery recharge. The battery is simultaneously ORed to the main bus as a power source by the battery diode.
Action 3—The controller of the shunt regulator is automatically switched to the voltage limit mode.
Action 4—Shunt regulator 2 instead of 1 is switched on (Fig. 3). This also permits the main bus to achieve the slightly higher voltage limit.

If the low voltage condition results from cause 1 or 2, action 1 will be helpful. If it results from cause 3, action 4 is helpful. If it results from cause 4, action 2 will be helpful. In the case of cause 1, actions 2 and 4 will help restore the battery to a charged condition and permit the determination of the particular subsystem causing the overload.

fifth day. Figure 4 illustrates the telemetered battery performance data obtained during recharge on Day 316, 1979. Small step jumps in the data are attributable to the granularity of a digital telemetry system. Relatively large perturbations in initial battery charge currents were caused by load variations that occurred as heaters were automatically switched on and off to maintain selected instrument module temperatures. The battery charging current was tapered as the selected instrument temperature was reached. The battery charge regulator was activated; it shunted excess current to maintain the appropriate bus voltage throughout the remainder of the charge period.

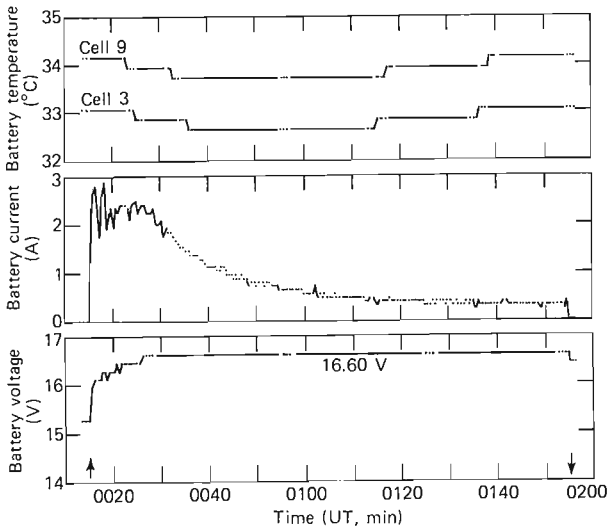

Fig. 4—Magsat battery 100 minute charge profile, Day 316, 1979.

Particularly noteworthy in Fig. 4 is the change in Magsat battery cell temperature during recharge. During the early part of the charge cycle, the temperatures of cells 3 and 9 dropped because of the endothermic nature of the chemical reactions taking place during recharge. During the last 40 minutes of the charge cycle, temperatures began to rise, indicating the onset of overcharge.

All telemetered performance parameters of the Magsat power system were nominal, including load currents and converter output voltages. The main bus voltage was closer to 16.5 V than to the predicted 16.7 V. This was a direct result of the somewhat higher than nominal operating temperature of the base module.

A significant loss in battery capacity was observed late in the Magsat mission lifetime. This loss is believed to be attributable to sustained high temperature operation. As a result of this capacity loss, operation of the spacecraft proved somewhat problematic during periods of solar eclipse; selected loads had to be switched off briefly during these periods in order to reduce the electrical load imposed on the battery.

ARK L. LEW, BRUCE C. MOORE, JOHN R. DOZSA, AND RONALD K. BUREK

THE MAGSAT TELECOMMUNICATIONS SYSTEM

The Magsat telecommunications system, consisting of the command and telemetry subsystems, performed the command, control, data-gathering, and transmission functions between Magsat and the NASA ground stations.

INTRODUCTION

The design of the Magsat telecommunications system was based in part on using hardware from the Small Astronomy Satellite (SAS-3) wherever possible. However, the telemetry modulation control and tape recorder interface electronics were new designs. In addition, the need to accommodate the new NASA phased shift keying (PSK) uplink format, together with other considerations, led to a new command processor design, supported by existing SAS-3 power switching modules and command DC/DC converters. Figure 1 illustrates the major telecommunications hardware functions and indicates the primary signal flow paths.

The NASA standard transponder and associated diplexers, couplers, and antennas were shared by the command and the telemetry subsystems. From each command receiver, the bit stream from the command decoding unit went to the command processor, where the commands were decoded, checked for validity, and distributed to the users, either as relay drive pulses from the pulse command matrix or as relay contact closures from the power switching unit. Command sequences could also be loaded into the command processor for delayed command execution at times when the satellite was out of range of a ground station. The command subsystem was completely redundant and was designed so that a single failure could not prevent commands from being processed.

The telemetry subsystem received data from all of the spacecraft systems, formatted the information into a single serial digital bit stream, and routed it to the transmitter and to the two tape recorders. Redundant precision crystal oscillators and digital clock divider logic in the telemetry subsystem provided timing signals for other spacecraft systems. The telemetry subsystem also had a data interface that allowed the command processors to preempt the entire telemetry frame for verification

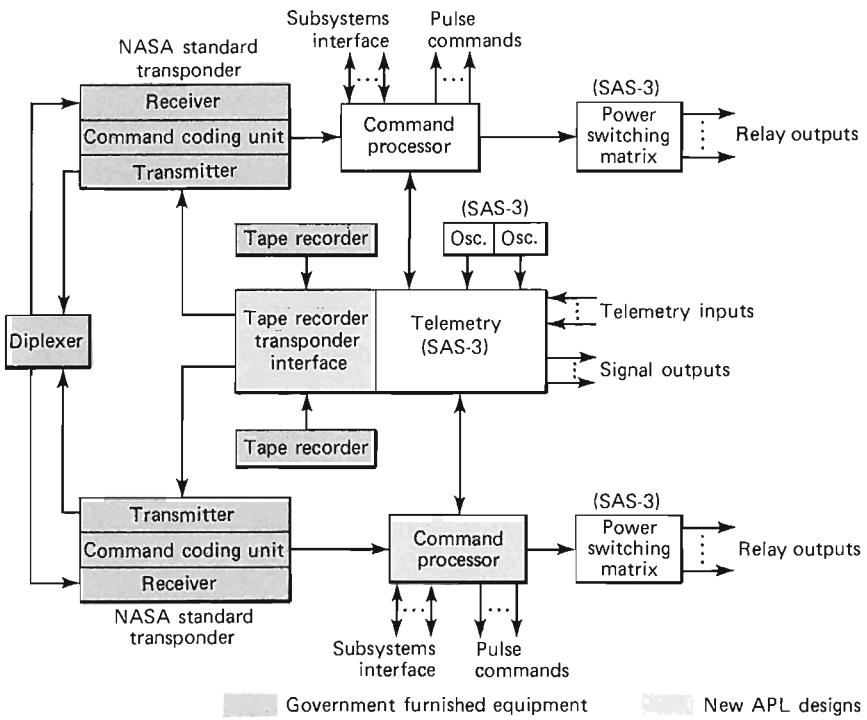

Fig. 1—Magsat telecommunications system.

of the stored command sequences before execution was begun.

COMMAND SUBSYSTEM

Since the introduction of the first integrated circuit controllers in the early 1970's, microprocessors have matured to the point where the design of complex spacecraft electronics must consider the alternatives of microprocessor-based versus random logic design. Trade-off evaluations resulted in the selection of a microprocessor-based design for the Magsat command subsystem.[1] This new design represented the first in a new generation of command subsystems, offering expanded capabilities and increased flexibilities in real-time and delayed commanding operations for APL satellites.

A block diagram of the command subsystem is shown as part of Fig. 1. Except for the S-band antenna, it incorporated full addressed redundancy. Two receivers detected the PSK RF uplink and delivered command data to each respective command processor for execution of the following functions: RELAY, SHORT DATA, LONG DATA, and PULSE commands. All command functions were executable in real time or on a delayed basis. Additionally, each command processor was programmed for limited semiautonomous operations with the telemetry, power, and attitude subsystems.

Multiple command execution was an important feature of this new design. Figure 2 shows the uplink command message depicting a real-time command sequence that must be limited to a maximum of 2048 bits (the equivalent of 32 real-time commands). Within the microstructure of each command, a truncated Hamming code byte was used for error control.

Both command processors processed the uplink command message; however, only the selected processor executed the desired command once all interlocks were enabled. Both processors would normally be in the main general polling routine shown in Fig. 3. The routine sampled flags according to a prescribed priority to determine the desired command operation: real-time commands, low battery-voltage commands for load minimization, delayed commands, spacecraft attitude maneuvers, and automatic transmitter power turn-off. The routine could be interrupted for the loading of a real-time command message bit stream by the INTRCDLD subroutine. Upon sensing a real-time hardware interrupt from the command decoder unit, the command sequence was loaded into a working area in the random access memory for processing by the general polling routine. All real-time commands were processed similarly for either RELAY, PULSE, SHORT DATA (24 data bits), or LONG DATA (memory load) commands. Delayed command sequences were extracted from the working random-access-memory space and loaded into a designated delayed-command random-access-memory space. The delayed-command storage area could accommodate up to five different sequences totaling 82 commands; however, each delayed-command load was limited to a maximum of 31 commands. For each load, an automatic telemetry readout was generated for ground verification before sequence execution was started with an epoch set command. The delayed commands were handled by two flags (for preservation of delayed-timing integrity) within the polling routine.

Subsystem Hardware

The considerations that led to the decision in favor of independent, redundant command channels were reliability, the reliance of other subsystems on the command subsystem for configuration and control, and their use as a troubleshooting tool with the telemetry subsystem. Both channels had equivalent command capabilities so that a failure in either channel would not impair any command function. Within each channel there existed a measure of circuit redundancy to reduce the probability of executing erroneous commands. Reinforcing the hardware redundancy were numerous software checks on the command message that had to be successfully verified before command execution could proceed.

Each channel consisted of a receiver, a processor, and the power switching electronics. The receivers are discussed in the transponder section.

The command processor was implemented with the RCA CDP 1802 family of circuits consisting of the CDP 1802 microprocessor, CDP 1852 interface circuit, CDP 1822 1K × 1 random access memory, and HA 6611 256 × 4 programmable read-only memories . Complementary metal-oxide semiconductor (CMOS) support circuits were utilized for power considerations. The CDP 1802 is the large-scale-integration CMOS, 8-bit register-oriented central processing unit with circuitry for fetching, interpreting, and executing instructions in external memory and generating input-output control signals.

Each command processor contained four electronics boards that were interconnected via flexible cabling, as is seen in Fig. 4. The four boards folded in accordion fashion and were housed in a magnesium casing.

The centralized power switching modules were housed separately. In addition to relay contact out-

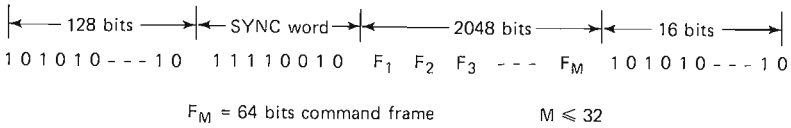

Fig. 2— Command message stream.

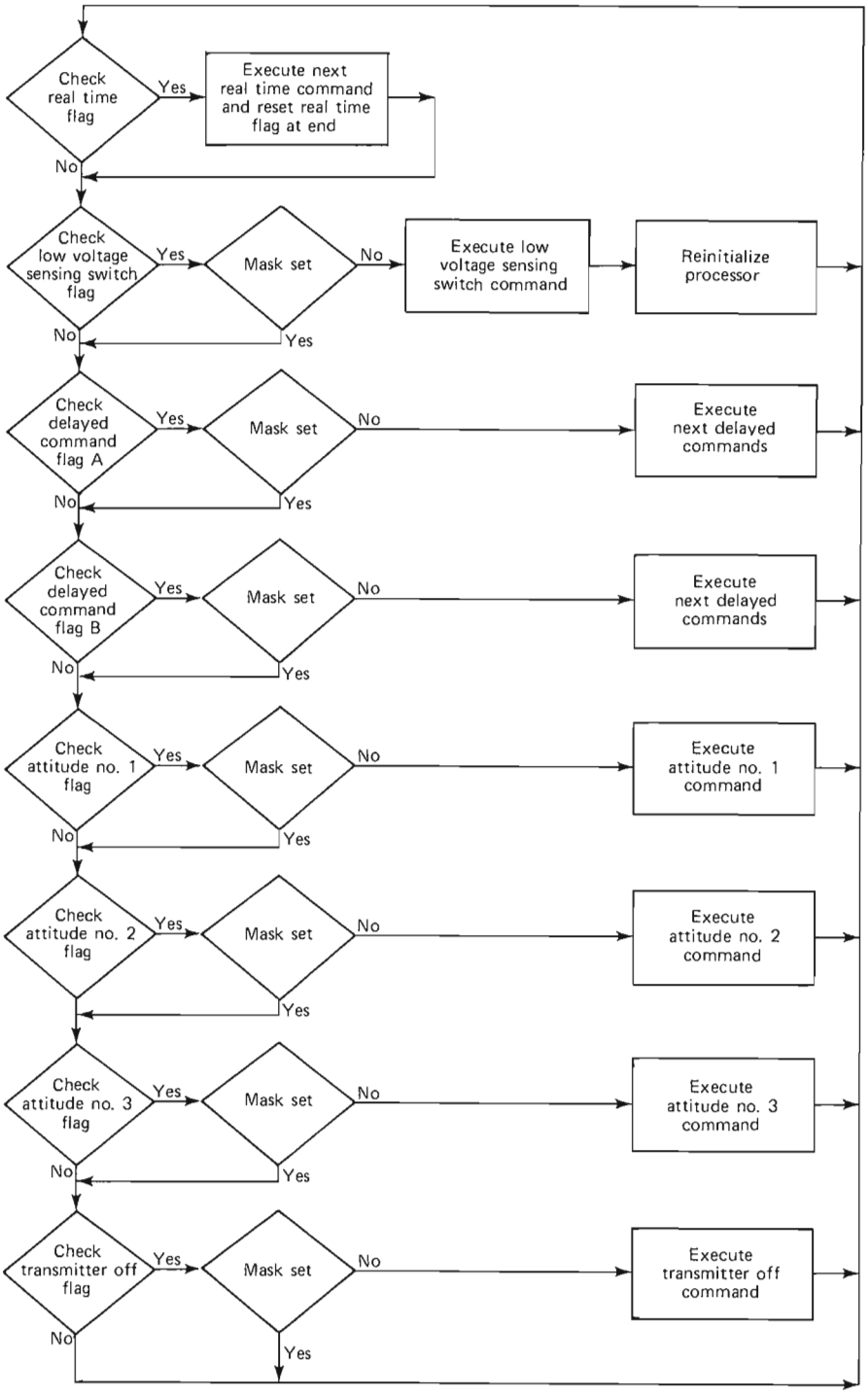

Fig. 3—Magsat command; general polling scheme.

puts, the two relay matrices also provided for low voltage sensing switch operations. A low voltage sensing circuit external to the command system provided a pulse to selected relays to switch off all nonessential loads upon sensing low battery voltages. The same pulse was also routed to each command processor to initiate the low-voltage stored commands. Functions not accommodated by the SAS-3 power switching modules were assigned to the pulse command matrices (board 4 of Fig. 4).

Subsystem Software

There are four routines for each command processor, labeled as follows: INGENPOL, CMDEX, INTRCDLD, and STORED CMDS. INGENPOL performed all initialization operations and continually executed the general polling routine during the background mode (Fig. 3). Within each loop the CMDEX routine was called to process command frames individually after each real-time command load.

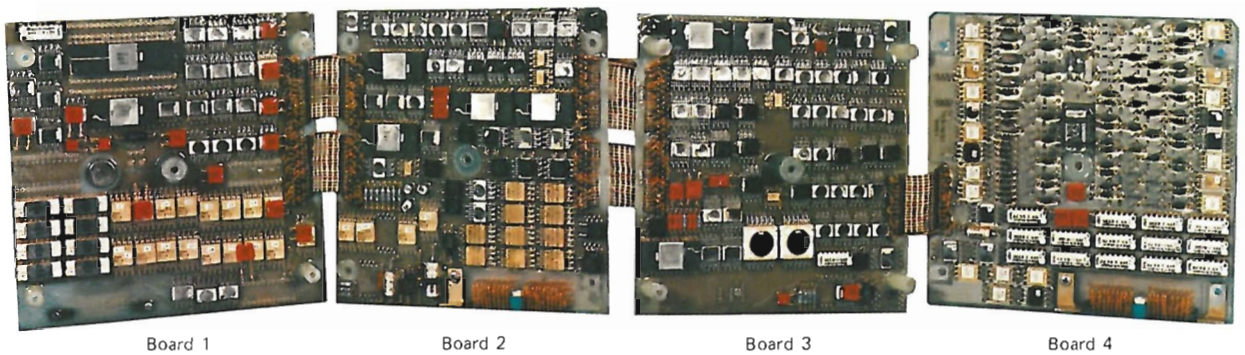

Fig. 4—Command processor. Each of the four electronics boards is 5.9 inches square.

After servicing subsequent flags, INGENPOL again invoked CMDEX to execute another real-time command until all real-time commands were executed.

Real-time command sequences were loaded into each processor's random access memory by interrupting INGENPOL with INTRCDLD. The STORED CMDS portion of the firmware consisted of stored commands that were executed via software for spacecraft operations.

The entire command firmware required 2.8 kilobytes of programmable read-only memory. Software for this project was developed with the aid of the APL 1802 cross assembler.

TELEMETRY SUBSYSTEM

For Magsat, the flight-qualified spare telemetry "books" from the SAS-3 spacecraft were modified and requalified. Some of the flexibility designed into the SAS-3 telemetry subsystem[2] was not required; this allowed some hardware to be deleted. The changes included deleting the variable format generator and its memory, the variable bit rate, and the transmitter and recorder interfaces, and changing the time code generator to a major frame counter. Also, the programmable read-only memories that contained the SAS-3 fixed format program were removed from the format generator board and replaced with programmable read-only memories containing the Magsat format. The relative ease with which the Magsat frame format was accommodated illustrates the flexibility inherent in a programmable controller like the SAS-3 format generator.

Since the interfaces to the transmitter, the NASA standard tape recorders, and the SAS-3 spare telemetry hardware were all predetermined and were not mutually compatible, a section of interface electronics had to be designed to interconnect them. The recorder-transponder interface represents the only new hardware design that was required for the telemetry subsystem. It provided the signal cross-strapping and mode selection that allowed data from either tape recorder to be played back via either of the transmitters. The telemetry subsystem as a whole was not completely immune to single-point failures, but there was much redundancy in the hardware (such as two independent format memories). In addition, the recorder-transponder interface was completely redundant. The interface unit required two standard welded wire boards of circuitry that fitted into the space that became available by eliminating the variable format generator. Pertinent characteristics of the telemetry electronics are summarized in Table 1.

Table 1

TELEMETRY CHARACTERISTICS

Bit Rate (b/s)
- 1953 Split phase PCM on 640 kHz subcarrier
- 312,000 Tape recorder playback on baseband

Frame
- Size
  - Minor frame: 960 bits
  - Major frame: 256 minor frames
- Rate (s)
  - Minor frame: 0.49
  - Major frame: 125.8
- Subcommutators
  - Number: 4 analog, 4 digital
  - Length: shortest, 4 channels; longest, 256 channels

Size (cm)

Main telemetry hardware	16.0 × 18.3 × 35.6
Crystal oscillators	10.4 × 13.0 × 15.5
Dual power converter	16.0 × 18.3 × 5.1

Weight (kg)
- 7.7 (excluding NST* and tape recorders)

Power (W)
- 9 (excluding NST* and tape recorders)

*NASA standard transponder

S-BAND TRANSPONDER

The S-band transponders used on Magsat were the NST—near earth type. They served as com-

mand receivers, phase-coherent ranging transponders, and telemetry transmitters. Each transponder consisted of a double-conversion, phase-coherent receiver and a transmitter that was integrally related in both frequency and phase with the receiver.

The transponder operated on a 2102.723 MHz uplink received signal and produced a 2283.5 MHz downlink transmitted signal. The phase-locked downlink RF carrier signal was precisely 240/221 times the uplink received RF signal frequency when operated in the ranging mode. On ground command, the transponder would provide a noncoherent downlink RF signal frequency. In this nonranging mode of operation, the transponder operated strictly as a command receiver and a telemetry transmitter that were independent of each other. In the absence of an uplink RF carrier signal, the downlink RF carrier signal was derived from a self-contained oscillator.

MAGSAT TAPE RECORDERS

Tape recording the real-time telemetry data ensured that no information was lost during the time the spacecraft was out of contact with a ground receiving station. Two recorders, manufactured by Odetics Corp., recorded up to 9×10^7 bits each, over a 12.5 hour maximum period. Upon command, the accumulation of data was played back to the ground at 312,000 b/s, which is 160 times the rate at which it was recorded. This took less than 4.7 minutes, well within the 6 to 10 minute duration of a satellite pass over a ground station. The reels of tape were stacked one above the other and contrarotated to minimize disturbances to the spacecraft attitude by recorder speed changes. To reduce angular momentum transients further and to eliminate rewind time, the tapes were played out backwards so that the last datum recorded was the first recovered. Each recorder had three capstans coupled by redundant Kapton belts and was driven by a servo-controlled brushless DC motor with optical commutation. Housings were pressurized by nitrogen to protect the recorders from the vacuum of space. Table 2 summarizes other tape recorder parameters.

Table 2

SALIENT CHARACTERISTICS OF THE MAGSAT TAPE RECORDERS

Record speed	0.55 cm/s
Playback speed	88.2 cm/s
Tape	256 m × 0.635 cm × 25.4 μm
Power consumption	9 W record, 25 W playback
Weight	7.85 kg
Size	35.4 × 22.9 × 15.5 cm

PERFORMANCE

Operation and performance of the telecommunication system were highly satisfactory both during prelaunch and in orbit. For the prelaunch qualifications, the command processor, power switching, and telemetry electronics were extensively tested in automated test configurations controlled by an SEL 32 computer. The spacecraft operators found the versatility, in orbit, of the command processor in handling delayed commands particularly useful. Successful execution of stored commands was crucial to spacecraft operations during the first orbit when the spacecraft was not in view of a ground station.

REFERENCES

[1]A. L. Lew, *The Microprocessor Based MAGSAT Command System*, JHU/APL CP 077 (1980).
[2]M. R. Peterson, "The SAS-3 Programmable Telemetry System," *APL Tech. Dig.* **14**, No. 4, pp. 7 – 13 (1975).

ACKNOWLEDGMENT — The authors wish to recognize the contributions of H. Goodnight, D. Guynn, J. Kroutil, M. Peterson, D. Stott, and G. Weaver in the production of this system.

KEVIN J. HEFFERNAN, GLEN H. FOUNTAIN, BARRY E. TOSSMAN,
AND FREDERICK F. MOBLEY

THE MAGSAT ATTITUDE CONTROL SYSTEM

An account is presented of techniques used for orienting Magsat in the desired three-axis controlled attitude in space. The pitch angle was sensed by an infrared horizon scanner and controlled by reaction torques from an internal reaction wheel. Roll angle was also sensed by the infrared scanner and controlled by torquing the satellite with a magnetic coil that interacted with the earth's magnetic field. A small on-board computer assessed the roll error and computed the proper strength of the magnetic coil in order to correct the error, accounting for the actual magnetic field strength and internal angular momentum. No direct measurement or control of yaw was necessary.

INTRODUCTION

The first two Small Astronomy Satellites, SAS-1 and SAS-2, are good examples of previous APL attitude control systems. A constant speed momentum wheel provided open-loop gyro stabilization of the Z axis in space (see Glossary, Fig. A and Ref. 1). X- and Y-axis coils were used to interact with the earth's magnetic field to control the satellite spin rate. A Z-axis coil was used to precess the Z axis to the desired orientation in space. Nutation damping was accomplished using a mechanical device to dissipate nutation energy in the form of heat. Only the Z-axis orientation was controlled, and that only by command from the ground.

The third Small Astronomy Satellite, SAS-3, had a somewhat more sophisticated attitude control system (ACS). An internal gyro system was used to sense the satellite spin rate, and closed-loop control of spin rate was achieved by modulation of the wheel speed to provide the necessary torque. The wheel also incorporated an IR earth horizon scanner for closed-loop pitch angle control of the satellite. While this was not the desired flight mode for SAS-3, we did have the opportunity to demonstrate its proper operation several times during the four years of SAS-3 life. This form of control became the primary operating mode for Magsat.

In Magsat, the satellite was three-axis controlled to follow the local vertical axis system as the satellite moved in orbit. The axis system makes one complete rotation about the pitch axis during each orbit. The angles describing the satellite attitude are called pitch, roll, and yaw, where pitch refers to nose-up or -down (B axis), roll is rotation about the flight path axis (A axis), and yaw is rotation about the local vertical axis (C axis).

The momentum wheel had its axis of rotation aligned with the satellite pitch axis. The angular momentum of the wheel, spinning at approximately 1500 rpm, provided a form of weak gyro stabilization to keep the roll and yaw angles from changing rapidly. However, the wheel momentum did not force the roll and yaw angles to return to zero. The IR earth horizon scanner provided a pitch error signal, and closed-loop control in pitch was achieved by modulation of the wheel speed. A pitch-axis gyro system provided a measure of pitch rate and was used to enhance the damping of the pitch control system. In time the accumulated effects of external pitch disturbance torques caused the wheel speed to drift away from 1500 rpm. When the deviation reached a specified threshold, a magnetic torquing system was turned on to restore the wheel speed to 1500 rpm.

The IR scanner also sensed the roll angle of the satellite. This information was used at four specific points in the satellite orbit to decide whether corrective action was necessary. If the roll angle exceeded a specified threshold (which could be set by command in the range from 0 to 16°), the B-axis magnetic coil was turned on with the correct polarity and strength to precess the roll error to zero. This calculation was done by a new electronic system called the attitude signal processor (ASP). It was a small on-board computer system using the RCA 1802 microprocessor. The ASP was the "brains" of the ACS — it sampled the roll angle and computed the necessary B-coil strength based on the sampled strength of the X and Y magnetic field components and the internal angular momentum as indicated by the wheel speed. In addition, it decided when to initiate momentum dumping, selected the proper polarity, and shut off momentum dumping when the wheel speed reached 1500 rpm.

No direct measurement or control of yaw was made, nor were they necessary. By controlling roll at four points 90° apart in the orbit, the yaw angle was automatically controlled. We relied on the fact that yaw would not change by more than 1 or 2° in the 23 minutes during which the satellite moved from one roll sample point to the next. This de-

pended on an adequate ratio of internal angular momentum to external torque. Being able to ignore yaw permitted a very important simplification in system design. Yaw is difficult to observe directly in a satellite; an inertial reference platform with three-axis gimbals and gyros would be required, with a substantial increase in complexity and cost, and a loss in reliability.

SYSTEM REQUIREMENTS

Four requirements played a major role in determining the design of the attitude control system. These were:

1. Stabilize pitch, roll, and yaw to $\pm 5°$ to orient the star cameras, sun sensor, and solar panels properly;
2. Minimize angular rates and short-term motion (jitter) to avoid boom bending and to ease the analysis of the star camera data;
3. Minimize the demand on the ground station operators for rapid attitude control; and
4. Minimize the amount of magnetic torquing activity because the associated magnetic fields would degrade the fields at the primary scientific data sensors.

SYSTEM DESIGN

A block diagram of the ACS is shown in Fig. 1. Some of these elements are in common with the SAS-3 design described in Ref. 2, namely, the IR scanner wheel, the redundant gyro system, the B-axis coil used for orientation of the B axis, the X and Y coils and X and Y magnetometer and electronics that make up the magnetic spin/despin system, and the passive nutation damper. The ASP and the yaw aerodynamics trim boom are new features for Magsat.

The control of pitch and the control of roll and yaw use quite different and independent schemes. Both schemes are managed and operated by the ASP.

Pitch Control

Maintaining pitch control of the spacecraft is vital to the success of the mission. Loss of control for more than one orbit could prove disastrous; the motion of the spacecraft could cause the B axis to move away from the sun line far enough to reduce the power-generating capability below that required by the critical loads. As a result, five pitch-control modes were designed into the system to be used during different phases of the mission or in failure situations.

The ASP monitored a number of points as a check on the system's ability to make correct control decisions and, upon detecting a malfunction, switched to a safe mode. A microprocessor bypass mode was provided in the event of a microprocessor failure.

Figure 2 is a block diagram of the Magsat pitch control system. There were five modes, four of which were closed loop. Relay position numbers in the diagram correspond to the mode numbers.

Mode 1: IR Scanner Pitch-Bias Mode with Gyro Damping — This was the primary mode of the mission. The IR scanner provided pitch angle feedback, and a gyro simultaneously provided pitch rate feedback for damping purposes. The error in pitch angle was reduced to zero by accelerating or decelerating the momentum wheel. The equilibrium pitch angle could be offset from zero by a command from the ground. This "pitch bias" could be commanded to any angle in the range of -10 to $+10°$. We correctly anticipated that this feature would be useful in seeking a pitch angle that had minimum pitch disturbance torque.

Mode 1 was designed with high damping and minimum bandwidth to provide a slow but smooth pitch response and thereby minimize the pitch jitter motion. The system bandwidth was approximately 0.01 Hz.

Great care was taken in the design to eliminate

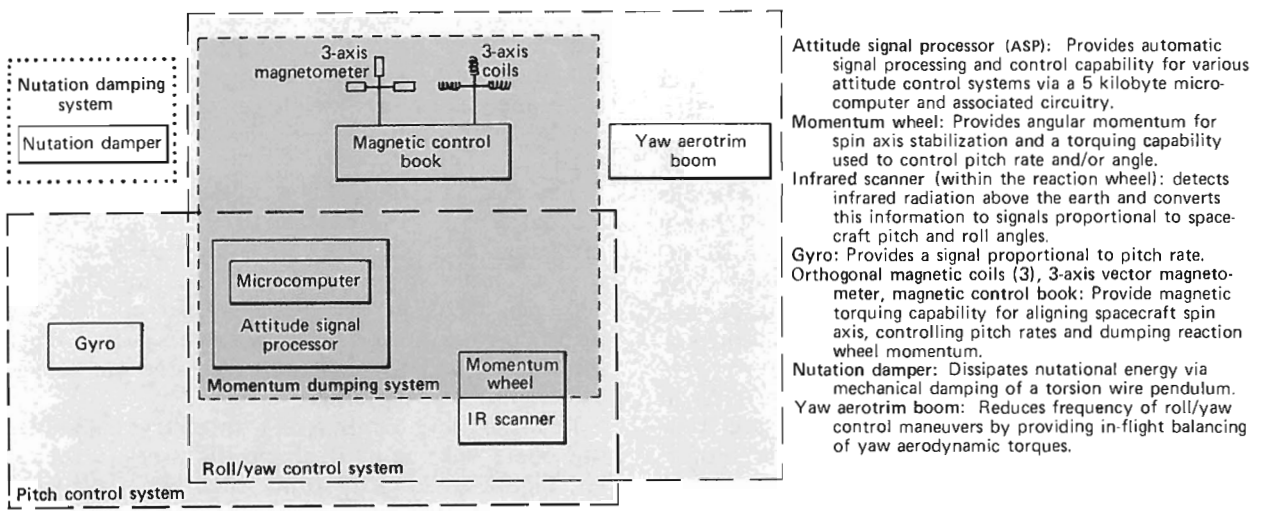

Fig. 1—Block diagram of the Magsat attitude control system.

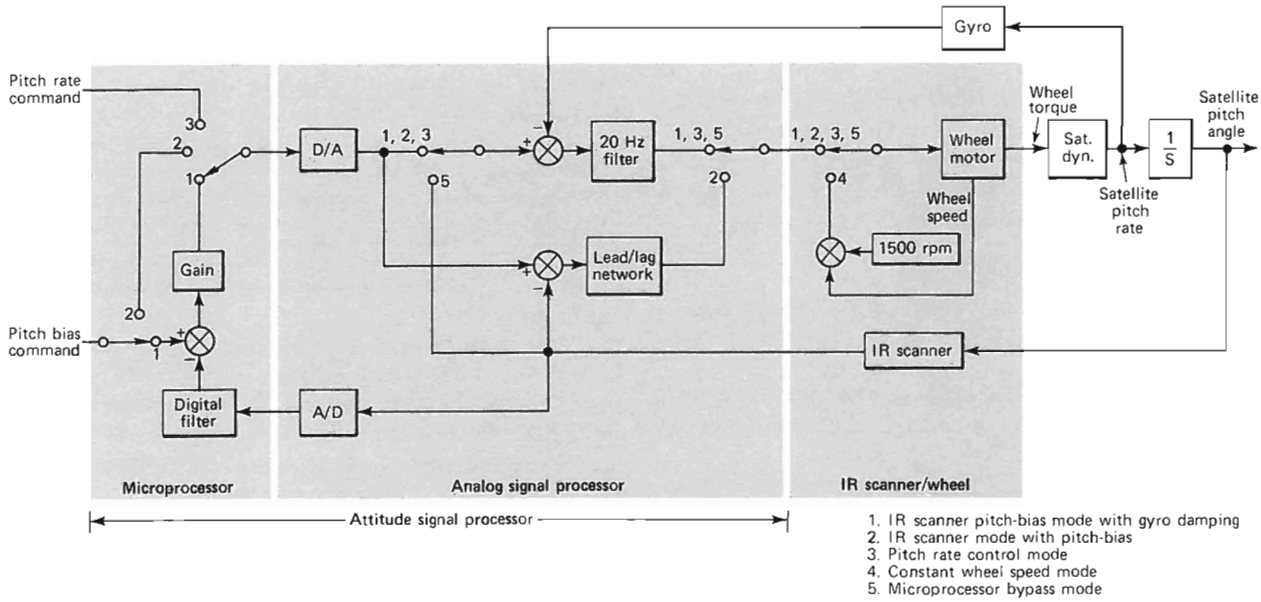

Fig. 2—Block diagram of the Magsat pitch control system.

any internal noise effects on system operation. The pitch voltage, which was noisy due to a differentiating network in the IR scanner, was digitally filtered at 0.02 Hz in the microprocessor. Gyro noise was measured and found to be negligible.

This mode was initiated approximately 24 hours following pitch capture and was intended to continue for the lifetime of the mission.

Mode 2: IR Scanner Mode with Pitch Bias — This was a pitch angle control mode, again with a commandable pitch bias capability to $\pm 10°$. However, the gyro was not required for this mode; it was a backup mode in case of gyro failure.

Mode 3: Pitch Rate Control Mode — In this mode the pitch rate was controlled, rather than the pitch angle. The gyro signal was used as a measure of the actual pitch rate, which was compared with the desired rate (as loaded by command). This mode was intended as a backup mode in case of an IR scanner failure or a roll angle so excessive that the IR scanner did not see the earth. The desired rate was set at 1 revolution per orbit.

Mode 4: Constant Wheel Speed Mode — In this mode the wheel speed was held fixed at 1500 rpm and no control of pitch angle or rate was attempted. The system was operating in this mode during launch and during the initial attitude maneuvers before closed-loop control was established.

Mode 5: Microprocessor Bypass Mode — As in the primary mode, both pitch angle and rate feedback information were provided. However, unlike Mode 1, this mode had no microprocessor interface and therefore no pitch bias capability or 0.02 Hz filtering of the pitch signal. This loop would have been used only in the event of a microprocessor failure and, due to loop gains, would have resulted in a steady state pitch angle of $-0.7°$. All microprocessor control and signal processing functions would have been disabled in this mode. This was the only pitch control mode that was not used during the lifetime of the mission.

Momentum Dumping

Momentum dumping was required to keep the wheel speed in the range where it was capable of producing reaction torque (1100 to 1900 rpm). Wheel speed changes were the result of external disturbance torques acting on the satellite. There were two techniques available to achieve momentum dumping, pitch angle bias and magnetic spin/despin torquing. The pitch angle bias was used to allow aerodynamic, gravity-gradient, and other disturbance torques to offset one another, the accumulated effect being to minimize the overall external pitch torques. The bias angle was determined from analysis by the satellite operators, and a command was sent to the satellite to implement the bias.

The magnetic spin/despin system was used automatically under the control of the attitude signal processor. If the wheel speed deviated from 1500 rpm by more than a predetermined amount, say 200 rpm, the ASP selected the proper polarity and turned on the magnetic spin/despin system. When the wheel speed reached 1500 rpm, the ASP turned off the magnetic torquing.

In order not to interfere with roll/yaw control, this could only be done at specific times in the orbit. Figure 3 shows the orbit track about the earth and the assigned points for various allowed activities by the ASP. Only at points A1 and A8 could

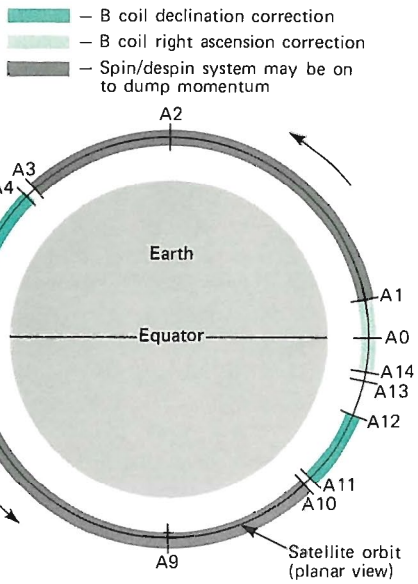

Orbit location	Action
A0	Orbit ascending node
A1, A8	B coil turned OFF after right ascension correction; wheel speed sampled, spin/despin system turned ON if desired and necessary
A2, A9	Roll angle sample for declination correction
A3, A6, A10, A13	Spin/despin system turned OFF to sample magnetometers
A4, A11	B coil turned ON for declination correction if desired and necessary
A5, A12	B coil turned OFF after declination correction
A7, A14	Roll angle sampled and B coil turned ON if desired and necessary for right ascension correction

Fig. 3—Orbit locations of roll/yaw control and momentum dumping events.

momentum dumping be initiated. Momentum dumping had to be completed by A3 or A10, respectively, or it would have been terminated in preparation for possible roll control maneuvers.

The magnetic spin/despin system worked in the following manner: Voltages proportional to the X and Y components of the earth's magnetic field were amplified and used to drive the Y and X coils, respectively. One of the signals was inverted. This produced a net magnetic dipole that led or lagged the earth's field by 90°. The result was a torque about the satellite spin axis, the sense of the torque being determined by the ASP.

Roll/Yaw Control

The roll/yaw control system was designed to maintain nominal alignment of the B axis with the orbit normal. The automatic roll/yaw control mode took advantage of the system's ability to detect both declination and right ascension errors from the roll output of the IR scanner and corrected these errors by using an application of a B-axis magnetic dipole at appropriate places in the orbit.

For example, at equatorial crossings the roll angle provided a measure of the error in right ascension between the B axis and the orbit normal. The earth's magnetic field is oriented north in this region. With knowledge of the roll error, magnetic field strength, and wheel speed, the B coil could be energized at a specific strength and for a specific length of time to precess the B axis in right ascension to correct the error almost exactly. By energizing the B coil for an integral number of nutation periods (150 seconds each), residual nutational motion of the spacecraft was minimized. Two nutation periods were used. This action was initiated at points A7 and A14 (Fig. 3) if the roll angle exceeded a specified threshold value. The torquing was terminated at A8 and A1, respectively.

In a similar manner, spacecraft roll angle at the orbit poles is a measure of the declination error of the B axis from the orbit normal. Energizing the B coil when the earth's magnetic field is nearly parallel to the earth's equatorial plane would precess the B axis in declination and correct the observed error. Figure 3 shows the orbit locations at which the roll angle was sampled (A2 and A9) and the B coil was energized (A4 and A11) if the roll angle exceeded the threshold.

In the interest of minimizing B-coil activity, a threshold on roll error was chosen below which no B-coil activity would occur. This threshold was normally set by command between 1 and 3°.

Computer analysis of the attitude dynamics showed that a significant yaw aerodynamic torque existed because the center of mass of the satellite was offset from the center of frontal area. This yaw torque would have continually perturbed the satellite, requiring frequent control activity. We therefore decided to balance the frontal area by installing a yaw aerodynamic trim boom. It was a motorized boom made up of a silver plated beryllium-copper tube 1.2 cm in diameter that could be extended to any length up to 12 m. Our analysis showed that about 5 m of extension would be required to balance the yaw torques. This boom protruded from the base of the satellite.

Nutation Damping

The primary means of reducing satellite nutational motion during the attitude acquisition phase was the nutation damper. It consisted of a damped pendulum pivoting on a torsion wire. The pendulum's arm swung in a plane normal to the intended spin axis and oscillated when the spacecraft nutated. Damping in the pendulum movement dissipated kinetic energy until all nutation ceased.

The predominant nutation damping mechanism for the mission phase used product-of-inertia coupling between nutational motions and the pitch control loop. Damping in the pitch loop simultaneously damped nutations via the passive coupling. Loop gains and phase shifts were analyzed to assure stability. The nutation period was approxi-

mately 150 seconds, and the damping time constant was 40 minutes.

ATTITUDE SIGNAL PROCESSOR

The attitude signal processor (ASP) coordinated and controlled the activity in the attitude control system. It used the RCA 1802 microprocessor with 4096 bytes[3] of programmable read-only memory (PROM) and 1024 bytes of random-access memory (RAM). The 1802 microprocessor employed a four-level, individually maskable, priority-interrupt scheme. The highest priority interrupt used a direct memory access to enter commands to the ASP directly into the RAM. The computer was synchronized to the telemetry clock by an interrupt generated every half second.

A command of 256 bits was required to initiate the ASP activity. This message contained such information as the orbital period, the time when the satellite would cross the equator north bound, the desired pitch mode, the pitch bias angle, the roll threshold, the desired pitch rate, etc. These data were stored in the RAM and used by the computer as it proceeded through its routine, which was stored in the PROM.

One of the most important features of the microcomputer was its diagnostic capability. The microcomputer performed a "checksum" every half second to verify that its embedded software had remained static. Also it checked for certain "faults" in the IR scanner and the gyro system; if any were detected, appropriate action was taken to change the pitch mode. Discrepancies in the command word were also detected and, depending upon the error, the command was either rejected or corrected. Flags were generated for each fault both in a 128-byte telemetry output and in a special 4-bit status word provided as a warning system for the ground operators.

In the event of a momentary loss of the 5 V power supply, the destruction of each copy of the resident ASP command, or a program sequencing anomaly, the ASP would automatically restart, initializing both the foreground and background portions of the firmware and placing the attitude control system in a safe mode. If the microprocessor had failed completely, a relay driven by the command system would have placed the attitude control system in a microprocessor-bypass pitch control mode and would have disabled all microcomputer control and signal processing capability.

The Magsat ACS was the first microcomputer-based ACS built at APL and quite possibly the first satellite microcomputer that was programmed in a high-level language (MICRO-FORTH). The 1802 microprocessor was chosen for the application because of its low power consumption, its compatibility with other systems on board, and its availability in a high reliability version. The ASP weighed 0.86 kg and consumed 0.95 W of power.

PERFORMANCE IN ORBIT

Initial satellite activity following launch included the yo-yo despin, pitch-axis alignment with the orbit normal, satellite despin using the spin/despin system, and acquisition of closed-loop pitch control. Details of the initial attitude maneuvers are given in the "Magsat Performance Highlights" article in this issue.

The satellite was commanded into the primary pitch control mode on November 1, 1979, and remained almost exclusively in that mode until June 10, 1980, the day before reentry. Attitude transfer system outputs indicated a peak-to-peak pitch oscillation of 1.5 arc-s at 0.6 Hz, well within the design specification.

Momentum dumping operations occurred periodically during the first week of the mission. Pitch angle bias was used very successfully to minimize magnetic momentum dumping for the majority of the mission. However, toward the end of satellite life, magnetic momentum dumping became quite frequent as the aerodynamic disturbance torques increased.

The yaw aerotrim boom was deployed to 4.63 m before the initial satellite maneuvers and subsequently was extended to 6.99 m after the magne-

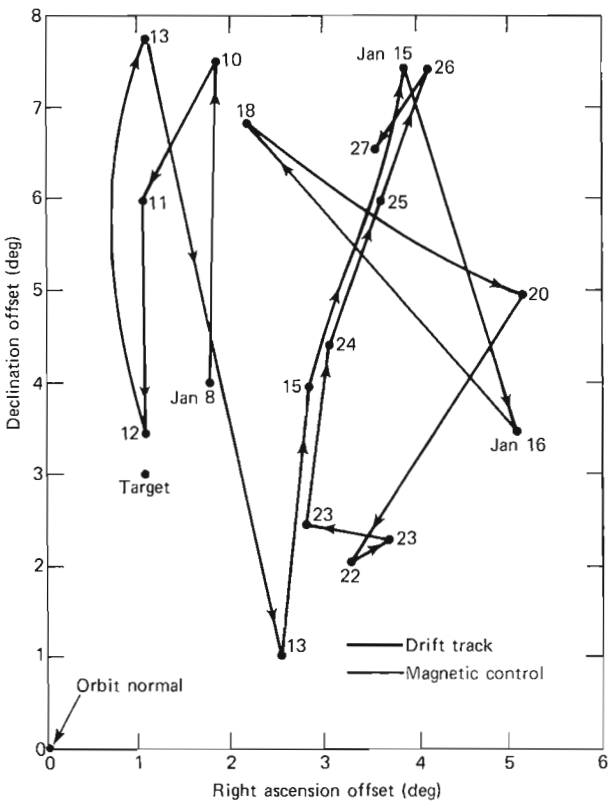

Fig. 4—Magsat attitude activity from January 8 to 27, 1980, showing drift of the +B axis in space. The roll angle had to exceed a threshold of ≈5° (with respect to target position) to initiate roll/yaw control activity. Lack of activity was due to the aerodynamic balancing effect of the yaw trim boom at the skewed target position.

tometer boom extension. Careful observation of the B-axis drift led to the decision to retract the boom to 4.88 m, which resulted in a minimum of B-coil magnetic torquing. Figure 4 shows the B-axis drift over a 17 day period in January 1980, during which only one roll/yaw control maneuver was required.

Nutational motion was reduced from 10 to 0.5° in 12 hours by the mechanical damper prior to magnetometer boom extension and was held to approximately 0.07° peak-to-peak by inertial coupling damping.

The entire ACS performed flawlessly in meeting each of its requirements. It oriented the satellite for optimum power generation and provided minimum aerodynamic torque needed to reduce magnetic torquing operations. In addition, it provided the stable platform needed for arc-second-quality attitude determination solutions and high-resolution magnetic field measurements.

REFERENCES and NOTES

[1]The B axis of Magsat is the same as the Z axis of SAS. The A and C axes are perpendicular to B. The X and Y axes are also perpendicular to B but are rotated 45° from the A and C axes.

[2]F. F. Mobley, P. Konigsberg, and G. H. Fountain, "The SAS-3 Attitude Control System," *APL Tech. Dig.* **14**, No. 3, pp. 16-23 (1975).

[3]A byte is an 8-bit word of data.

ACKNOWLEDGMENT — The authors wish to recognize the special efforts of T. Zaremba, D. Klein, and W. Schneider in designing the software for the ASP.

GLEN H. FOUNTAIN, FREDERICK W. SCHENKEL, THOMAS B. COUGHLIN,
AND CLARENCE A. WINGATE

THE MAGSAT ATTITUDE DETERMINATION SYSTEM

The Magsat mission required knowledge of the magnetic field orientation with respect to a geocentric coordinate system with an accuracy of better than 20 arc-seconds. Attitude sensors were therefore incorporated into the spacecraft. The design, construction, and verification of these sensors as a system became a major task of the spacecraft development.

INTRODUCTION

The Magsat mission requirement for measurements of the earth's magnetic field with an accuracy of 6 nanoteslas (1 nT = 10^{-9} Weber/m^2) root sum square (rss) per vector axis imposed a stringent requirement on the spacecraft's attitude determination system (ADS) of 14.5 arc-s (0.00028°) rss. The major sources of error in making such field measurements were the vector magnetometer, the satellite tracking system, and the ADS. The vector magnetometer measured the magnetic field at a given position in a geocentric coordinate system as determined by the satellite tracking network. The orientation of the field was determined by the spacecraft attitude sensors. Initial estimates of the errors associated with the vector magnetometer and the spacecraft tracking system required the errors caused by attitude measurement to be less than 4.5 nT rss; for the maximum field strength anticipated (i.e., 64,000 nT) the angular error inferred was 14.5 arc-s.

The design, fabrication, and verification of the ADS was one of the major challenges of the Magsat program. It is interesting, as a point of reference, to note that an angular measurement of 1 arc-s is equivalent to measuring the eye of a needle at a distance of 164 meters!

The Magsat ADS, shown schematically in Fig. 1, was a collection of sensors whose required accuracies were a few arc-seconds. These accuracies had to be verified by ground tests where component weight effects and thermal environments differed slightly from the flight conditions. From these measurements the instrument alignment and accuracies in orbit were inferred.

The ability to determine the attitude of satellites has been steadily improving. The Small Astronomy

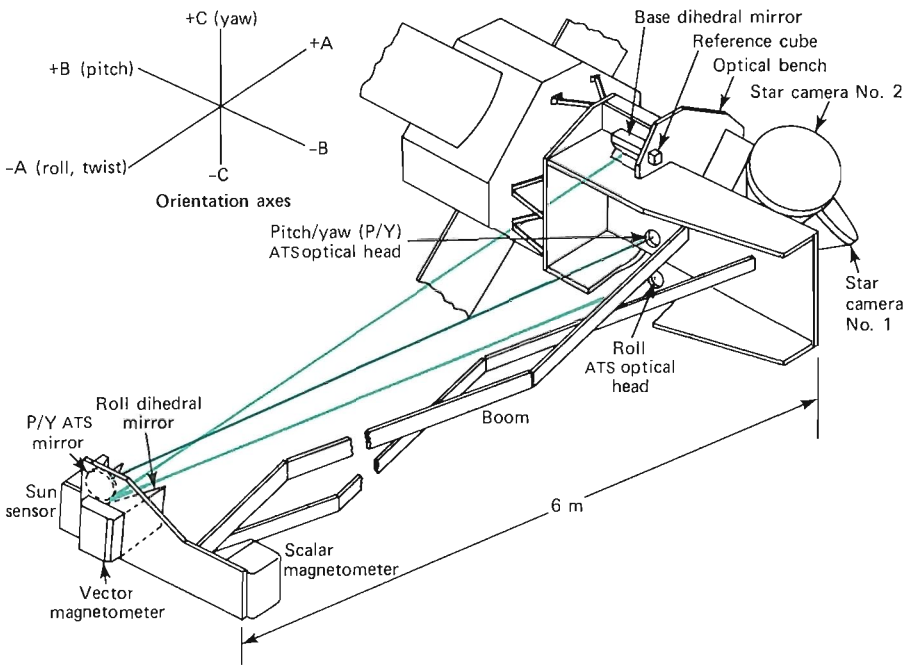

Fig. 1—The attitude determination system consists of two star cameras mounted on an optical bench, which also contains an attitude transfer system for relating the orientation of the star cameras to the vector magnetometer. The sun sensor (and a rate gyro located in the spacecraft) provides additional information to allow interpolation between star sightings.

Satellites SAS-1 and -2 made measurements with accuracies of a few arc-minutes. Large complex satellites such as the Orbiting Astronomical Observatory (OAO) made angular measurements of 1 arc-min. SAS-3 was the first small spacecraft to attempt to make measurements in the sub-arc-minute range, but only after in-flight calibration. It was for that mission that a "strap down" star camera for high accuracy attitude determination was developed. Analysis of the in-orbit performance of SAS-3 indicated that the star cameras had the inherent accuracy to provide primary attitude data for Magsat.[1] However, to meet the entire Magsat attitude requirements, significant changes in the SAS-3 design were required, including better ground calibration, a more stable structure, and additional angular (or rate) sensing to interpolate between star sightings.

The three rotations chosen to describe the angular orientation of the vector magnetometer are roll, pitch, and yaw. As shown in Fig. 1, these rotations are measured about a set of body-fixed axes that would nominally be aligned to the spacecraft velocity vector (roll), the orbit normal (pitch), and the local vertical (yaw). For the sun-synchronous orbit chosen for Magsat, the pitch (B) axis also pointed in the general direction of the sun. For each of these axes, a detailed error budget was determined. The error budget established in November 1977 for each axis had the form shown in Table 1.

Table 1

ERROR BUDGET FOR VECTOR MAGNETIC FIELD MEASUREMENT

	arc-s		*nT*
Vector magnetometer			3.8
Attitude determination			
Star camera	11		
Attitude transfer system	5		
Optical bench	4		
Subtotal (rss)	13	→	4.1
Satellite position error			1.7
Total error (rss)			5.8

STAR CAMERAS

The two star cameras that provide the primary attitude determination data were built by the Ball Brothers Research Corp., based on the SAS-3 star camera design. Each camera consisted of a Super-Farron objective lens that focused an 8 by 8° star field onto the photocathode of an image-dissector tube. The image dissector consisted of a photomultiplier with a small aperture in front of the first dynode and a gradient-free drift space between the aperture and the photocathode on which the optical image was focused. Deflection coils steered electrons from a given portion of the photocathode surface through the aperture. By programming the deflection current the entire area of the photocathode was scanned for the presence of star images. Figure 2 shows the scanning pattern for the Magsat cameras.

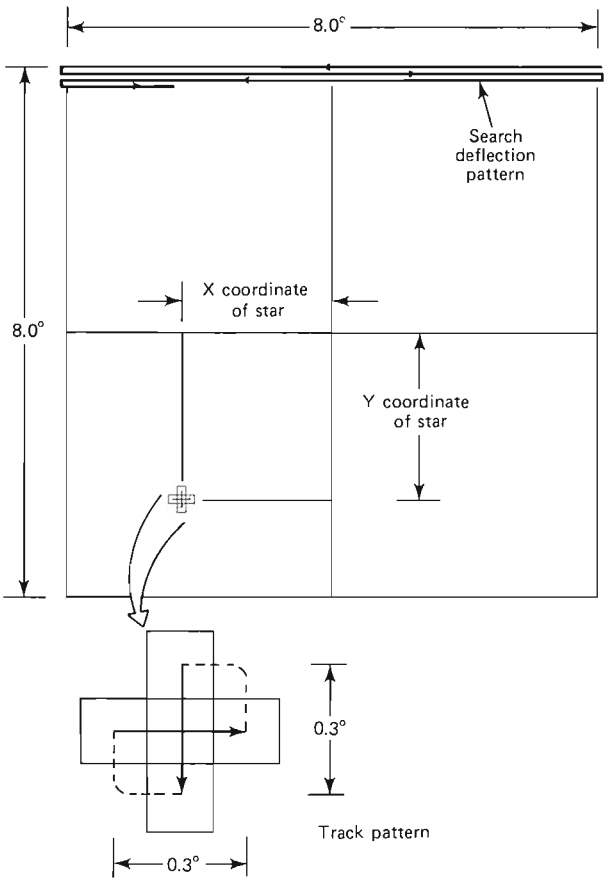

Fig. 2—When searching for a star, the camera field is searched in a left-to-right, right-to-left pattern. If an illuminated area is detected during the scan pattern, the camera will automatically initiate a small cruciform scan about the center of the illuminated area. If the illuminated area moves in the field of view, the camera automatically recenters the cruciform scan and tracks it. The deflection coil currents required to keep the aperture centered on the illuminated spot are direct measures of the star coordinates.

The cameras were designed to detect stars as dim as 6.0 visual magnitude with a probability of 0.98. In fact the cameras were typically tracking stars as dim as 7.2 visual magnitude. This guaranteed that several detectable stars were in the camera's field of view at all times.

The cameras were mounted on the spacecraft in such a way that both swept the same circle on the celestial sphere while the spacecraft rotated at one revolution per orbit. This circle was 32° off a great circle to minimize the effect of both sun and earth albedo interference. As each camera swept out its circle, the stars appearing in its field of view were tracked for a specific time. The tracking time was commandable between 4 and 128 s; for Magsat a time of 30 s was selected. After the 30 s period (or loss of track caused by the star falling outside the

camera's field of view), the camera was commanded to break lock and search for another star. In this manner a "snapshot" of stars was located in the camera field of view.

Like most real devices the camera outputs were not truly linear or independent. As a result there were variations from an idealized linear response of several arc-minutes. The camera's ultimate accuracy was achieved by calibrating these effects during ground tests and removing them during post-flight data processing. Each observed position, once these effects were removed, was accurate to 10 arc-s or better with respect to the camera optical axis.

ATTITUDE TRANSFER SYSTEM

The transfer of each observed star position to the vector magnetometer depended on the accuracy of the attitude transfer system (ATS). The system, built by the Barnes Engineering Corp., measured the relative orientation of the vector magnetometer with respect to the star cameras via two optical systems that measured the rotational angles of pitch, yaw, and roll. Both optical systems used a 125 Hz, 50% duty cycle, modulated infrared beam at 930 nanometers to perform the optical measurement. This allowed both optical filtering and a synchronous detection scheme to eliminate effects of interfering light sources such as sun or earth albedo.

The simplest system was one that measured the pitch and yaw angles of the vector magnetometer with respect to the optical bench. The pitch/yaw transceiver generated at the transceiver exit pupil a 1.8 cm square beam that was reflected by the flat mirror mounted on the vector magnetometer platform. The return beam formed a square image in the focal plane of the transceiver 0.03 cm on a side. When perfectly collimated, the image was centered on two split detectors as is shown in Fig. 3. Pitch or yaw rotations of the vector magnetometer platform produced displacements of the image. The two detectors were oriented so that, to first order, the pitch sensor was insensitive to yaw motion and the yaw sensor was insensitive to pitch motion. A 1 arc-s rotation in either pitch or yaw produced displacement of the image on the order of 1.3×10^{-4} cm, which generated an output in the appropriate split detector. The maximum angular rotation, allowed to keep the pitch/yaw system within its linear region, was ±3 arc-min. A second constraint on the pitch/yaw system was the allowable translation of the vector magnetometer. If the flat mirror translated more than ±1.9 cm, the collimated beam would be vignetted or possibly not returned to the pitch/yaw transceiver.

The roll system was much more complicated. It was, in essence, trying to measure the rotation (twist) about the line of sight of the optical system. The measurement was made by generating an off-axis collimated beam that produced a pseudo-yaw signal as a function of roll rotations. The roll optical system is illustrated in Fig. 4. A transceiver was located on the optical bench but was displaced from the roll axis. The collimated signal was transmitted to a dihedral mirror on the magnetometer platform that reflected the beam to a second dihedral mirror on the optical bench. From this base dihedral mirror the beam was reflected back on itself to the transceiver.

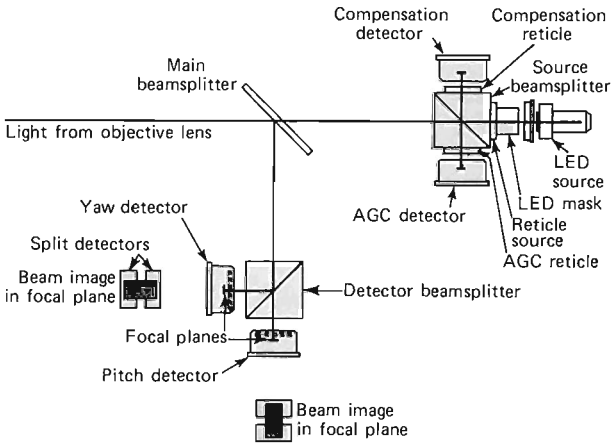

Fig. 3—The light-emitting diode (LED) of the attitude transfer system generates an infrared signal that is formed into a square image by the LED mask at the focal plane of the objective lens. The source beamsplitter diverts a small amount of the transmitted and received energy to the compensation and automatic gain control detectors, which stabilize the sensor performance. The majority of the returned signal is diverted to the pitch and yaw detectors by the detector beamsplitters. There the image formed by the LED mask is focused on the two silicon cells in each detector. Yaw motion causes the beam image to move along the horizontal axis of each detector, producing a change in the differential output of the yaw detector while leaving the output of the pitch detector unchanged. Pitch motion causes the image to move along the vertical axis of the detector, producing change in the output of the pitch detector.

In its simplest form the dihedral mirror on the magnetometer platform can be thought of as reflecting the transmitted image onto a circle whose radius is defined by how far the transceiver is off the roll axis. As the magnetometer dihedral mirror rotates, the transmitted image moves around the circle, producing a pseudo-yaw motion. In fact, the two dihedral mirrors could be flat mirrors tilted at the appropriate angles and produce the same result, but both pitch and yaw motion of the magnetometer would corrupt the roll measurement. The dihedral mirrors are insensitive to rotations about the ridge line. Thus the dihedral mirror on the magnetometer platform effectively decoupled yaw from the roll measurement and the decoupled pitch motion of the base dihedral mirror.

The transmitted roll image was focused onto another split detector in the transceiver that detected the pseudo-yaw motion. In this case, how-

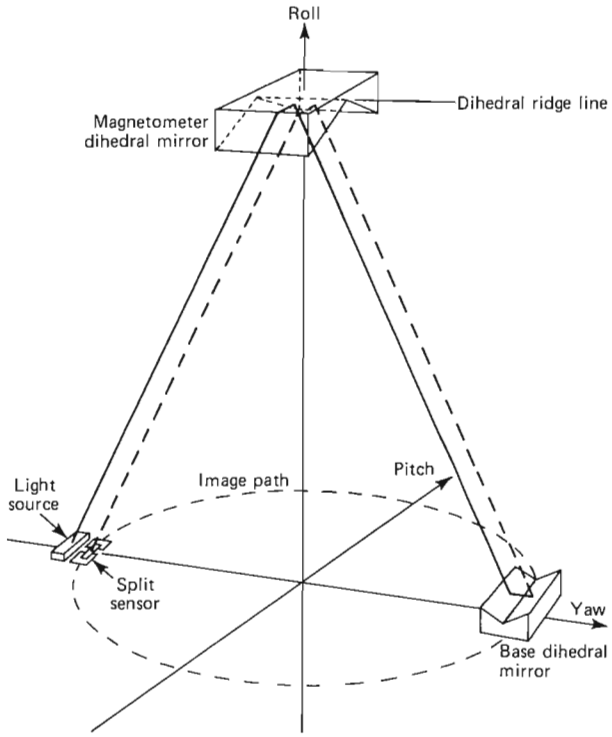

Fig. 4—The roll system transceiver generates a collimated beam that is reflected by the magnetometer dihedral mirror. As the dihedral mirror rotates about the roll axis, the reflected beam traces out a circle in the pitch/yaw plane. The base dihedral mirror causes the reflected beam to be returned to the transceiver when the magnetometer dihedral ridge line lies in the roll/yaw plane. For small roll rotations, the returned image is translated parallel to the pitch axis (as a yaw rotation would produce in an autocollimator), which is measured by the split detector.

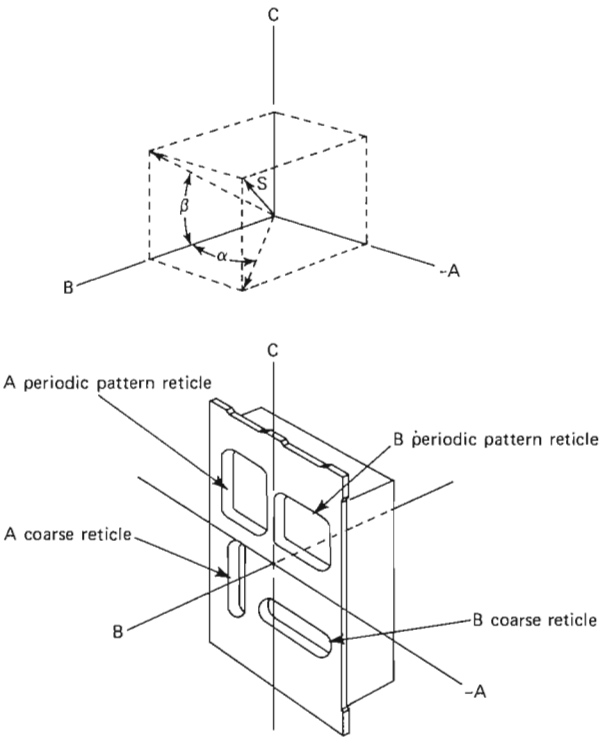

Fig. 5—The precision sun sensor resolves the orientation of the sun line into two angles (α and β) in the sensor coordinate system by means of the A and B reticle assemblies. The periodic patterns determine the α and β angles with a precision of 2 arc-s in a 2.2° repeating pattern. The coarse reticles determine which one of the 2.2° segments (in the 32° field of view) actually contains the sun line.

ever, the pseudo-yaw motion for a 1 arc-s roll rotation was only 1×10^{-5} cm. In addition, because the roll rotation appeared as a yaw motion, actual yaw rotations between the transceiver and the base dihedral mirror appeared as roll motion and, unfortunately, at an even more sensitive level than the true roll rotation. This put a very stringent requirement on the Magsat optical bench and required the rotation about the line connecting the transceiver and the base dihedral (yaw) in the plane of the bench to be less than 0.2 arc-s if such motion was to affect the roll measurement by less than 2.5 arc-s. This effect was noted during ground calibration of the roll system. Measurements taken with the spacecraft in two configurations that reversed gravity-induced distortion in the optical bench produced significant changes in the roll output. This 1 g bias was removed by the roll system calibration.

PRECISION SUN SENSOR

The precision sun sensor (see Figs. 5 and 6), manufactured by the Adcole Corp., was the only primary attitude sensor that was sufficiently clean

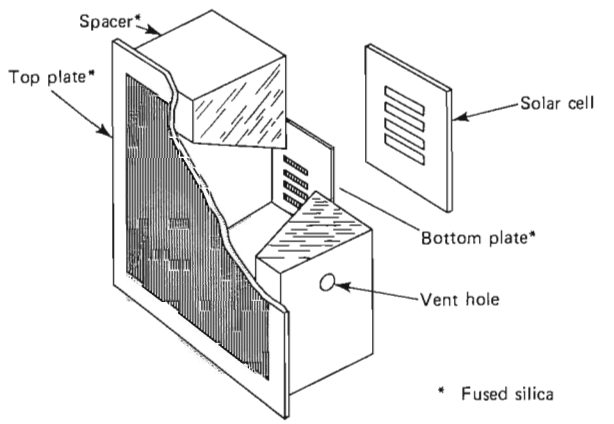

Fig. 6—The periodic pattern reticle assemblies consist of two thin, fused, silica plates separated by a fused silica spacer. Four photocells are located beneath the bottom plate. A periodic grating deposited on the lower surface of the top plate has equal-width lines and spaces with a grating period *w*. The bottom plate has four identical periodic patterns deposited on the upper sun-facing surface, with the same grating period as the upper plate. However, each of these four lower patterns is displaced by one-quarter of the grating period. When combined, these four periodic patterns form a 4-phase filter for light reaching the photocells beneath the four patterns.

magnetically to be mounted near the vector magnetometer. The sensor optical system resolved the angle between the sun line and a sensor coordinate system into two angles with a resolution of better than 2 arc-s and an accuracy of 12 arc-s root mean square (rms) based on preflight calibration. The sensor optics contained two reticle assemblies for each angle measurement. Each assembly consisted of one periodic pattern reticle and one coarse angle reticle. The periodic pattern reticle provided angular information with 2 arc-s resolution over repeated angular periods of 2.2°. The coarse angle reticle determined which of the periodic patterns the sun line was in over a range of ±32°.

The periodic pattern reticle acted as a 4-phase filter for the incident sunlight with a spatial distribution of intensity. The position of the intensity distribution, and consequently the amount of light transmitted by the 4-phase grating to the photocells, was a function of the sun angle. As the sun angle moved in the plane perpendicular to the grating lines, the output of each of the 4 photocells varied sinusoidally with a period of 2.2° and with each cell in phase quadrature. The sensor electronics converted the photocell outputs to digital data.

By combining the periodic pattern reticle outputs with the coarse pattern reticle outputs, which unambiguously determine the angles α and β with a resolution of 1°, the sun angle could be determined with a resolution of 2 arc-s.

Like most other highly accurate sensors, small imperfections in the system created nonlinearities in the actual sensor output. For the sun sensor, these nonlinearities were caused by a number of factors such as the flatness of the grating substrates, the photocell spectral response, the skew (misalignment) between the input and output gratings, and the thickness of the grating patterns. Analysis by the Adcole Corp. resulted in a transfer function dependent on higher order harmonics of the fine reticle period that reduced the errors to the level of 12 arc-s rms.

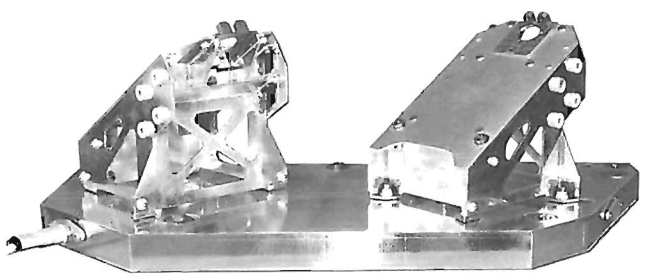

Fig. 7—The Magsat optical bench shown here was fabricated by the Convair Division of General Dynamics. The inclined planes on the top surface hold the star cameras. The ATS components are mounted on the underneath side as illustrated in Fig. 1. The silver-like surface of the structure is the aluminum moisture barrier.

OPTICAL BENCH REQUIREMENTS

For the ADS to function, the attitude sensors had to be connected by means of extremely stable structures. The spacecraft optical bench (Fig. 7) and the magnetometer platform were designed and built to hold the alignment of the system elements mounted on them to deflections of 1 to 2 arc-s during orbital operations. In addition, they could suffer no alignment changes during the launch and prestabilization phases of the mission. Severe weight constraints, in conjunction with the thermal, structural, and magnetic requirements, led to the choice of graphite-fiber reinforced epoxy (GFRE) for the construction of both structures. Active temperature control was necessary to meet thermal deflection objectives. The optical bench was attached to the spacecraft by means of a kinematic mounting arrangement to prevent significant deflection caused by spacecraft bending.

The selected material was superior to the other materials (such as aluminum or beryllium) in strength and stiffness ratios and in coefficient of thermal expansion, and it is not magnetic. It has some unique properties that require special care but are tractable. GFRE consists of graphite fibers lying in a single plane, held together by resin. The desirable properties of GFRE exist only in the fiber plane. Normal to the plane, the thermal properties of GFRE degrade, approaching those of epoxy. By using an egg crate construction technique degradation of the anisotropic properties was reduced.

Another factor considered was hygroscopicity. Strains caused by water absorption by GFRE during satellite construction and testing can approach 100 μm/m and can produce deformations far exceeding those caused by thermal sources. Critical alignments of bench-mounted components, performed when the bench had a high moisture content, were likely to change in orbit as the moisture was released in vacuum. This undesirable property was reduced to tolerable levels by the application of a moisture barrier to the external surfaces of the optical bench. The moisture barrier consisted of 0.017 mm aluminum foil bonded to the GFRE.

A comparison of the critical alignment goals and the expected thermal deflections of the satellite structure when in orbit indicated that the bench should be attached to the structure in a manner that would not introduce bench bending. This analysis led to a kinematic arrangement for attaching the bench to the spacecraft. Of the three attachments, one restricted all three translational degrees of freedom and the other two restricted the three rotational degrees of freedom without introducing additional translational constraints.

Even with the use of GFRE, the requirement for temperature control was reasonably stringent. For the optical bench, which was 3.8 cm thick and had a maximum separation between any two components of 66 cm, a temperature gradient through the

bench of 0.5°C would produce a deflection of 1 arc-s. In addition to controlling the bench temperature, it was necessary to maintain each of the bench-mounted components at a constant temperature. The basic approach taken was to prevent large temperature gradients by minimizing heat flow within the bench. The bench was first enclosed in its own multilayer thermal blanket within the spacecraft to reduce heat transfer by radiation to its surroundings. Second, the five components and three mounting points that must penetrate the blanket were heated to 25.0 ± 0.2°C. Third, thermal connections between the bench and the heater-controlled surfaces had relatively high thermal resistance.

The three spacecraft attachment fittings were designed to minimize heat flow between the bench and the spacecraft structure by controlling the temperature to 25°C through the use of thermostatically controlled heaters. Thermal resistance introduced between the bench and the spacecraft reduced the required heater power substantially. Also, in those few cases when the temperature of the structure was greater than 25°C, the heat flow into the bench was limited by the resistance.

Because the optical components (i.e., the two ATS optical heads, the base dihedral mirror, and the two star cameras) have direct heat leaks to space, they had to be directly controlled to the desired temperature. In addition, they had to be mounted so that precise alignment was maintained through all mission phases. Thus titanium, a material with low thermal conductivity, was used for the joints between the bench and each component. A heater placed directly on the bottom of each component served the dual function of preventing heat flow from the bench and controlling the component's temperature. This design resulted in a bench with minimal thermal gradients through and across the bench. Post-launch data show that gradients were less than 0.1°C.

SYSTEM VERIFICATION AND PERFORMANCE

The Magsat attitude determination system was a composite of individual units that had to be assembled into a calibrated system. Each of the sensors was tested and calibrated by its manufacturer to various levels depending on the manufacturer's facilities and the ability of that particular component to operate without assembly into the spacecraft. Verification of the primary attitude system was performed at the Calibration, Integration, and Alignment Facility at the NASA/Goddard Space Flight Center. Tests were performed to determine the alignments of the star cameras and the ATS components to an optical reference mounted on the spacecraft optical bench. The star camera calibration algorithms generated by the Massachusetts Institute of Technology's Center for Space Research, based on the calibration data furnished by the Ball Brothers Research Corp., were verified. The calibration of the ATS system related the sensor outputs to the angular relationships between the spacecraft optical bench reference cube and a reference cube on the vector magnetometer (see Fig. 1). The alignments between the precision sun sensor and the vector magnetometer were also measured at this time, but no verification of the Adcole calibration of the sun sensor was performed.

The flexure induced in the bench by the weight of the components was measured by making all alignment measurements with the spacecraft B axis both up and down (i.e., ±1 g). The measurements indicated that star camera No. 1 moved 9 arc-s and star camera No. 2 moved 30 arc-s because of weight reversal. The ATS pitch/yaw system moved less than 3 arc-s, but the roll system changed by 70 arc-s because of the sensitivity of the roll output to yaw rotation between the roll transceiver and the base dihedral mirror. Changes of 10 arc-s in the sun sensor alignment were measured when the vector magnetometer plate assembly was flipped to reverse the weight loading. The final calibration of the system used these measured changes to determine the relative alignments when in space. The weight loading effect was removed by averaging the difference in alignment in the ±1 g cases.

A second set of alignment measurements was made after the spacecraft had been exposed to environmental testing. Residual changes caused by environmental stress were less than 3 arc-s for the ATS and star camera No. 2. Changes in star camera No. 1 were slightly larger, reaching 10 arc-s.

The data from the various attitude sensors were used as inputs to a computer program developed by the Computer Sciences Corp., that generated three-axis attitude information at 0.25 s intervals.[2] The program computed the attitude for each 0.25 s interval based on the sensor data available. If both cameras were tracking identified stars, the magnetometer orientation was computed using the two star sightings and ATS data. If only one star camera was tracking an identified star, the second vector required for an attitude solution was derived from the sun sensor data. If neither star camera was tracking an identified star, a motion model was used to interpolate between valid star tracks. This motion model determined the right ascension and declination of the B axis from sun sensor data and the rotation (pitch) about the B axis by integrating the output of the pitch axis gyro.

The attitude determination program was capable of making certain self-consistency checks to ascertain the validity of the data and the stability of the system throughout the mission. One major check was the determination of biases in the system from data sets in which all three sensors generated valid data simultaneously. These bias determinations, computed from data taken early in the mission, in-

dicated that the two star cameras were within 6 arc-s of the prelaunch alignment measurements. Differences between the attitude as computed by the star cameras, the ATS, and the sun sensor were larger than expected (based on ground testing). Since the star camera alignment did not appear to have changed, the discrepancy appeared to lie either in the ATS or the sun sensor. Further analysis, using a least squares fit of the observed magnetic field data, determined the distribution of the error. The best fit of the data to a model of the earth's field indicated that the major discrepancy of 200 arc-s in roll was due to the ATS (i.e., the precision sun sensor measures the roll angle correctly). Likewise, a smaller yaw discrepancy of 55 arc-s was associated with the sun sensor. The sources of these errors in the individual instruments have not been determined.

In time, the input of each sensor varied over a large portion of its range; i.e., the sun moved in a circle about the B axis during each orbit of the spacecraft, the ATS angles varied, and many stars were tracked over the entire field of view. During such a period of time, variation in the difference between a reference vector (determined by star camera No. 2, the ATS, and the sun sensor) and the same vector determined solely by star camera No. 1 was computed to be 5 arc-s root mean square (rms).[3] This variation was a measure of the system noise and the ability of all sensor transfer functions to remove the system nonlinearities.

Computations of system biases were performed several times during the mission life. Variations in system alignments were small, but with some drift that was correlated with temperature changes. A failure of the heater on one of the star cameras in December 1979 caused a shift of 6 arc-s. The data set of attitude measurements for the Magsat mission has good internal consistency and, with resolution of the observed bias, the system has an absolute accuracy of 20 arc-s rms.

REFERENCES

[1]R. L. Cleavinger and W. F. Mayer, "Attitude Determination Sensor for Explorer 53." AIAA Paper 76-114, *Proc. 14th Aerospace Science Meeting* (1976).

[2]D. M. Gottlieb *et al.*, *MAGSAT Fine Aspect Baseline System Overview and Analysis,* Computer Science Corp. Document CSC SD-78-6067 (1978).

[3]F. Van Landingham, personal communications (March 1980).

JAMES F. SMOLA

THE MAGSAT MAGNETOMETER BOOM SYSTEM

The boom connecting the sensor platform with the Magsat spacecraft provided position and tilt adjusting capabilities for the remote mirrors referenced to the vector magnetometer. Once set in orbit, the mirror positions were to be maintained passively. Only vanishingly small angular deviations caused by thermally and dynamically induced structural distortions were permissible, which made the design and test problems extremely difficult.

INTRODUCTION

The need for a simple, extendable, lightweight, precisely alignable, virtually distortion-free structure for Magsat, capable of overcoming the stiffness of sizable multiconductor electrical cabling, presented a most difficult design requirement. The critical requirement was the need to position with precision magnetically sensitive instruments at a considerable distance from sources of magnetic contamination in the spacecraft. The problem was particularly acute because the magnetometer sensors were designed to measure a 60,000 nanotesla (1 nT = 10^{-9} weber per square meter) magnetic field with a precision of ± 1 nT.

Very precise knowledge of the vector magnetometer sensor's angular orientation was important. Because of the extremely narrow bandwidth of the attitude transfer system (ATS), which measured the angular orientation of the magnetometer, special precautions were taken to control thermal distortions, mechanical misalignments, and dimensional instabilities in the design of the structural system that supported the sensors and separated them from the spacecraft instrument section.

SYSTEM DESCRIPTION

The magnetometer boom system consisted of a 14-link scissors boom, a 3-axis gimbal, and the sensor platform (see Fig. 1). The platform was connected to the instrument module electrically with multiconductor cabling that was routed through the interior of each boom link. Two independent, pyrotechnically actuated caging systems were used during launch to contain and protect the boom and platform in their stowed configurations. The 3-axis gimbal located at the boom base provided the boom with pitch, yaw, and roll capabilities of ± 2,

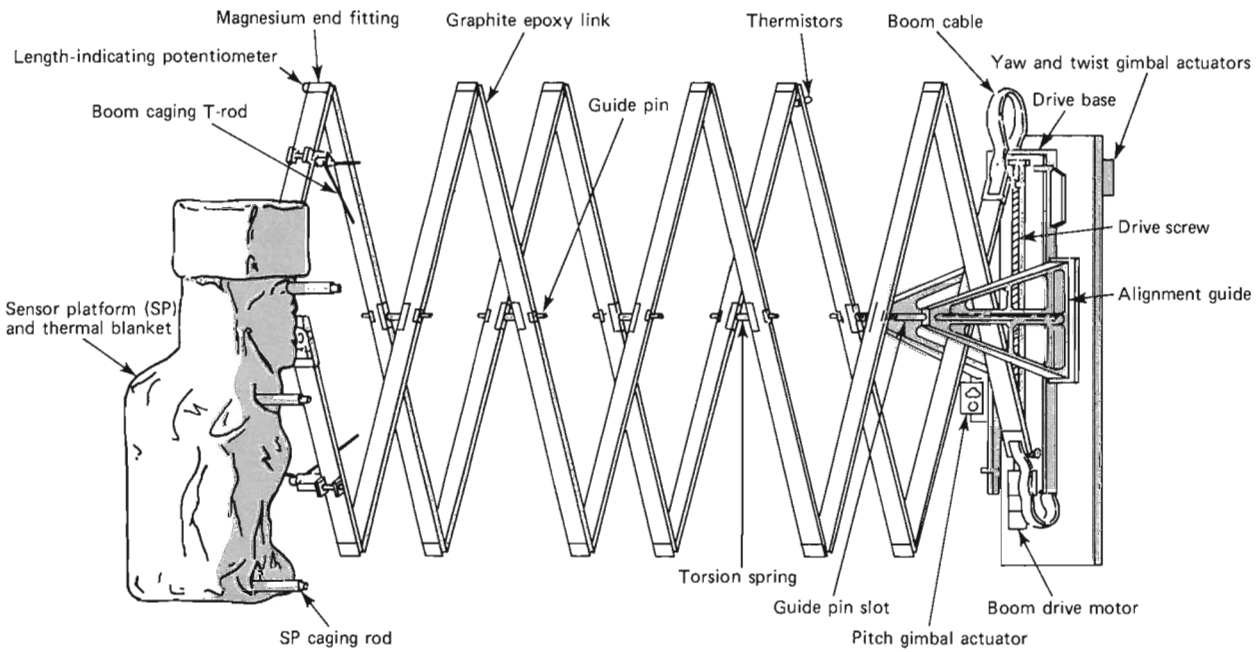

Fig. 1—Magnetometer boom system (partially extended).

±2, and ±5°, respectively, for acquisition of the ATS. The drivers for each gimbal actuator, consisting of a 491-Hz square-wave inverter powering two phase-synchronous hysteresis gear motors coupled to gearboxes, provided average pitch, yaw, and roll scan rates of 30 arc-s/s . A pair of tension springs attached to the drive base and the instrument module structure eliminated all unrestrained play in the gimbal actuator adjusting screws. Rotary potentiometers geared to the output shafts of each of these gearboxes were calibrated to give the angular orientation of the drive base.

The boom drive consisted of a right- and a left-handed ball screw that was rotated by a fourth, inverter-driven, synchronous hysteresis gear motor. A rotary potentiometer geared to the output shaft of the gearbox was calibrated to indicate boom length during deployment. Confirmation of total extension was given by a second potentiometer made of nonmagnetic materials and pinned to one of the boom hinges closest to the platform. Total deployment time was about 20 minutes.

Weight and thermal distortion dictated the use of graphite-epoxy material for the boom links. The basic link was 94 cm long and 1.07 × 5.08 cm in cross section. Magnesium fittings were fastened to the ends and the center of each link with semirigid epoxy to prevent interface cracking caused by differential expansion. Each link was a hollow box with a 0.076 cm thick wall and was covered internally and externally with an aluminum foil moisture barrier to control moisture absorption and desorption — sources of dimensional instability — in the inherently hygroscopic graphite epoxy. A final wrapping of aluminized Kapton coated with aluminum oxide was added for temperature control. The links were hinged to each other with pins that were forced through compliant undersized bushings. This permitted rotation but eliminated all unrestrained mechanical side play.

The aluminum-foiled, graphite-epoxy platform was attached to the tip of the boom through a hollow graphite-epoxy box-like spacer and a "figure-eight" mechanism that enabled the platform to translate while maintaining its attitude normal to the boom axis as the boom extended. Attached to the platform with a kinematic suspension was the temperature-controlled vector magnetometer base, which in turn had attached to it the vector magnetometer sensor, the remote plane and dihedral ATS mirrors, and a precision sun sensor. The kinematic suspension provided a compliant mount for the magnetometer base and isolated it from thermally induced structural distortions that would be detrimental to the alignment of the vector magnetometer and the remote mirrors. The scalar magnetometer was attached to a 1.27 cm thick epoxy-glass thermal isolator that was fastened to the side of the graphite-epoxy spacer.

The weight breakdown for the boom system is shown in Table 1.

Table 1

WEIGHTS OF BOOM SYSTEM COMPONENTS (kg)

Link structure	2.72	
Drive assembly	2.93	
Gimbal actuators (3)	3.09	
Caging subsystems	1.13	
		9.87
Inverters (2)	0.62	
Electrical subsystem	0.76	
		1.38
Sensor platform assembly	7.03	
Boom cable	2.72	
		9.75
Total weight		21.00

OPERATIONAL REQUIREMENTS

Magnetic contamination of the magnetometer sensors was avoided by locating the star cameras (which were magnetic) on an optical bench in the spacecraft instrument module. (Since the potential for magnetic contamination of the sensors was so great, the urge to locate the cameras on the sensor platform was dispelled well in advance of any serious design effort.) On command, the boom was to uncage and displace the sensor platform 6 m away from the instrument module. To satisfy requirements imposed by the ATS, which measured the vector magnetometer tilt relative to the star cameras, the boom was to maintain the platform position so that the center of a plane mirror, precisely attached to the backside of the vector magnetometer sensor, remained within a ±1.91 cm square target zone. This zone was centered on the axis defined by an infrared light beam emanating from an ATS optical head located in the instrument module. The plane mirror had to remain orthogonal to the optical axis within 3 arc-min; this turned out to be the greatest challenge.

AREAS OF MAJOR CONCERN

Although the precision scissors boom was a flight-proven concept, the remote, precisely aligned platform was not. Concern over magnetic interference disallowed electrically powered adjusting mechanisms at the platform end. Consequently, tilt adjustments could only be achieved by gimballing the boom at its base, which would cause the platform to translate. This side effect, coupled with the narrow field of view of the ATS, severely limited the tilt adjusting capability. For this reason considerable engineering analysis and testing were necessary to demonstrate that the Scout launch environment, uncaging, deployment, thermal distortions, and attitude control disturbances would not compromise the ability to achieve the precise alignments that were required.

The following three major areas of concern received considerable attention.

Control of Thermal Distortion

The requirement was to limit initial boom thermal distortions caused by broadside solar illumination sufficiently to permit acquisition of the ATS remote mirrors by gimballing the boom at its base. Although the gimbals were adjustable ±2° in pitch and yaw and ±5° in roll, any tilting of the boom at its base would translate as well as rotate the remote mirrors. Since the target zone was ±1.91 cm square, any mirror tilting that was necessary for acquistion had to be achieved within 0.33° once the mirrors entered the target zone. This made the initial tilt angle of the mirrors and direction of tilt extremely important. If, for instance, the mirrors were perfectly centered within the target zone initially, acquisition would have to be achieved within 0.16° or 9.6 arc-min of angular displacement.

The ±3 arc-min requirement on mirror angle limited the permissible transverse offset of boom tip position to ±0.51 cm for simple mechanical misalignment and ±0.25 cm for misalignments caused by thermal distortion. It was important for the system to be free of play and for the boom elements to be made of some material that is virtually immune to thermal distortion. (Active temperature control was ruled out because of the complexity required for implementation and lack of sufficient electrical power.) Graphite fiber-reinforced plastic (graphite epoxy) with a coefficient of thermal expansion of very nearly zero ($+0.34 \times 10^{-6}$/°C) was chosen to cope with the thermal distortion problem.

To control boom-link temperatures and temperature gradients in the presence of the solar and earth infrared environments, each link was taped with aluminized Kapton coated with aluminum oxide. This thermal covering was selected to give link equilibrium temperatures close to 25°C where all mechanical alignments would be checked.

Thermal distortion tests conducted in the Goddard Space Flight Center simulator on a four-link version of the flight boom yielded favorable results and indicated that the transverse and angular displacements of the platform caused by boom thermal distortion would be well within the allowable range.

Uncaging, Separation, and Extension

Two independent caging systems were provided to contain the boom during launch and to prevent the 7 kg sensor platform from transmitting damaging loads into the relatively delicate boom structure. Both were actuated by pyrotechnic piston-type actuators. Because the boom system was stowed in an unheated external compartment, boom-link and cable temperatures as low as −70°C were expected. Resistive heaters attached to the boom drive base were to provide 16 W of power to warm the boom cable and drive just prior to platform separation and boom extension. Torsion springs located at each boom-link pivot were designed to overcome cold-cable stiffness as well as hinge frictional resistance. The existence of many single-point failure mechanisms in this area of concern resulted in a considerable amount of cold temperature testing to demonstrate and guarantee system integrity.

Pre-Launch Mechanical Alignments

To bring the remote mirrors mounted on the sensor platform into the fields of view of the ATS pitch/yaw and roll optical heads and then into linear range by fine adjustment, a terrestrial test that negated the 1 g bias had to be contrived. The best proposal utilized a pair of 6.1 m long water troughs (Fig. 2). Specially designed floats with gimballed pulleys were attached to each of the boom-link pivots. The idea was to simulate a zero-g condition in a plane parallel to the plane of the water. Remote mirror transverse or angular offsets could then be corrected by gimballing the boom at its base or introducing shims at the platform interface. The boom system was installed in a special fixture that was attached to a rotary table, the purpose of

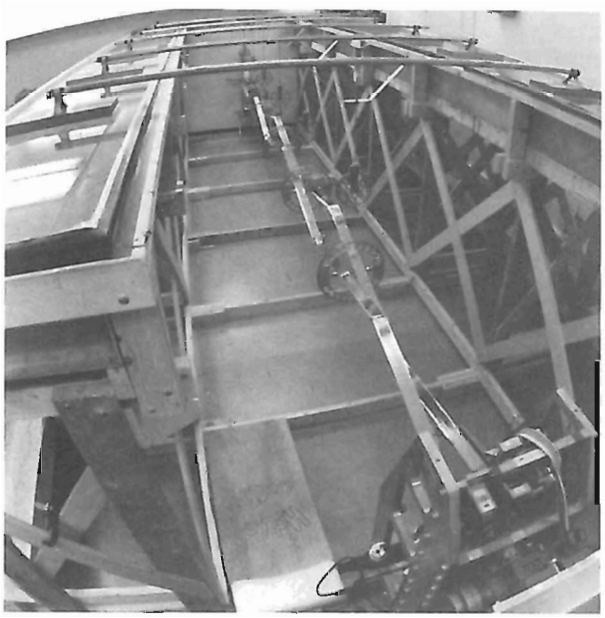

Fig. 2—The Magsat magnetometer boom float system. The magnetometer boom is suspended from floats in 6.1 m long flotation tanks that provided zero-g simulation in the horizontal plane. The boom was rotated about its longitudinal axis into four positions 90° apart. Measurements of inclinations of sensor platform-mounted mirrors provided data that were used to align the mirrors by operating the gimbal at the base of the boom or by shimming the vector magnetometer base at the sensor platform end. Final measurements, adjustments, and checks were made by the attitude transfer system with the instrument module mounted on the rotary fixture.

which was to rotate the boom into its pitch and yaw planes for orthogonal plane, zero-g measurements, and adjustments. With the aid of an autoreflecting telescope, a theodolite, and numerous mirrors to measure the transverse and angular offsets of the plane remote mirror, sufficient data were obtained to guarantee remote mirror acquisition in orbit.

OPERATIONAL PERFORMANCE

On November 1, 1979, following a successful launch a few days earlier, the spacecraft attitude was stabilized. At 6:27:53 PM EDT, after successful uncaging, the magnetometer boom was extended. Telemetry indicated that the extension was proper and complete (see Fig. 3 of the Mobley article in this issue). Surprisingly, telemetry indicated that the remote mirrors were within the field of view of the ATS optical heads. This obviated the need for extensive gimbal searching for ATS acquisition. On the following day slight gimbal adjustments were made to bring the remote mirrors into the ATS linear range. Subsequent gimbal adjustments were unnecessary.

Figure 3 — data from one orbit 92 days into mission life — shows roll, pitch, and yaw angles relative to orbital time and boom-link temperatures as measured by thermistors attached directly opposite one another on a boom link. Oscillations are evident, with periods approximately equal to the orbital period and amplitudes well within the ±180 arc-s pitch and yaw and ±300 arc-s roll limitations of the ATS. The boom-link temperatures exhibit

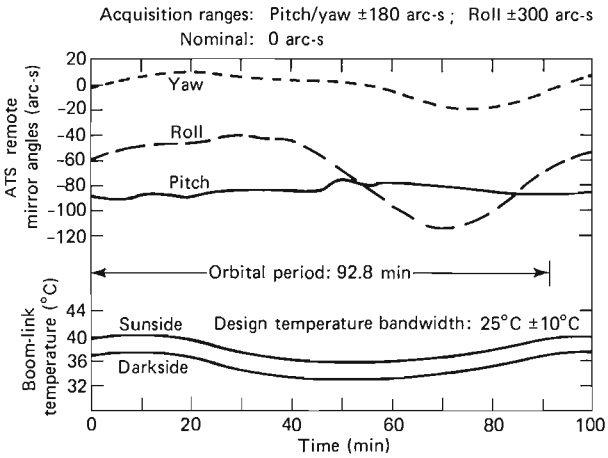

Fig. 3—Magsat ATS remote mirror angles and magnetometer boom-link temperatures, 029:22:40:15 (January 29, 1980, orbit 1410).

this same cyclical characteristic. This coincidence leads to the inference that the boom is being thermally excited at the orbital frequency. The continually varying temperatures are caused by the once-per-orbit coning of the solar vector. Their magnitudes are functions of the boom-link angle relative to the sun, which is set by the link angle relative to the boom axis and the seasonal variation in the solar vector.

The landmark performance of the boom system in orbit is an endorsement of the concept and of the special precautions that were exercised to guarantee its successful use.

WINFIELD H. FARTHING

THE MAGSAT SCALAR MAGNETOMETER

The Magsat scalar magnetometer is derived from optical pumping magnetometers flown on the Orbiting Geophysical Observatories. The basic sensor, a cross-coupled arrangement of absorption cells, photodiodes, and amplifiers, oscillates at the Larmor frequency of atomic moments precessing about the ambient field direction. The Larmor frequency output is accumulated digitally and stored for transfer to the spacecraft telemetry stream. In orbit the instrument has met its principal objective of calibrating the vector magnetometer and providing scalar field data.

INTRODUCTION

The cesium vapor optical pumping magnetometer used on Magsat is derived from the rubidium magnetometers flown on the Orbiting Geophysical Observatories (OGO) between 1964 and 1971. The Polar Orbiting Geophysical Observatories (Pogo) used rubidium-85 optical pumping magnetometers,[1] while those on the Eccentric Orbiting Geophysical Observatories (Eogo) used the slightly higher gyromagnetic ratio of rubidium-87.

Data generated by the Pogo instruments provided the principal data base for the U.S. input to the World Magnetic Survey,[2] an international cooperative effort to survey and model the geomagnetic field. It is partly this body of data that underlies the most accurate analytical models of the main geomagnetic field in present use.[3] Further studies of the Pogo data base and other sources led to the recognition of the need for a dedicated mission, such as Magsat, to increase the resolution for crustal studies, to incorporate vector measurements, and to correct the models for secular variation.

When considering various options for implementing a scalar magnetometer for use in space, optical pumping instruments are clearly superior in view of requirements for accuracy, dynamic range, information bandwidth, ease of data collection and storage, power and weight requirements, and reliability. For the self-oscillating type used in OGO and Magsat, cesium-133 is superior to other alkali vapors because of its narrower resonance line width, followed by rubidium-87 and rubidium-85. When instrumentation for Pogo was selected, cesium had not been used extensively in magnetometry and thus was not considered sufficiently developed to use in spaceflight. Rubidium-87, with its higher gyromagnetic ratio, would have resulted in a wide range of frequencies over which it would have been difficult to control the electronic phase shifts that are so important to accuracy. Rubidium-85, with its gyromagnetic ratio of 4.66737 Hz per nanotesla (nT), was therefore used even though, from the standpoint of resonance line width, it is the poorest of the three. In the interim between OGO and Magsat, cesium-133 came to be the most commonly used isotope in alkali vapor magnetometry and was thus the natural selection for Magsat.

PRINCIPLE OF SENSOR OPERATION

The alkali vapor magnetometer is based on the phenomenon of optical pumping reported by Dehmelt[4] in 1957. The development of practical magnetometers followed rapidly, evolving in one form finally to the dual-cell, self-oscillating magnetometer[5] shown in Fig. 1. Two of these twin-cell magnetometers are combined in the Magsat magnetometer. In each twin-cell sensor an electrodeless discharge lamp driven by the RF exciter produces resonance radiation that is collimated and passed through an interference filter, which selects the D_1 spectral line (894.5 nm for cesium-133) and rejects the D_2 spectral line (852.1 nm for cesium-133). The light is then circularly polarized before it is allowed to optically excite cesium vapor contained in the absorption cells.

Two identical sets of optics are employed, with the direction of light propagation antiparallel, thus defining the "optical axis" of the system. The transmission of each absorption cell is monitored by a photodetector, amplified, and cross-fed back to solenoidal coils wound about the absorption cells coaxially with the optical axis. A closed loop is thus formed that oscillates if the loop gain is greater than unity at the frequency where the loop phase shift is zero. The frequency of oscillation is a direct measure of the strength of the ambient magnetic field, i.e., the Larmor frequency of atomic magnetic moments precessing about the ambient field direction.

The modulation of light transmission obtained through application of a Larmor frequency signal to the solenoidal coil, termed the "H_1" coil, results from transitions between the discrete hyperfine

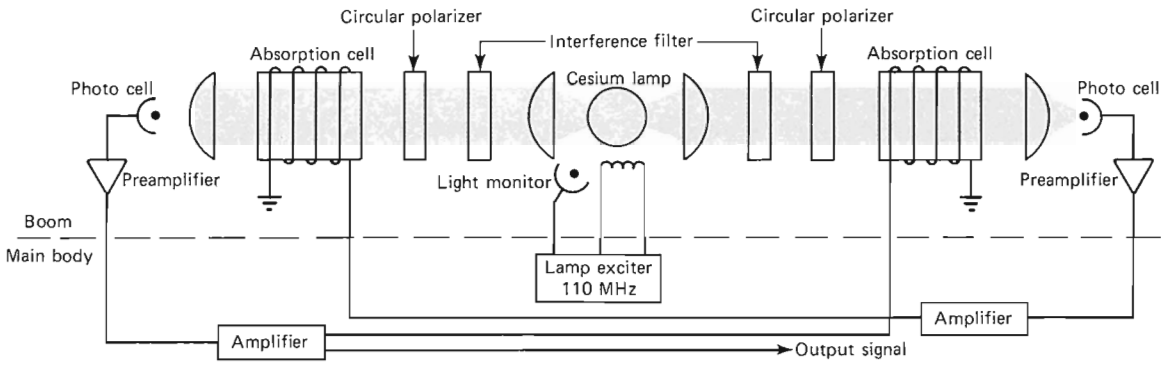

Fig. 1—Dual-cell cesium magnetometer. The loop, composed of absorption cells, photocells, and amplifiers oscillates at a frequency proportional to the ambient field magnitude.

energy states that exist in the cesium atom when it is subjected to a magnetic field. The hyperfine splitting of cesium-133 is shown in Fig. 2. Prior to the application of pumping light, the atoms can be considered to have a Boltzmann distribution among the energy states. Optical pumping polarizes the sample so that a nonequilibrium concentration of atoms in either the m (the Larmor frequency for transition) $= +4$ or $m = -4$ sublevel of the ground state is obtained, depending on both the sense of circular polarization and the direction of the optical axis component of the magnetic field.

Application of a (Larmor frequency) signal to the H_1 coil at the transition frequency for $m = +4, +3$ (or $m = -4, -3$) causes the selective depumping of a group of atoms having a certain phase with the driving signal. Since the pumping probability depends on the angle to the light wave normal as the group of depumped atoms precesses, the light transmission is modulated at the Larmor frequency.

A single-cell absorption cell process is subject to "heading error" in that the Larmor frequency for transition $m = +4, +3$ differs from that for transition $m = -4, -3$. The dual-gas-cell configuration has a strong advantage over single-cell magnetometers in that the sense of circular polarization is such that when one cell is pumped to the $m = +4$ state, the other is pumped to the $m = -4$ state, resulting in a reverse skew for the two absorption cells. Since the dual-cell loop transfer function includes the product of the individual absorption lines, a symmetrical two-cell composite line is obtained. Thus the frequency of operation should not change under reversal of the ambient field with respect to the sensor.

The frequency of oscillation of the loop is determined by the open loop phase shift of all the components. If the net phase shift from all sources other than the absorption cells is zero at any frequency, the closed loop oscillates at the frequency where the phase shifts of the two absorption cells are equal and opposite. By the symmetry of the system, this frequency is the average of the eight

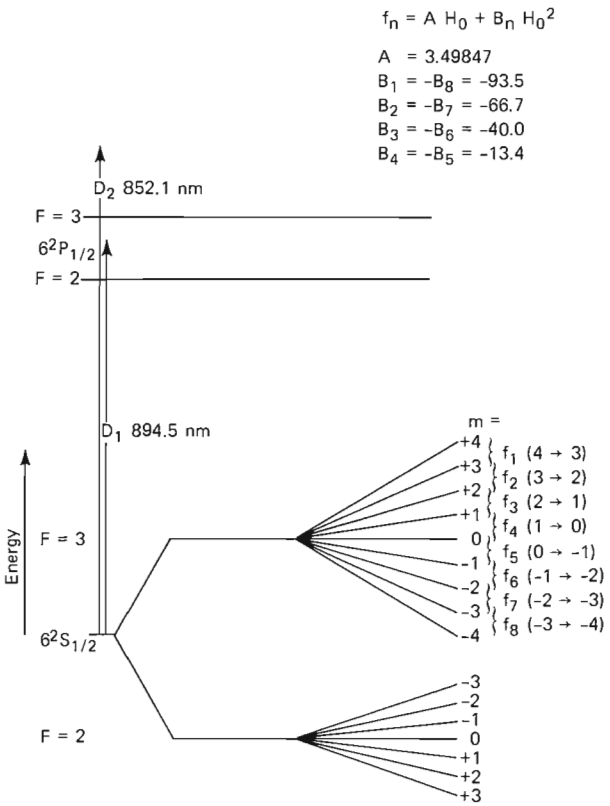

Fig. 2—Energy diagram for cesium-133. Transition frequencies f_1 to f_8 are in hertz for the applied field H_0 in gauss (1 gauss = 10^5 nT).

absorption frequencies of the Zeeman spectrum for $F = 3$. This yields for the theoretical oscillation frequency

$$f = 3.49847\, H_0 ,$$

where f is given in hertz if the ambient field H_0 is expressed in nanoteslas.

The various processes of modulating and monitoring light in the twin-cell sensor are such that the loop gain depends on the product $\sin^2 \theta \cos \theta$, where θ is the angle between the optical axis and

the applied field. Thus null zones are to be expected in a twin-cell sensor when the ambient field is either along or perpendicular to the optical axis. These zones are termed "polar" and "equatorial" null zones, respectively. The Magsat magnetometer incorporates two such sensors, with their optical axes crossed at 55°. The polar null zones are thereby eliminated because they have no intersection, and the only remaining composite null zone is the intersection of the two equatorial null zones, shown in Fig. 3. In the Magsat magnetometer, the composite null zone is directed normal to the orbit plane, such that in normal operation in near-polar orbit the ambient field will never lie within the composite null zone.

It is desired, of course, to minimize the width of the null zones for each individual sensor. It is thus necessary to use high gain amplifiers in the system, the limitations being the noise level of the system and the requirement to maintain near-zero phase shift over the operating frequency range. The width of the null zones is also quite dependent on the operating temperature of the absorption cells. For cesium-133, the optimum cell temperature is 52°C. The four absorption cells in the Magsat magnetometer are maintained at the desired temperature by individual thermostatically controlled heaters. The heaters are made from bifilar-wound resistance wire to avoid magnetic signature, and each heater dissipates 0.5 W at 30 V when the thermistor-operated control circuitry closes the circuit. The overall thermal environment is achieved by controlling separately the beryllia yoke (into which the sensors are mounted) at 41°C, and enclosing the entire sensor in a passive thermal enclosure with a radiator whose area is selected to radiate the required amount of energy. Figure 4 shows the Magsat scalar magnetometer sensor configuration without its thermal enclosure or radiator.

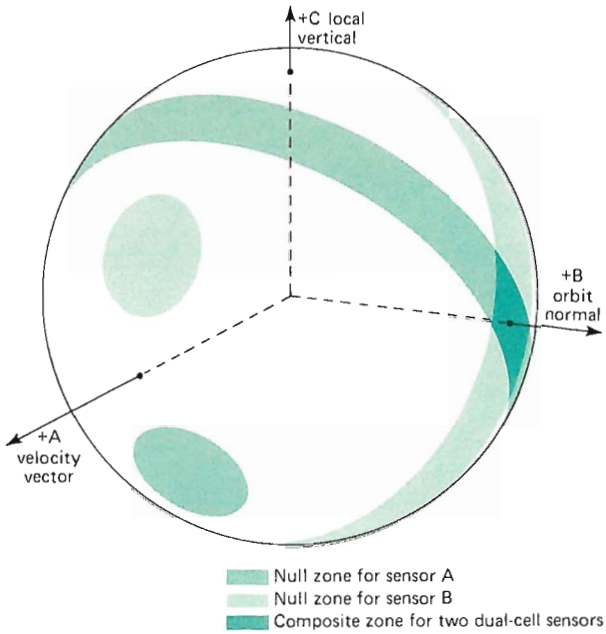

Fig. 3—Spatial coverage of the scalar magnetometer. The composite null zone, or intersection of the two individual sensor null zones, is oriented normal to the spacecraft orbit plane. It should never contain the magnetic field vector.

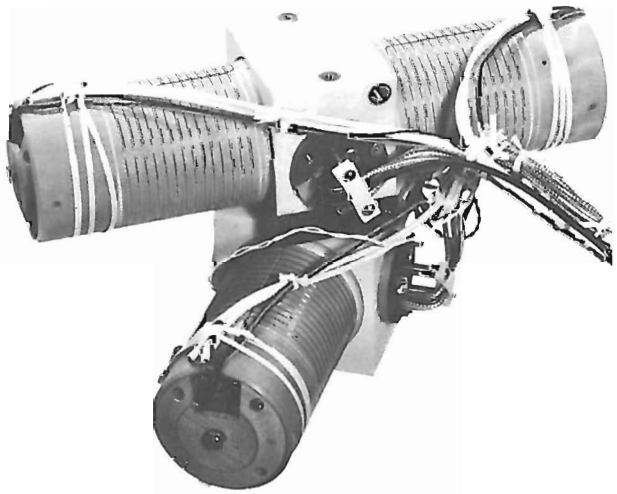

Fig. 4—Magsat scalar magnetometer sensor. Each cylinder contains optics and hybrid preamplifiers for one dual cell magnetometer. The central yoke is made of beryllia to minimize the temperature gradient. A flat beryllia radiator (not shown) is attached to the top of the yoke. The entire structure is housed in a fiberglass and multilayer thermal blanket enclosure.

DIGITAL DATA GENERATION

Figure 5 is a diagram of the electronics necessary to operate the sensors and to interface the spacecraft telemetry system. In order to prevent interference between the two sensors, they must be operated in frequency lock. This is accomplished by using a combining amplifier on one side of the sensors. The combining amplifier is repeated in order to implement fully the design objective of maintaining the maximum amount of redundancy for single sensor operation. The output signals from the two combining amplifiers are processed through completely independent signal processors consisting of phase-locked loop tracking filters, accumulators, and readout gates. In each signal processor chain, the bandwidth of the tracking filter is set at 25 Hz to ensure that the loop will track the varying input frequency adequately and to make negligible any errors associated with time lag in the closed-loop transfer function. The accumulators are of a commandable aperture type, a design feature that was incorporated to allow the sampled data to vary from the normal situation of a 30 ms aperture time (in which the information bandwidth is primarily that of the tracking filter) to a maximum aperture case (where the frequency characteristic of the sampling function is primarily determined by the aperture time and the resulting output data are substantially protected from frequency aliasing effects). In

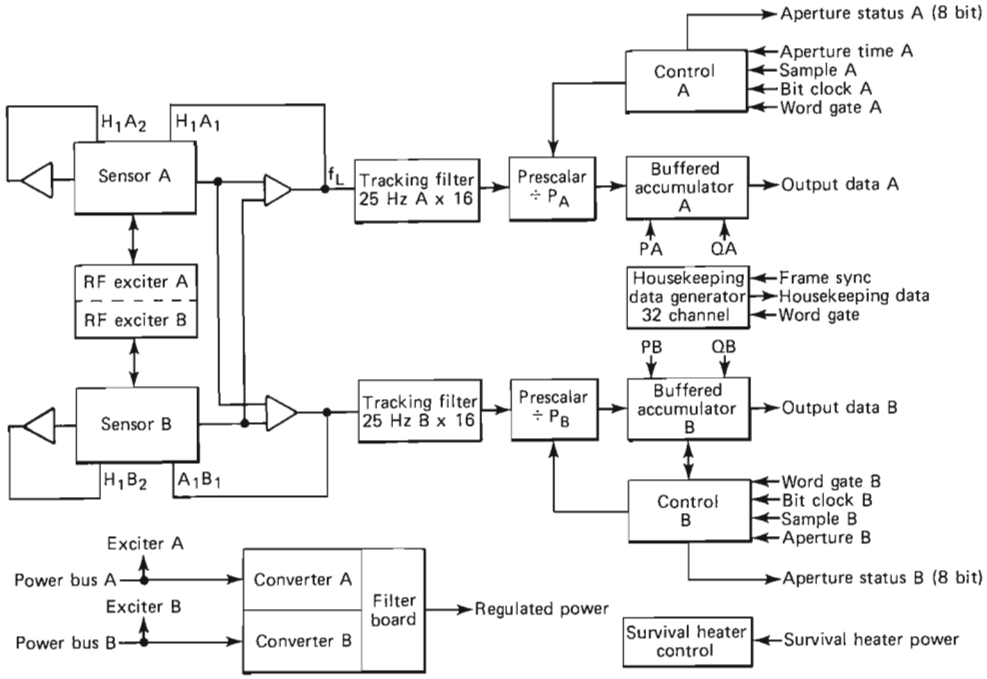

Fig. 5—Block diagram of scalar magnetometer electronics.

order to make this design objective compatible with resolution requirements, the tracking filters were designed to multiply the Larmor frequency by a factor of 16.

The output data word assigned to each scalar magnetometer data point is 20 bits long. The last bit is made a parity bit, and the next to last bit was desired to be a data quality flag associated with that particular sample. This leaves 18 bits for the primary data sample, which was not compatible with the full range of commandable aperture times. Thus a prescalar is included in each data processing chain. The prescalar is under the control of the commanded aperture time, which is delivered to the experiment in the form of a binary number, N, that specifies the aperture time as $(2N + 1)Tb$, where Tb is the telemetry bit time of 0.512 ms. For $N \leq 63$, the prescalar factor, P, is 1. For $64 \leq N \leq 127$, the prescalar factor is 2. For $N \geq 128$, the prescalar factor divides by 4.

The logic equation for the data quality flag, Q, associated with each data point is, for instance, for scalar A,

$$Q_A = T_{FA} \cdot (\mathrm{SIGA} + \mathrm{SIGB}) \cdot (\mathrm{BRA} + \mathrm{BRB}) ,$$

where each term in the logic function has to be true over the accumulation time in which that particular data sample was collected. $T_{FA} = 1$ means that the tracking filter associated with that data point was in lock throughout the accumulation time. SIGA + SIGB = 1 is a condition that the signal amplitude in either sensor A or sensor B is above a predetermined threshold throughout the accumulation interval. BRA + BRB = 1 is a condition that one or both of the lamps must be operating within a predetermined brightness range throughout the accumulation interval. This form of the logic function was selected in order to be compatible with the operation of both processing chains with a single sensor and yet to be an efficient rejector of a number of possible malfunctions within the instrument.

The sampling of each scalar is done at 4 samples per second, and the samples of scalar A and scalar B are interleaved to obtain a total of 8 equidistant samples per second.

OPERATION IN ORBIT

The Magsat scalar magnetometer met its principal in-orbit objective of calibrating the vector magnetometer and returned scalar field data, although intermittent noise in the lamp excitation circuitry caused loss of lock in the tracking filters and, therefore, a reduction in the expected data rate.

Engineering data returned from the instrument verified that the thermal control circuitry performed as expected in controlling lamp and absorption cell temperatures. Monitors in the lamp RF control loops were only reliable when the intermittent noise was absent but at such times showed that lamp A operated at control parameters identical to those observed during ground thermal-vacuum testing. Lamp B, which ran extremely efficiently during ground testing, required slightly more RF power in orbit. Sensors A and B were operated independently at times to serve as a cross check on absolute accuracy and to verify the integrity of the Larmor sensors.

The lamp noise problem manifested itself differently in the two lamps. It first appeared in lamp A about 12 hours after the instrument was turned on and, except for a few periods after the lamp had been off for a day or more, was consistently present in the lamp excitation until the spacecraft entered the eclipse season, when a dramatic improvement occurred. The problem was first observed in lamp B two weeks after turn-on and was present intermittently over a period of several hours in a way that has not been explained. Transitions from one state to another often occurred when one of the tape recorders was played back, but the problem was not associated with a particular tape recorder. The lamp problem was most likely caused by a feedback mechanism to the spacecraft power that was not present to the same degree on the ground.

The effect of the interference on tracking filter lock was much more serious when the noise was present in lamp B. Thus the operational mode was to operate lamp A continuously and to operate lamp B approximately one day out of five in order to fill in the A sensor null zones and to provide a more complete data set for calibration of the vector magnetometer.

Incorporation of the data quality flag in the output word proved indispensable to the rejection of data when the tracking filter was out of lock and enabled the combination of vector and scalar magnetometers to meet substantially all the objectives, even in the presence of the lamp excitation noise.

REFERENCES

[1]W. H. Farthing and W. C. Folz, "Rubidium Vapor Magnetometer for Near Earth Orbiting Spacecraft," *Rev. Sci. Instrum.* **38**, pp. 1023 – 1030 (1967).

[2]A. J. Zmuda (ed.), *The World Magnetic Survey*, IAGA Bulletin No. 28 (1971).

[3]Ibid., p. 148.

[4]H. G. Dehmelt, *Phys. Rev.* **105**, p. 1487 (1957).

[5]A. L. Bloom, "Principles of Operation of the Rubidium Vapor Magnetometer," *Appl. Opt.* **1**, pp. 61 – 68 (1962).

ACKNOWLEDGMENT — The Magsat scalar magnetometer was built for the NASA/Goddard Space Flight Center by Bell Aerospace Systems Division, Western Laboratories, and Varian Associates, Canada, Ltd. Mr. David Synder, BASD, was program manager for the project. The RF exciters were provided by Mr. L. J. Rogers of GSFC.

MARIO H. ACUNA

THE MAGSAT PRECISION VECTOR MAGNETOMETER

The Magsat precision vector magnetometer was a state-of-the-art instrument that covered the range of ±64,000 nanoteslas (nT) using a ±2000 nT basic magnetometer and digitally controlled current sources to increase its dynamic range. Ultraprecision components and extremely efficient designs minimized power consumption.

INTRODUCTION

The instrumentation aboard the Magsat spacecraft consisted of an alkali-vapor scalar magnetometer and a precision vector magnetometer. In addition, information concerning the absolute orientation of the spacecraft in inertial space was provided by two star cameras, a precision sun sensor, and a system to determine the orientation of the sensor platform, located at the tip of a 6 m boom, with respect to a reference coordinate system on the spacecraft.

The two types of instruments flown aboard the spacecraft provided complementary information about the measured field. The scalar magnetometer measured the magnitude of the field independent of its orientation with respect to the sensor, with an absolute accuracy that is determined by atomic constants and thus is not subject to change as a function of time. On the other hand, the precision vector magnetometer measured the projections of the ambient field in three orthogonal directions with an absolute accuracy determined by calibrations with respect to a standard; thus they were subject to error and drift. Accuracy goals for the mission required a vector magnetometer capable of measuring the ambient field with a maximum error of ±1 part in 64,000 in magnitude and 5 arc-s in orientation (1 arc-s = 0.00028°). The development of such an instrument within the constraints imposed by the spacecraft represents a major technological achievement that would have been impossible without parallel developments in the areas of ultraprecise linear integrated circuits and miniature resistors. The design implemented for Magsat represented an optimum compromise among many conflicting requirements and limitations imposed by available resources, reliability considerations, and state-of-the-art electronics. This paper presents a brief description of this unique instrument.

INSTRUMENT DESCRIPTION

Figure 1 is a block diagram of the vector magnetometer. The heart of the instrument is a highly stable and linear triaxial fluxgate magnetometer with a dynamic range of ±2000 nT (1 nT = 10^{-9} weber per square meter). The principles of operation of fluxgate magnetometers are well known and will not be repeated here. The reader is directed to Refs. 1, 2, and 3 for further information concerning the detailed design of these instruments.

To extend the range of the basic magnetometer to the 64,000 nT required for Magsat, three digitally controlled current sources with 7 bit resolution and 17 bit accuracy were used to add or subtract automatically up to 128 bias steps of 1000 nT each. The X, Y, and Z outputs of the magnetometer were digitized by a 12 bit analog-to-digital converter that, in conjunction with the 7 bits associated with the digital current sources, yielded an overall instrument resolution of ±0.5 nT.

The ambient magnetic field was sampled 16 times per second along each of the three orthogonal directions, and the digital current sources were updated at the same rate. The digital data corresponding to the "fine" (12 bit) and "coarse" (7 bit) information were fed directly to the spacecraft through a serial interface. The fine data were sampled at 16 samples per second; the coarse data were sampled at only 4 samples per second. This sampling scheme took advantage of the fact that the ambient magnetic field changed slowly over the Magsat orbit; hence, coarse updates were not needed as frequently as fine updates. The response of the instrument to increasing and decreasing ambient fields is shown in Fig. 2. The current steps, which are added or subtracted depending on the magnitude and direction of the external field, maintained the effective magnetic field seen by the fluxgate sensor within its operating range of 2000 nT. The stepping threshold was actually 1000 nT to allow the magnetometer to follow rapid changes in the field between two adjacent updates of the bias steps without loss of data.

As can be seen from Fig. 1, the magnetometer electronics, analog-to-digital converters, and digitally controlled current sources were implemented with redundant designs. This was also true for the

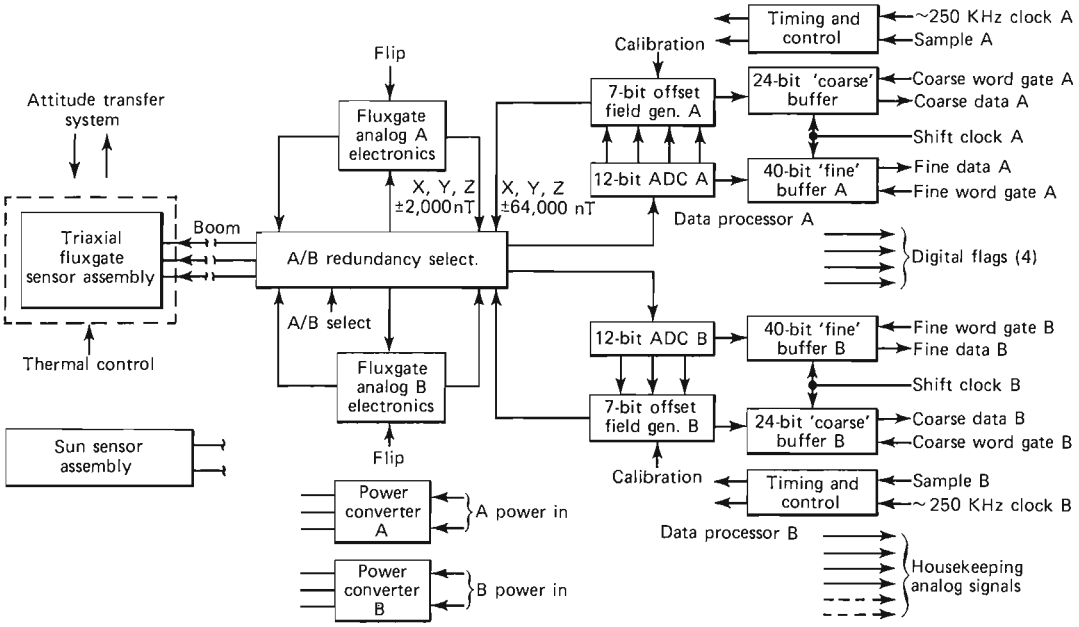

Fig. 1—Block diagram of the precision vector magnetometer. All subsystems are implemented with redundant designs to avoid loss of data in case of failures.

digital processors and power converters. The block-redundancy approach provided a fundamental measure of reliability to this important instrument and eliminated from consideration single-point failures in the electronics. Selection of the particular system used (A or B in Fig. 1) for both the analog and digital portions of the instrument was executed by ground command.

TRIAXIAL FLUXGATE SENSOR

The fluxgate sensor used in the Magsat vector magnetometer was a unique design that took advantage of the ring core geometry. This particular geometry exhibits superior performance characteristics in terms of noise and zero-level stability. In addition, its uniform expansion characteristics were essential for achieving the angular stability required. Figure 3 is a schematic diagram that shows the construction of each sensor. Crucial elements in the Magsat fluxgate sensor design were the feedback coil that nulls the external field, and the sensor core itself; they constitute the most important sources of error in terms of alignment stability as well as variation of scale factor with temperature. Any distortion or motion of the sensor core within the feedback coil represents an effective alignment shift. Structural deformations larger than 50 μm were sufficient to exceed the alignment stability tolerance.

The fundamental strategy followed for the Magsat vector magnetometer was to match the expan-

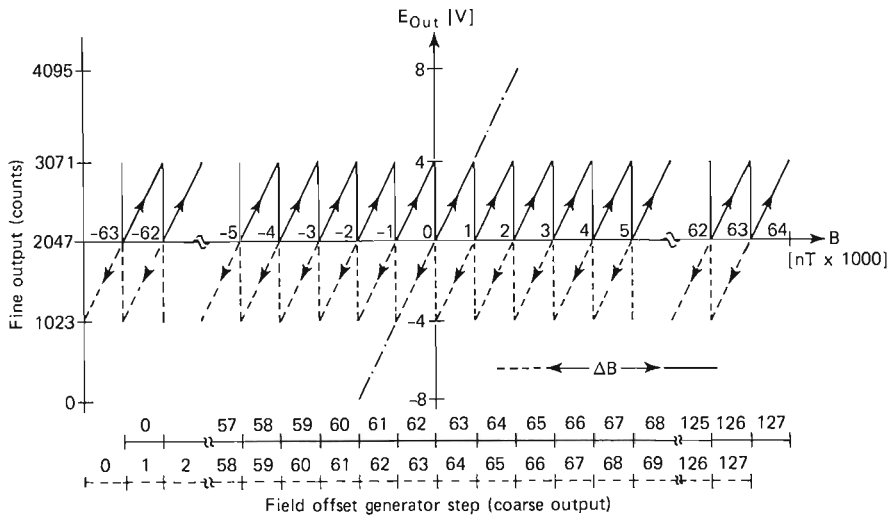

Fig. 2—Instrument response for increasing (solid curve) and decreasing (dashed curve) ambient field. Note the large safety margin in the switching threshold (half scale).

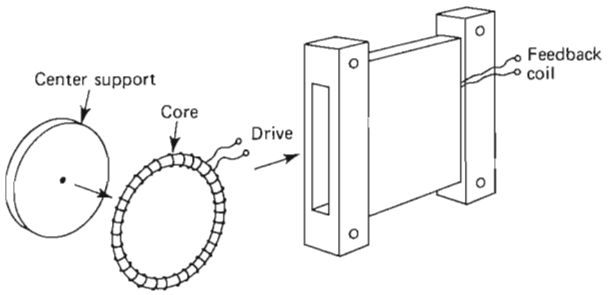

Fig. 3—Individual fluxgate magnetometer sensor construction. All parts have identical expansion coefficients.

sion coefficients of all the materials used in the construction of the sensor assembly (core, feedback coil, and support structure) so that differential stresses induced by temperature variations were minimized. Since the sensor core expansion coefficient is approximately 10 ppm/°C, platinum wire was used to wind the feedback coil, and the support structures were machined from solid blocks of Macor, a machinable glass-ceramic. The triaxial sensor assembly was mounted on a temperature-stabilized baseplate whose temperature was actively maintained at 25 ± 1°C. The attitude transfer system mirrors were mounted under this baseplate. Their expansion coefficient was nearly zero; hence, active thermal control of this crucial interface was needed.

Since the overall expansion coefficient of the sensor feedback coil was nonzero, the magnitude of the feedback field was a strong function of temperature. To minimize this effect, the magnetometer electronics incorporated a correction circuit that sensed the coil temperature by changes in its resistance and adjusted the feedback current to make the generated field independent of temperature.

The external magnetic field generated by the triaxial fluxgate sensor assembly was less than ±1 nT at the location of the scalar magnetometer. This low field value minimized the interference with the accuracy of the measurements obtained by the scalar instrument.

To determine the absolute orientation of the sensors with respect to a reference coordinate system, two optical cubes were bonded to the sensor mount. They allowed the sensor assembly to be rotated exactly 90° during calibrations to establish the absolute direction of the magnetic axes and later to reference the scalar instrument measurements to the principal spacecraft coordinate system.

MAGNETOMETER ELECTRONICS

The electronics design for the vector magnetometer incorporated a number of advanced developments derived from the Voyager 1 and 2 magnetic field experiments[1,2] that were directly applicable to this instrument. However, the extreme accuracy required of the analog signal processing circuits dictated the use of ultraprecise components, some of which had to be specifically developed for Magsat. The maximum allowable error voltage for the digitally controlled current sources was only 125 μV so considerable attention had to be paid to the problem of thermally generated electromotive forces that are produced across dissimilar metal junctions. Circuit layouts with a minimal number of solder joints, the proximity of essential conductors in order to minimize thermal gradients, and the use of cadmium-tin alloys for soldering and assembly reduced the instrument errors to an absolute minimum. The resistors used in the digital current sources as well as the magnetometer feedback circuit were ultraprecise, hermetically sealed units with an absolute temperature coefficient of less than 0.5 ppm/°C and a long term stability of 20 ppm/year. The calibration of the analog circuits required special test instrumentation with accuracies established by the National Bureau of Standards and resolution of about 1 ppm (a type of design usually restricted to laboratory-grade instruments). Extensive reliability and performance trade-off analyses were carried out to ensure mission success.

The digital processors were implemented with CMOS digital integrated circuits to reduce power consumption to a minimum. Only one processor was powered at any given time by its respective power converter; the same was true for the analog electronics subsystem. As is illustrated in Fig. 1, there were then four possible arrangements for these subsystems, depending on how they were interconnected. To simplify testing, the "A-A" and "B-A" combinations were calibrated by an indirect analysis of the "A-A" and "B-B" configurations test data. A summary of performance parameters and technical characteristics of the magnetometer and the electronics system is given in Table 1.

CALIBRATION AND ALIGNMENT

The problem of determining the orientation of a given magnetic field vector traditionally has been solved by assuming that the field orientation can be established accurately by the geometry of a calibration coil. This method is generally sufficient to determine sensor orientation within a few arcminutes from its true direction, but it is certainly not accurate enough for the Magsat case where accuracies of the order of 2 arc-s were required. The method to determine the sensor alignment assumed that the deviations from orthogonality of the sensor assembly and triaxial test coil system were small. In this case, a very accurate alignment of the sensor and test coil system can be obtained simultaneously by rotating the sensor twice through exactly 90° in two planes. This method has been described in Refs. 4 and 5. An accurate optical reference coordinate system was first established at the Goddard Space Flight Center (GSFC) Magnetics

Table 1

SUMMARY OF TECHNICAL CHARACTERISTICS OF THE MAGSAT PRECISION VECTOR MAGNETOMETER

Basic Fluxgate Magnetometer
- Dynamic range: ±2000 nT
- Resolution: 12 bit A/D converter (±0.5 nT)
- Noise: 0.008 nT rms (8 Hz bandwidth)
- Zero level stability:
  - Sensor (−60 to +60°C): ±0.2 nT
  - Electronics (−20 to +50°C): ±0.2 nT
- Drive frequency: 12.5 kHz
- Linearity error (compensated): less than 1 part in 10^5
- Angular stability better than ±3 arc-s over a temperature range of 10 to 40°C

Offset Digitally Controlled Current Sources
- Dynamic range: ±64,000 nT
- Quantization step: 1000 nT
- Temperature coefficient: less than 0.5 ppm/°C
- Long-term stability: within 2 parts in 10^5 per year

Sensor Assembly
- Mass: 0.6 kg
- Dimensions: 11.4 × 5.72 × 5.8 cm

Electronics (redundant)
- Mass: 2.6 kg
- Dimensions (approximate): 22.23 × 17.8 × 11.4 cm
- Total power consumption:
  - 1.8 W at 25°C
  - 2.0 W at 0°C

Test Facility by means of a pair of first-order theodolites referenced to a 400 meter baseline. Numerous magnetic contamination problems associated with the optical system had to be solved to realize the intrinsic accuracy obtainable by this method. The short- and long-term mechanical stability of the triaxial coil system presented very difficult problems at times in terms of the consistency of test results. Nevertheless, after many hours of dedicated testing to determine the true performance of the magnetometer and coil system, excellent results were obtained, as is evident by the outstanding in-orbit performance of the vector magnetometer.

The individual axis scale factors were calibrated using a proton precession magnetometer as a reference standard for fields greater than 20,000 nT. For small fields, the calibration constants were synthesized from selected incremental measurements above 20,000 nT to determine the exact "weights" of each of the 7 bits in the digitally controlled current sources. Final overall calibration included coordinated tests with the scalar magnetometer to determine mutual interference and relative accuracy. Significant problems were encountered in this respect with the relatively large RF power required for operation of the scalar magnetometer. Prior to the installation of RF shielding on the spacecraft, this interference was rather serious, and considerable effort was dedicated to its elimination.

REFERENCES

[1]M. H. Acuna, "Fluxgate Magnetometers for Outer Planets Exploration," *IEEE Trans. Magn.* **MAG-10**, No. 3, p. 519 (1974).

[2]K. W. Behannon, M. H. Acuna, L. F. Burlaga, R. P. Lepping, N. F. Ness, and F. M. Neubauer, "Magnetic Field Experiment for Voyagers 1 and 2," *Space Sci. Rev.* **21**, pp. 235–257 (1977).

[3]M. H. Acuna, C. S. Scearce, J. B. Seek, and J. Scheifele, *The MAGSAT Vector Magnetometer—A Precision Fluxgate Magnetometer for the Measurement of the Geomagnetic Field,* NASA Technical Memorandum 79656 (1978).

[4]R. L. McPherron and R. C. Snare, "A Procedure for the Accurate Calibration of the Orientation of the Three Sensors in a Vector Magnetometer," *IEEE Trans. Geosci. Electron.* **GE-16**, No. 2, pp. 134–137 (1978).

[5]M. H. Acuna, *MAGSAT - Vector Magnetometer Absolute Sensor Alignment Determination,* NASA Technical Memorandum 79648 (1978).

ACKNOWLEDGMENTS — The author would like to acknowledge the dedication and support provided during the development, test, and integration of this instrument by J. Seek, C. Scearce, J. Scheifele, and E. Worley of GSFC; C. Fewell of Northrop Services; R. Lundsten, and J. Scarzello of NSWC; and F. Mobley, J. Roberts, E. Marshall, and J. Smola of APL. The outstanding optical support provided by S. Hinkal was essential to the success of the calibration activity. The GSFC Magnetics Test Facility personnel, C. Harris, R. Bender, and R. Ricucci, spent many hours waiting for us to understand our spacecraft; their contribution is deeply appreciated.

ROBERT A. LANGEL

MAGSAT SCIENTIFIC INVESTIGATIONS

The nature of the geomagnetic field and of presatellite and early satellite measurements is described. The objectives of each investigation in the areas of geomagnetic modeling, crustal magnetic anomaly studies, investigations of the inner earth, and studies of external current systems are presented, along with some early results from Magsat.

INTRODUCTION

The near-earth magnetic field, as measured by the magnetometers on Magsat, contains contributions from three sources: the earth's core, the earth's crust, and external current systems in the earth's ionosphere and beyond. By far the largest in magnitude is the field from the core, or the "main" field. The main field is nearly dipolar in nature. Its strength is more than 50,000 nT (nanoteslas) at the poles and near 30,000 nT at the equator. Its variation with time ("secular" variation) is slow, with a maximum of about 1% per year. External current systems are time varying on a scale of seconds to days and can vary in magnitude from a fraction to thousands of nanoteslas. The current systems are located in a cavity-like region surrounding the earth, known as the "magnetosphere." Although these currents are always present, their strength and location vary considerably between periods of magnetic quiet and periods of magnetic disturbance.

Magnetic fields from the earth's crust are by far the smallest in amplitude of the three sources at satellite altitudes. Their strength at Magsat altitudes is between 0 and 50 nT. Also called "anomaly fields," the sources are associated with variations in the geologic or geophysical properties in the earth's crust; accordingly, their temporal variations are on a geologic time scale.

Prior to the satellite era the earth's magnetic field was (and still is) monitored by means of permanent magnetic observatories that measure the ambient field continuously and by periodically repeating measurements at selected sites. Field surveys are necessary to fill in the spatial gaps between observatories and repeat sites. Such surveys were first conducted by early mariners and land surveyers. Edmund Halley made a sea voyage during 1689-1700 expressly to survey the magnetic field over the oceans. In 1701 he published the first chart of the magnetic declination in the region of the Atlantic Ocean; in the following year he extended his chart to the Indian Ocean and to the sea near China.

In addition to land and sea surveys, some aircraft have been especially adapted for the measurement of magnetic fields. Such surveys usually, although not always, measured only the scalar magnitude of the field. Many countries have been surveyed in their entirety, some more than once. Unfortunately, the United States has not yet been totally surveyed. In addition to their obvious value for modeling the earth's main field, such surveys are particularly useful for mapping the anomaly field at low altitude and, as a result, have been conducted by the oil and mineral exploration industries on a local scale.

Satellite measurements of the geomagnetic field began with the launch of Sputnik 3 in May 1958 and have continued sporadically in the intervening years. Table 1 is a list of spacecraft that have made significant contributions to our understanding of the near-earth geomagnetic field. Each had its own limitations, ranging from a lack of global coverage caused by the absence of on-board tape recorders to limited accuracy due either to instrumental shortcomings or to ambient spacecraft fields. Prior to Magsat, only the Polar Orbiting Geophysical Observatory (Pogo) satellites (OGO -2, -4, and -6) had provided an accurate, global geomagnetic survey. Their alkali vapor magnetometers provided measurements of the field magnitude about every half second over an altitude range of about 400 to 1500 km.[1,2]

A new era in near-earth magnetic field measurements began with NASA's launch of Magsat in October 1979. Magsat has provided the first truly global geomagnetic survey since the Pogo satellites and the very first global survey of vector components of the geomagnetic field. Designed with two major measurement tasks in view, Magsat provided a global vector survey of the main geopotential field and a lower altitude measurement of crustal anomalies. These tasks stemmed directly from the Magsat mission objectives outlined by Ousley in this issue. Data from Magsat are being analyzed by many investigators, some of whom are working cooperatively.

OVERVIEW OF INVESTIGATIONS

Investigations are being carried out by scientists at the Goddard Space Flight Center (GSFC) and

Table 1

SATELLITES THAT HAVE MEASURED THE NEAR-EARTH GEOMAGNETIC FIELD

Satellite	*Inclination (degs)*	*Altitude Range (km)*	*Dates*	*Instrument*	*Approximate Accuracy (nT)*	*Coverage*
Sputnik 3	65	440 – 600	5/58 – 6/58	Fluxgates	100	USSR
Vanguard 3	33	510 – 3750	9/59 – 12/59	Proton	10	Near ground station*
1963-38C	Polar	1100	9/63 – 1/74	Fluxgate (1-axis)	30 – 35	Near ground station
Cosmos 26	49	270 – 403	3/64	Proton	Unknown	Whole orbit
Cosmos 49	50	261 – 488	10/64 – 11/64	Proton	22	Whole orbit
1964-83C	90	1040 – 1089	12/64 – 6/65	Rubidium	22	Near ground station
OGO-2	87	413 – 1510	10/65 – 9/67	Rubidium	6	Whole orbit
OGO-4	86	412 – 908	7/67 – 1/69	Rubidium	6	Whole orbit
OGO-6	82	397 – 1098	6/69 – 7/71	Rubidium	6	Whole orbit
Cosmos 321	72	270 – 403	1/70 – 3/70	Cesium	Unknown	Whole orbit
Azur	103	384 – 3145	11/69 – 6/70	Fluxgate (2-axis)	Unknown	Near ground station
Triad	Polar	750 – 832	9/72 – present	Fluxgate	Unknown	Near ground station

*"Near ground station" indicates no on-board recorder. Data were acquired only when the spacecraft was in sight of a station equipped to receive telemetry.

the U.S. Geological Survey (USGS), and by scientists selected in response to a NASA Announcement of Opportunity (AO). The work at GSFC includes derivation of the first geomagnetic field models from Magsat, derivation of the global anomaly map from Pogo, and some interpretations of that map in terms of geologic/geophysical models of the earth's crust. The USGS effort, under the direction of Frank Frischknecht, includes both field modeling and magnetic charting as carried out by Joseph Cain and Eugene Fabiano, and crustal modeling by Jeff Phillips and others. A total of 19 domestic and 13 foreign investigators were selected from responses to the AO. Table 2 lists these investigators, their institutions, and a brief description of their proposed investigations. More detailed information regarding the investigations will be given in the remainder of this paper, which is divided into four sections corresponding to four relatively distinct areas of scientific investigation, namely:

1. Geomagnetic field modeling;
2. Crustal magnetic anomaly studies, i.e., postulating the crustal structure and composition that cause the magnetic anomalies;
3. Investigations of the inner earth (the core, mantle, and core/mantle interface area); and
4. Studies of external current systems.

GEOMAGNETIC FIELD MODELING

Geomagnetic field modeling derives the spherical harmonic potential function that best represents the main field of the earth in a least-squares sense. Theoretically, such a potential function could be made to represent both the core and crustal fields exactly. Practically, a restricted model must be chosen because of the finite limitation on computer size and speed. Most researchers attempt only to represent the core field with a potential function and use alternate methods of describing the crustal fields.

One of the principal contributions of satellite magnetic field measurements to geomagnetism has been to make available a truly global distribution of data. Surface measurements are notably sparse, particularly in oceanic and remote regions. The problem is compounded by the secular variation in the main geomagnetic field that, as was stated earlier, can amount to as much as 1% per year in some localities. This means that to represent the global geomagnetic field accurately at any given time (epoch), worldwide measurements must be made at times near that epoch, a feat only achieved by satellite observations and even then only by the Pogo and Magsat satellites with their on-board tape recorders and near-polar orbits. Accurate global representation of the secular variation itself would require periodic worldwide surveys, something often spoken of but yet to become a reality. The Pogo satellites accomplished one such survey and Magsat provided another. These, together with existing surface data, permit accurate global representation of secular variation for the period beginning with OGO-2 until the demise of Magsat. Future

Table 2

LIST OF MAGSAT INVESTIGATORS

Investigator	*Institution/Country*	*Title*	*Objectives*
David R. Barraclough	Institute of Geological Sciences, United Kingdom	Spherical Harmonic Representation of the Main Geomagnetic Field for World Charting and Investigation of Some Fundamental Problems of Physics and Geophysics	Produce an accurate model of the main geomagnetic field, together with reliable estimates of the accuracy of coefficients
Charles R. Bentley	University of Wisconsin	Investigation of Antarctic Crust and Upper Mantle Using Magsat and Other Geophysical Data	Using Magsat data, devise a general framework for the structure of Antarctica into which more specific and local measurements can be integrated
Edward R. Benton	University of Colorado	Geomagnetic Field Forecasting and Fluid Dynamics of the Core	Adjust the gauss coefficients of the main field model of the Magsat data set to satisfy dynamic constraints; use Magsat data to test the ability to forecast the structure of the internal geomagnetic field
B. N. Bhargava	Indian Institute for Geomagnetism	Magsat for Geomagnetic Studies in the Indian Region	Prepare a regional geomagnetic reference field and magnetic anomaly maps over Indian and neighboring regions: (a) to gain a clearer understanding of secondary effect features and the variability of the dawn/dusk field, and (b) to study in detail the equatorial electrojet and transient variations
Robert F. Brammer	The Analytic Sciences Corporation (TASC)	Satellite Magnetic and Gravity Investigation of the Eastern Indian Ocean	Produce magnetic anomaly maps of the Indian Ocean; quantify the comparison between Magsat data and Geos-3 gravity data; interpret the magnetic data using ancillary data
J. Ronald Burrows	National Research Council of Canada	Studies of High-Latitude Current Systems Using Magsat Vector Data	Understand the physical processes that control high-latitude current systems; improve the confidence level in studies of internal field sources
Robert S. Carmichael	University of Iowa	Use of Magsat Anomaly Data for Crustal Structure and Mineral Resources in the U.S. Midcontinent	Analyze Magsat anomaly data to synthesize a total geologic model and interpret crustal geology in the midcontinent region; contribute to the interpretation and calculation of the depth of the Curie isotherm
Richard L. Coles	Energy, Mines and Resources, Canada	The Reduction, Verification and Interpretation of Magsat Magnetic Data over Canada	Select quiet-time data; correct Magsat data for disturbance fields and apply the routines; compare Magsat and vector airborne data; combine Magsat and aircraft data of magnetic anomalies; produce regional interpretations relating to earth structure
James C. Dooley	Bureau of Mineral Resources, Australia	Magsat Data, the Regional Magnetic Field, and the Crustal Structure of Australia and Antarctica	Incorporate Magsat data into regional magnetic field charts to improve their accuracy; determine if differences exist in temperature-depth curves for different tectonic areas; study the boundaries between major tectonic blocks and between continental and oceanic crust; determine Curie point depth and crustal magnetization for Antarctica
Naoshi Fukushima	Geophysics Research Laboratory, Japan	Proposal from Japanese National Team for Magsat Project	Analyze the regional geomagnetic field around Japan and Japanese Antarctica; study the contributions to magnetic variations by electric currents and hydromagnetic waves in and above the ionosphere
Paolo Gasparini	Osservatorio Vesuviano, Italy	Crustal Structures under the Active Volcanic Areas of Central and Eastern Mediterranean	Calculate the depth of the Curie temperature for the Mediterranean area and relate to areas of volcanic activity; investigate the Italian and Tyrrhenian anomaly
Bruce P. Gibbs	Business and Technological Systems, Incorporated	Geomagnetic Field Modeling by Optimal Recursive Filtering	Produce a state vector to predict field values for several years beyond the Magsat model; obtain optimal estimates of field values throughout the 1900-1980 period
M. R. Godivier	Office de la Recherche Scientifique et Technique, Outremer (ORSTOM), France	Magnetic Anomaly of Bangui	Improve the explanation of the cause of the Bangui anomaly, using Magsat data, other magnetic data, and gravity, seismic, and heat flow data
Stephen E. Haggerty	University of Massachusetts	The Mineralogy of Global Magnetic Anomalies	Interpret Magsat data to locate mafic and ultramafic source rocks and lineament expressions of anomalies that can be correlated with crustal of upper mantle depths; determine mineral stabilities pertinent to magnetic anomalies to ascertain the magnetic properties of metamorphic rocks

Table 2 (continued)

LIST OF MAGSAT INVESTIGATORS

Investigator	*Institution/Country*	*Title*	*Objectives*
D. H. Hall	University of Manitoba, Canada	Identification of the Magnetic Signatures of Lithostratographic and Structural Elements in the Canadian Shield Using Magnetic Anomalies and Data from Individual Tracks from Magsat	Confirm and extend the model for crust mantle magnetization
Christopher G. A. Harrison	University of Miami	Investigations of Medium Wavelength Magnetic Anomalies in the Eastern Pacific Using Magsat Data	Determine the relationship of magnetic anomalies with surface geological features
David A. Hastings	U.S. Geological Survey, EROS Data Center	An Investigation of Magsat and Complementary Data Emphasizing Precambrian Shields and Adjacent Areas of West Africa and South America	Determine the Magsat magnetic signatures of various tectonic provinces; determine the geological associations of these signatures; synthesize Magsat and other data with mineral resources data globally
John F. Hermance	Brown University	Electromagnetic Deep-Probing (100-1000 km) of the Earth's Interior from Artificial Satellites; Constraints on the Regional Emplacement of Crustal Resources	Evaluate the applicability of electromagnetic deep-sounding experiments using natural sources in the magnetosphere
William J. Hinze	Purdue University	Application of Magsat to Lithospheric Modeling in South America: Part I— Processing and Interpretation of Magnetic and Gravity Anomaly Data	Use magnetic anomalies to develop lithospheric models to determine the properties of principal tectonic features; correlate magnetic anomalies of South America with those of adjacent continental areas to attempt to reconstruct Gondwanaland (see Keller below)
B. David Johnson	Macquarie University, Australia	An Investigation of the Crustal Properties of Australia and Surrounding Regions Derived from Interpretation of Magsat Anomaly Field Data	Produce a map of surface magnetization to understand the evolution of the crust and to aid in mineral exploration
G. R. Keller	The University of Texas at El Paso	Application of Magsat to Lithospheric Modeling in South America: Part II— Synthesis of Geologic and Seismic Data for Development of Integrated Crustal Models	Provide models of the seismic velocity structure of the lithosphere (see Hinze above)
David M. Klumpar	The University of Texas at Dallas	Investigation of the Effects of External Current Systems on the Magsat Data Utilizing Grid Cell Modeling Techniques	Apply a modeling procedure to the vector Magsat data in order to separate the terrestrial component from that due to extraterrestrial sources
John L. LaBrecque	Lamont-Doherty Geological Observatory	Analysis of Intermediate-Wavelength Magnetic Anomalies over the Oceans in Magsat and Sea Surface Data	Determine the distribution of intermediate wavelength magnetic anomalies of lithospheric origin in the oceans, the extent to which Magsat describes the distribution, and the cause of these anomalies
Jean-Louis LeMouel	Institut de Physique du Globe de Paris, France	Magsat Investigations Consortium	Reduce Magsat vector data for a global analytic field model and constant altitude field maps; compare Magsat data to regional studies; study features of the core field; correlate globally and regionally Magsat and gravimetric data
Michael A. Mayhew	Business and Technological Systems, Incorporated	Magsat Anomaly Field Inversion and Interpretation for the U.S.	Construct a regional crustal temperature/heat flow model based on a developed magnetization model, heat flow/production data, and spectral estimates of the Curie depth
Michael A. Mayhew	Business and Technological Systems, Incorporated	Equivalent Source Modeling of the Main Field Using Magsat Data	Model the core field; compute equivalent spherical harmonic coefficients for comparison with other field models; examine the spectral content of the core field
Igor I. Gil Pacca	Instituto Astronomico e Geofisico—UPS, Brazil	Structure, Composition, and Thermal State of the Crust in Brazil	Construct preliminary crustal models in the Brazilian territory; point out possible variations in crustal structure among different geological provinces

Table 2 (continued)

LIST OF MAGSAT INVESTIGATORS

Investigator	*Institution/Country*	*Title*	*Objectives*
Thomas A. Potemra	The Johns Hopkins University Applied Physics Laboratory	A Proposal for the Investigation of Magsat and Triad Magnetometer Data to Provide Corrective Information on High-Latitude External Fields	Identify and evaluate high-latitude external fields from the comparison of data acquired by the Magsat and Triad spacecraft that can be used to improve geomagnetic field models
Robert D. Regan	Phoenix Corporation	Improved Definition of Crustal Magnetic Anomalies in Magsat Data	Develop an improved method for the identification of magnetic anomalies of crustal origin in satellite data by defining better and removing the most persistent external field effects
David P. Stern	NASA/Goddard Space Flight Center	Study of Enhanced Errors and of the Secular Magnetic Variation Using Magsat Models and Those Derived in Pogo Surveys	Estimate the secular variation over the period 1965-80 by removing mathematical instability based upon scalar field intensity alone
David W. Strangway	University of Toronto, Canada	Proposal to Analyze the Magnetic Anomaly Maps from Magsat over Portions of the Canadian and Other Shields	Examine the expected difference between the Grenville and Superior provinces
Ihn Jae Won	North Carolina State University	Compatibility Study of the Magsat Data and Aeromagnetic Data in the Eastern Piedmont of the U.S.	Evaluate the compatibility between the Magsat and aeromagnetic data in the eastern North Carolina Piedmont

satellite surveys will be needed for accurate global representations beyond the lifetime of Magsat.

Although Pogo data were global and taken over a short time span, the limitation of measuring only the field magnitude resulted in some ambiguity in the field direction in spherical harmonic analyses based on Pogo data alone.[3-6] This ambiguity is being removed by the acquisition of global vector data with Magsat.

The USGS is currently in the process of updating world and national magnetic charts and field models. Three sets of charts are being prepared: a U.S. chart of declination, a U.S. chart of total field intensity, and a set of world charts for all components. The declination chart was finalized in early 1980, the total intensity charts will be by the end of 1980, and the world charts by August 1981. Magsat data will contribute to all of these charts.

To provide timely input for all applications, a series of field models will be derived from data during magnetically quiet times over the period of data accumulation. One model has already been generated from two full days of data.[7] At appropriate intervals it will be updated with additional data, culminating in a final model incorporating all data with fine attitude coordinate accuracy, to be available about October 1981. Magsat data will also be combined with data from the Pogo satellites and other sources to derive predictive models with temporal terms.

Of the Magsat data currently available for analysis, November 5 and 6, 1979, showed the lowest value of magnetic activity indices. Plots of the data indicated that those days were indeed very quiet magnetically. Accordingly, a selection of 15,206 data points from those days was used to derive the first geomagnetic field model from Magsat, designated MGST (6/80).[7] The spherical harmonic coefficients are given in Table 3. Vector data above 50° latitude were not included because of non-curl-free fields from field-aligned currents. Such fields are transverse to the main field and, as shown by Langel,[2] have little or no effect on the field magnitude. However, 3354 values of B_r, 3345 of B_θ, and 3361 of B_ϕ were included for latitudes below 50°. (B_r, B_θ, and B_ϕ are the radial, north-south, and east-west components — in a spherical coordinate system — of the geomagnetic field.)

This model fits the selected data with the mean and standard deviations as follows:

Component	*Mean Deviation (nT)*	*Standard Deviation (nT)*
Scalar magnitude	0.1	8.2
B_r	2.5	6.5
B_θ	−0.1	7.6
B_ϕ	0.5	7.4

The deviations are mainly due to a combination of fields from unmodeled external and crustal sources.

As part of our preparation for Magsat, Pogo data were combined with surface data from observatories between 1960 and 1977, with selected repeat data, and with selected shipborne data to derive what we consider to be the best possible pre-Magsat model.[8] Constant and first-, second-, and third-derivative time terms were included to degree and order 13, 13, 6, and 4, respectively. This model, designated PMAG (7/80), used a new technique for dealing with the observatory data. As at

Table 3

SPHERICAL HARMONIC COEFFICIENTS FOR MAGSAT GEOMAGNETIC FIELD MODEL MGST (6/80)

Internal Coefficients (nT)

n	m	g_n^m	h_n^m	n	m	g_n^m	h_n^m
1	0	−29989.6		9	8	1.4	−5.9
1	1	−1958.6	5608.1	9	9	−5.1	2.1
2	0	−1994.8		10	0	−3.3	
2	1	3027.2	−2127.3	10	1	−3.5	1.4
2	2	1661.6	−196.1	10	2	2.5	0.4
3	0	1279.9		10	3	−5.3	2.6
3	1	−2179.8	−334.4	10	4	−2.1	5.6
3	2	1251.4	270.7	10	5	4.6	−4.2
3	3	833.0	−251.1	10	6	3.1	−0.4
4	0	939.3		10	7	0.6	−1.3
4	1	782.5	211.6	10	8	1.8	3.5
4	2	398.4	−256.7	10	9	2.8	−0.5
4	3	−419.2	52.0	10	10	−0.5	−6.2
4	4	199.3	−297.6	11	0	2.4	
5	0	−217.4		11	1	−1.3	0.7
5	1	357.6	45.2	11	2	−1.9	1.7
5	2	261.0	149.4	11	3	2.2	−1.1
5	3	−73.9	−150.3	11	4	0.1	−2.7
5	4	−162.0	−78.1	11	5	−0.4	0.6
5	5	−48.3	91.8	11	6	−0.3	−0.1
6	0	48.3		11	7	1.7	−2.4
6	1	65.2	−14.5	11	8	1.8	−0.3
6	2	41.4	93.4	11	9	−0.6	−1.4
6	3	−192.2	70.6	11	10	2.1	−1.6
6	4	3.5	−42.9	11	11	3.5	0.6
6	5	13.7	−2.4	12	0	−1.6	
6	6	−107.6	16.9	12	1	0.4	0.6
7	0	71.7		12	2	−0.1	0.6
7	1	−59.0	−82.4	12	3	−0.1	2.3
7	2	1.6	−27.5	12	4	0.6	−1.5
7	3	20.5	−4.9	12	5	0.5	0.5
7	4	−12.6	16.1	12	6	−0.6	0.2
7	5	0.6	18.1	12	7	−0.4	−0.4
7	6	10.6	−22.9	12	8	0.1	0.0
7	7	−2.0	−9.9	12	9	−0.4	0.0
8	0	18.4		12	10	−0.2	−1.5
8	1	6.8	6.9	12	11	0.7	0.3
8	2	−0.1	−17.9	12	12	0.0	0.7
8	3	−10.8	4.0	13	0	0.0	
8	4	−7.0	−22.3	13	1	−0.5	−0.4
8	5	4.3	9.2	13	2	0.3	0.4
8	6	2.7	16.1	13	3	−0.7	1.6
8	7	6.3	−13.1	13	4	0.0	0.0
8	8	−1.2	−14.8	13	5	1.2	−0.6
9	0	5.6		13	6	−0.4	−0.1
9	1	10.4	−21.1	13	7	0.4	0.8
9	2	1.1	15.2	13	8	−0.6	0.2
9	3	−12.6	8.9	13	9	0.2	0.8
9	4	9.5	−4.8	13	10	0.1	0.5
9	5	−3.3	−6.5	13	11	0.4	−0.1
9	6	−1.3	9.0	13	12	−0.4	0.0
9	7	6.8	9.5	13	13	0.0	−0.1

External Coefficients (nT)

n	m	$\bar{g}_n^m$	$\bar{h}_n^m$
1	0	20.4	
1	1	−0.6	−0.4

The mean radius of the earth is 6371.2 km
The mean epoch is 1979.85

the satellite, surface fields contain contributions from the three sources. For field modeling the annual mean value for each observatory is usually used so that the external contribution is some averaged value (we hope, small). However, crustal anomaly fields are typically quite large. For past models the rms residual of surface data to the model has been typically between 100 and 200 nT.[9] We have incorporated a procedure for solving independently for the "bias" or anomaly field in each component at each observatory. This procedure was used for the first time in the derivation of the PMAG (7/80) model. After solving for the coefficients of the potential function and the observatory biases, the rms residual of the observatory data was reduced to below 28 nT for all components. For repeat data this procedure was not feasible because of a lack of extensive temporal coverage. These data were incorporated by including only locations where three or more measurements, made at different times, were available. Each component at each location was then represented by a linear fit; only the rate of change was used in deriving PMAG (7/80). The residual to the fit was 10 nT per year for all components. For shipborne data, 39 long tracks in regions devoid of other surface measurements were selected. These were low-pass filtered with a cutoff of 500 km to eliminate the crustal anomaly field. The rms residual to the fit was 38 nT. Extension of this model by the addition of Magsat data does not change the above quoted residuals a great deal, and the resulting model, GSFC (9/80), is in good agreement with MGST (6/80) at the Magsat epoch.

Using quick-look data from the first few days of Magsat operation, various pre-Magsat models were evaluated. These results are summarized in Table 4.

Global geomagnetic models will be undertaken by the USGS (Cain, Fabiano) and by the French investigators under the direction of LeMouel and the British investigators under the direction of Barraclough. The USGS investigators, in addition to publishing charts of the field, will pay particular attention to the problem of separating the core, crustal, and external contributions to the field, and of developing an adequate mathematical representation of each. The French and British will attempt a very accurate model of secular variation for predicting the field in the future and for studying properties of core fluid motions and interactions at the core/mantle boundaries. In addition to the global models, several investigators will attempt more accurate regional models for particular areas in order to isolate better the crustal anomaly fields in those areas.

Magsat will provide an accurate model of the main geomagnetic field, but its lifetime was too short for determining the secular variation of the field. The secular variation can be determined through comparison with earlier global surveys of the geomagnetic field from space, but such surveys are known to suffer from enhanced errors in certain sequences of harmonic terms. Stern (GSFC) will use the Magsat model to evaluate the extent of such enhanced errors, correct them, and then use the corrected models for deriving the mean secular variation over the 1965-1980 period.

Gibbs (Business and Technological Systems) will attack the secular variation problems from a statistical point of view by using recursive estimation theory to combine conventional models into optimal estimates of the field parameters for any given time. The statistical information so derived should enable a more accurate prediction capability as well as more accurate *a posteriori* models.

An alternative to the classical spherical harmonic representation will be attempted by Mayhew (Business and Technological Systems). He will

Table 4

RESIDUALS OF SELECTED MAGSAT DATA TO SOME PUBLISHED FIELD MODELS (nT)

	POGO (2/72)[10]	*IGRF 1975*[11]	*AWC/75*[12]	*IGS/75*[13]	*WC80*[14]	*PMAG (7/80)*[8]
Scalar: mean deviation	9	−91	60	21	−21	−2
standard deviation	105	124	125	119	117	79
rms deviation	105	154	139	121	119	82
B_r: mean deviation	6	12	25	20	31	13
standard deviation	208	192	152	134	121	93
rms deviation	208	192	154	135	125	94
B_θ: mean deviation	18	51	−4	15	22	33
standard deviation	114	108	93	84	89	59
rms deviation	115	120	94	86	92	67
B_ϕ: mean deviation	0	1	2	0	1	1
standard deviation	165	125	89	89	61	61
rms deviation	165	125	89	89	61	61

adopt methods of anomaly modeling by equivalent sources, representing the main field with an array of dipoles at a fixed radius within the core. If such a method proves feasible, it will potentially use less computer time than the usual methods.

CRUSTAL MAGNETIC ANOMALY INVESTIGATIONS

A crustal magnetic anomaly is the residual field after estimates of the core and external fields have been subtracted from the measured field. An anomaly map is a contour map of the measured average anomaly field at the altitude of the data. Anomaly maps have been derived from aeromagnetic and shipborne data for many years and used in the construction of geologic/geophysical models of the crust. Investigations with aeromagnetic and shipborne magnetic data have mainly concentrated on the very localized anomalies associated with small-scale geologic features and localized mineralization. However, in the past few years there has been an increased interest in studies of the broad-scale anomalies that appear in regional compilations of aeromagnetic and shipborne data.[15-19] Satellite anomaly maps are of recent origin and describe only the very broadest scale anomalies. Aeromagnetic and shipborne anomaly maps have usually been interpreted assuming a flat earth and a constant ambient field over the region of interest. Because of the extremely large scale of satellite-derived anomalies, both of these assumptions become invalid, thus necessitating development of new analysis techniques.

Originally, it was thought impossible to detect fields of crustal origin in satellite data. However, while analyzing data from the Pogo satellites, Regan *et al.*[20] discovered that the lower altitude data contained separable fields caused by crustal anomalies, thus opening the door to a new class of investigations. None of the satellites shown in Table 1 was designed for solid earth studies, yet results from the Pogo satellites have demonstrated the capability of mapping broad-scale anomalies. Although the map of Regan *et al.* was partially contaminated by "noise" from magnetospheric and ionospheric fields, the reality and crustal origin of several of the anomalies defined by the map were clearly demonstrated. More recently Langel *et al.*[10] have compared a Pogo-derived anomaly map with upward-continued aeromagnetic data from western Canada. Figure 1 shows the results of that comparison. The two maps are in substantial agreement, demonstrating further both the reality and crustal origin of the anomalies.

The techniques for preparing such a map include selecting suitable quiet-time data, removing the best estimate of the fields not originating in the earth's crust, and averaging data at the appropriate resolution. It is believed that these techniques can be readily adapted to Magsat data, both scalar and vector. It will be some months before an anomaly map is available from Magsat data. Individual pass residuals, however, clearly show the presence of

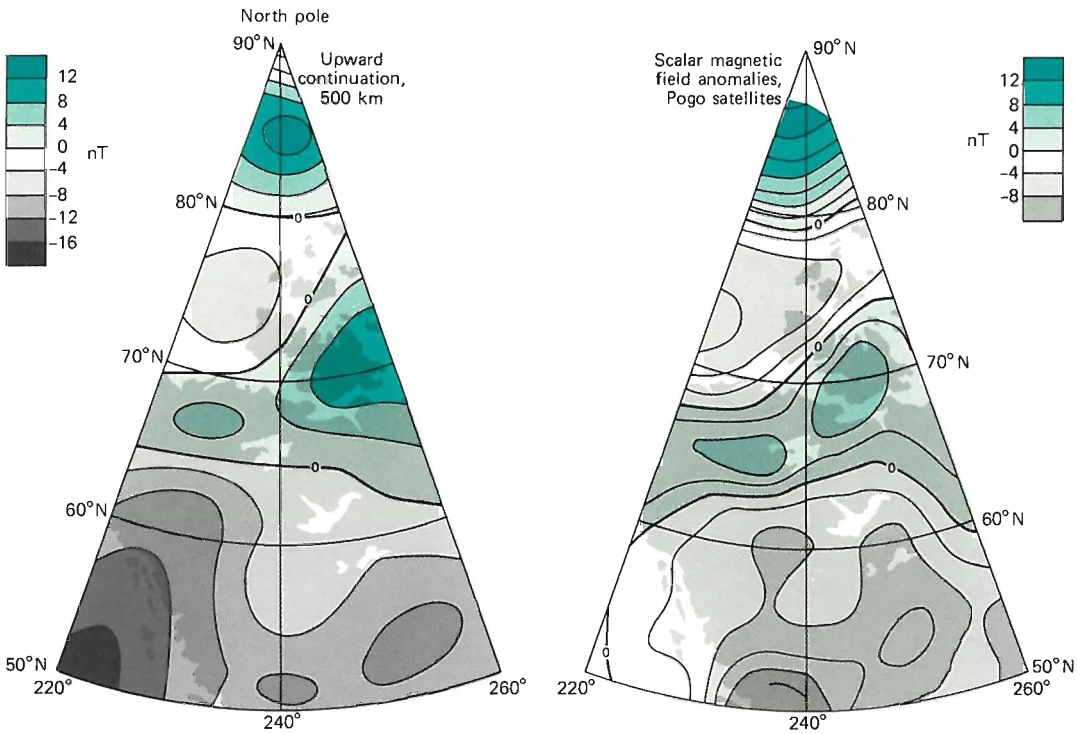

Fig. 1—Comparison of anomaly maps from upward continued aeromagnetic data and from Pogo data. Units are nanoteslas (nT).

these crustal fields. Figure 2, for example, shows the Bangui or Central African anomaly first discovered by Regan *et al.*[20]

The basic anomaly maps are only a starting point for interpretation. To maximize their usefulness they must be transformed to a common altitude and to the anomalies that would be present if the earth's field had the same inclination everywhere (reduction to a common inclination). Preliminary techniques for reduction to common altitude now exist and have been applied to Pogo data between ±50° latitude. The resulting map is shown in Fig. 3.

For geologic studies such anomaly maps must be inverted to a description of the magnetic properties of the crustal rocks. The inversions are not unique; constraints from other data sources will be required in their interpretation. As a first step in such modeling, traditional equivalent source methods, adapted for the case of a spherical earth with changing field inclination, have been applied to the United States[21] and Australia.[22] This technique assumes a constant 40 km thickness of the magnetic crust and derives the magnetization in such a crust that would cause the anomalies seen at the spacecraft. All of the anomalous field is assumed to be induced; i.e., remanent magnetization is assumed to be zero. The results for the United States are shown in Fig. 4. In many regions, known geologic features are clearly outlined (e.g., the Basin and Range Province, Colorado Plateau, Rio Grande Rift, Michigan Basin, and Mississippi Embayment) whereas some features are notable by the absence of magnetic features (e.g., the mid-continent gravity high). It will be some years before these maps are fully understood and interpreted, but they promise to shed new light on the geology of the deep crust.

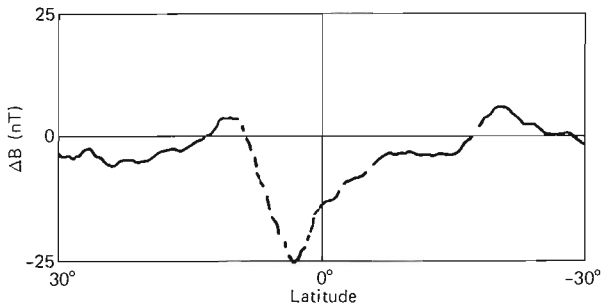

Fig. 2—The Bangui or Central African anomaly as seen in Magsat data. The equatorial longitude is 14.6°; the altitude is 425 km. ΔB is the residual anomalous field after subtracting a model of the core field from the measured field.

Anomaly maps, or even magnetization maps, are not an end in themselves. The object of these efforts is to derive models of the crust and upper mantle for large-scale regions of the globe. There are many kinds of models; their common purpose is to generalize observations and prediction. Through synthesis of particular models, complex models of crustal geologic systems are built up in terms of structural and compositional variations and the movements of material and energy. Conclusions can then be drawn about the evolution of regions that lead to inferences about the distribution of natural resources.

Figure 5 is an outline of an example of how one might think of the process of synthesizing models, beginning with satellite magnetic field data and including correlation with other data types. Models of gross variations in mean magnetization to the Curie isotherm can be developed from satellite data. This serves to quantify the anomaly map and can be of great utility in more detailed analysis of the data. Correlatively, from gravity measurements, variations in mean density to some fixed depth can be inferred, assuming homogeneity below that depth. These models can be combined with velocity

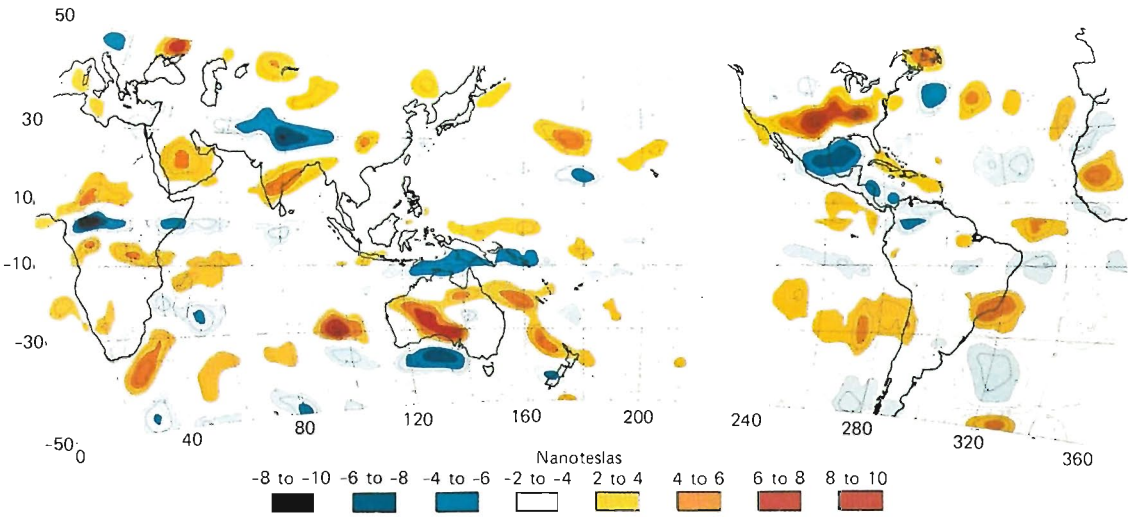

Fig. 3—Scalar magnetic anomaly map from the Pogo satellites reduced to 500 km altitude.

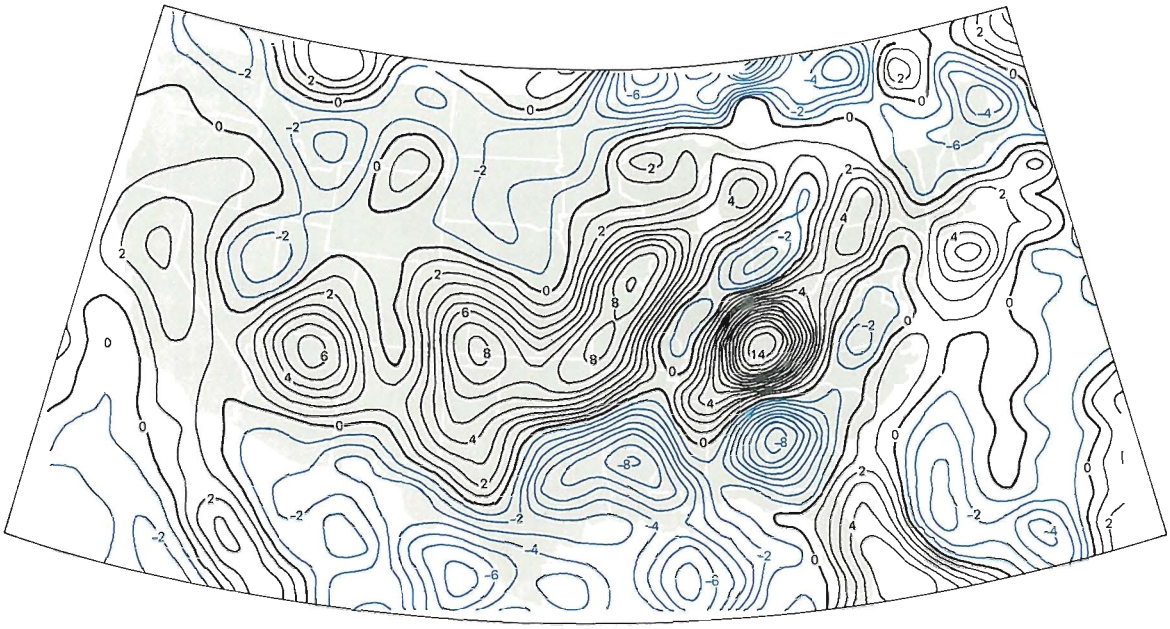

Fig. 4—Equivalent bulk magnetization derived from Pogo satellite data assuming a constant-thickness magnetic crust of 40 km. Units are EMU/cm^3 × 10^4.

models based on seismic data and with compositional models based on laboratory measurements of rock properties to give large-scale models of crustal structure and composition. Similarly, models of relative movements and of temperature distribution can be built for very large regions. These large-scale models can then be used to make more detailed models for smaller regions using a variety of data, some of which are also listed in Fig. 5. There are no hard and fast rules about the combination sequence, which depends on the region and the data available. Further, the process is an iterative one in which new data are sought based on predictions from interim models.

The Pogo satellites from which these maps were derived had two severe limitations for the studies: the altitude range was high (most data were from above 500 km), and the data were of field magnitude only. Magsat addresses both shortcomings. Its lower altitude increases the resolution by roughly a factor of 2 and the field strength of the anomalies by a factor of between 2 and 5, depending on the geometry of the source region. This is dramatically illustrated in Fig. 6, which shows a comparison between the lowest altitude Magsat data and low-altitude Pogo data. The Magsat data are at 187-191 km, while the Pogo data are at 414-420 km. The tracks are nearly coincident geographically.

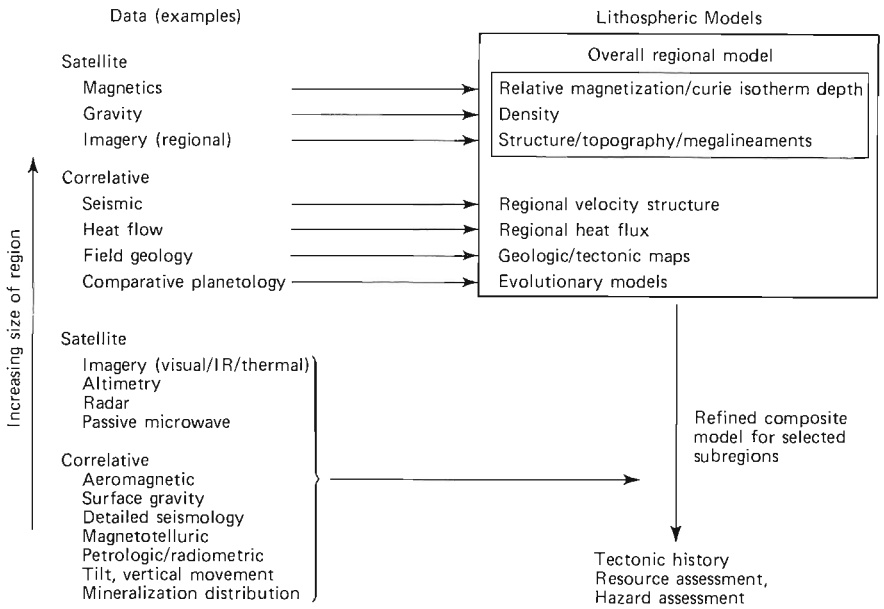

Fig. 5—Synthesis of geologic/geophysical models (idealized outline).

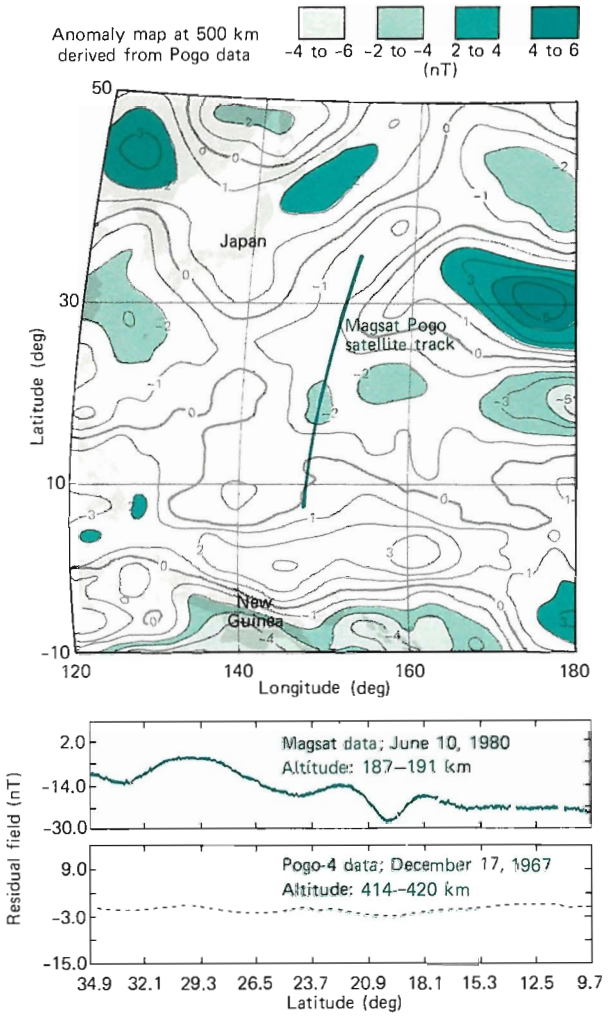

Fig. 6—Comparison between Pogo (OGO-4) data and the lowest altitude data from Magsat.

Magsat's lower altitude greatly enhances the resolution and signal strength of the anomalies. With field magnitude data, only indirect estimates of remanent magnetization are possible.[23] The vector data from Magsat measure anomaly directions other than along the earth's main field.

GSFC will derive a basic global magnetic anomaly map from the Magsat data. Many investigators will use that map or the associated magnetization map directly in their investigations. Other investigators will reexamine the basic derivation of the anomaly map and seek to extend or modify these techniques. Among the latter are:

Investigator	*Region Investigated*
Bhargava	India
Fukushima	Japan and vicinity
Coles and Hall	Canada
Hinze and Keller	South and Central America
Mayhew	United States
Johnson and Dooley	Australia and Antarctica
LeMouel	Europe and Central Africa

This type of modeling will be used by the investigators just listed for the continent-size regions indicated. When the larger region has been modeled, features of particular interest will become the subject of more intensive investigations. In some cases existing tectonic features have already been singled out for more localized modeling, such as the Narmada-son lineament in central India (Bhargava), the Superior province of Canada (Strangway), or the Japan Trench (Fukushima).

Continental-scale studies will utilize maps made at GSFC, including those of Pacca (Brazil), Bentley (Antarctica), and Hastings (Africa and South America).

Mayhew, Hinze, Coles, and Pacca will pay particular attention to mapping the Curie isotherm. Hinze, Keller, and Hastings are interested in the implications of the Magsat data for the plate-tectonic reconstruction of Africa and South America, a topic now under study by Langel, Frey, and Mead at GSFC using the Pogo data.

In addition to the continental-scale studies, several investigators will study more limited areas or particular tectonic features. Godivier (ORSTOM) will extend the work of Regan and Marsh[24] in the region around the Central African Republic where ORSTOM has a large amount of correlative data. Gasparini (Osservatorio Vesuviano) will investigate the Curie depth and volcanism in the Mediterranean area. Won (North Carolina State University) will study a combination of Magsat, aeromagnetic, and regional gravity data in the eastern Piedmont of the United States. Carmichael and associates (University of Iowa) will study the central midcontinent of the United States with particular attention to the known midcontinent geophysical anomaly.

In contrast to the large number of investigators studying continental-type regions, only three investigators are giving concentrated attention to oceanic regions. There are several reasons for this. First, the satellite anomaly maps derived from Pogo data show very few anomalies in oceanic regions compared to continental regions. Second, theoretically, the thinner oceanic crust should not contain anomalous features of comparable size to continental crust. Harrison (University of Miami) notes that a minimum in the power spectrum should occur between the contributions from core and crustal sources but that such a minimum is not present in spectra from shipborne data over oceanic basins. He will use Magsat data to study the intermediate wavelength anomalies. Brammer (TASC) will concentrate his efforts on a study of Magsat and Geos-3 altimeter gravity data in the eastern Indian Ocean.

LaBreque (Lamont-Doherty) will organize the ex-

isting shipborne data in an effort to help describe the secular variation over oceanic areas and to provide surface anomaly maps suitable for upward continuation and comparison with Magsat data.

Underlying all crustal models derived from Magsat and correlative data is a need for understanding the basic magnetic properties of crustal rocks. Such understanding depends on careful laboratory measurements, some at the higher temperatures and pressures of the lower crust. Preliminary studies[25] have already claimed to show the extremely significant result that the Moho is a magnetic boundary even when the Curie isotherm lies in the mantle. Wasilewski and the other GSFC investigators are continuing these efforts. Particular attention to petrologic constraints, the effects of oxygen fugacity, and other properties will be given by Haggerty (University of Massachusetts). A substantial refinement of the petrology of source rocks responsible for deep crustal anomalies is expected.

INVESTIGATIONS OF THE INNER EARTH

Man has directly penetrated only a few kilometers of the 6371 km distance to the earth's center. Information about the inner earth must be obtained by indirect methods such as seismology and measurements of the gravitational and magnetic fields.

Combining Magsat data with Pogo and near-surface surveys will permit more accurate determination of the secular variation of the core field. This variation will be used by Benton (University of Colorado) to study properties of the fluid motions in that core; in turn, appropriate magnetohydrodynamic constraints will be investigated to determine if they can aid in better modeling the secular variation.

When they are time-varying, magnetospheric fields result in induced fields within the earth because of the finite conductivity of the earth. The characteristics of these induced fields are determined by the properties of the materials in the earth's mantle (i.e., composition, temperature). At present the limiting factor in determining a precise conductivity profile within the earth, with adequate spatial resolution, is the accuracy possible in determining the external and induced fields. Hermance (Brown University) will use Magsat vector measurements together with surface data for a more accurate analysis than was previously possible.

STUDIES OF EXTERNAL CURRENT SYSTEMS

Early observers of the earth's magnetic field discovered that it continually undergoes transient changes. These changes include systematic variations that occur with daily regularity and irregular variations, both of amplitude and of a totally different kind, superimposed on the regular variations. Periods of time when the changes are mostly regular are called magnetically quiet; periods when the magnetic disturbances become irregular are called magnetically disturbed. When the irregular fields are large but mainly confined to high latitude, the condition is called a magnetic substorm; when the irregular fields are large and worldwide, it is called a magnetic storm. To understand such changes in field, one must realize that the space surrounding the earth contains several "species" of electric current. The energy for these currents comes ultimately from the sun. Figure 7 is an artist's conception (based on Fig. 1 of Heikkila,[26] wherein there is a more detailed explanation) of the magnetic environment of the earth. A stream of charged particles from the sun, called the solar wind, confines the earth's magnetic field to a cavity known as the magnetosphere. This cavity is compressed on the front, or sunward, side and drawn

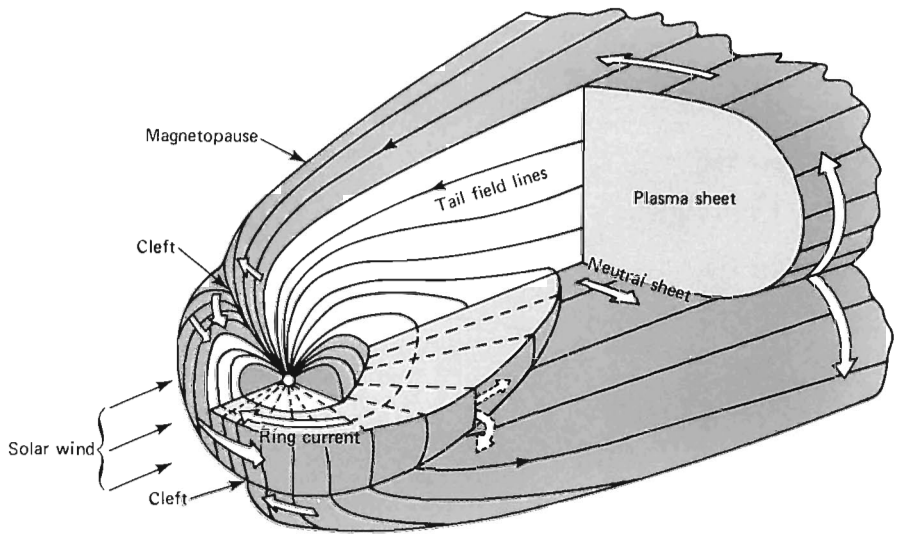

Fig. 7—Artist's conception of the configuration of the magnetosphere, adapted from Heikkila.[26] The magnetosphere is the region into which the earth's magnetic field is confined by the solar wind.

out in a "tail" to the antisunward side. Currents flow, as shown, on the boundaries of this cavity and across the tail. Also, trapped particles within the cavity flow in a "ring current" in a westward direction around the equatorial plane. Most of these currents are relatively distant from the earth and cause only small fields at Magsat locations. However, the ring current intensifies considerably during periods of magnetic disturbance and causes substantial fields at Magsat altitude.

In addition to the currents shown in Fig. 7, a variety of currents flow in the conducting layer of the atmosphere known as the ionosphere. The regular daily variations of the field observed at the surface are from such a current system, known as Sq (S for solar daily variation and q for quiet times). Sq is mainly a low- and mid-latitude phenomenon. At high latitudes very intense currents flow, often associated with auroral phenomena. These currents, illustrated schematically in Fig. 8,[27] are coupled to the ring current and to currents in the tail of the magnetosphere.

Because the Magsat orbit was near sun-synchronous, it sampled mainly twilight local times, a distinct disadvantage for synoptic studies of the magnetospheric fields, which are relatively fixed in local time. However, because it is the first near-earth satellite to obtain global vector measurements and because its measurement accuracy far exceeds that of spacecraft that obtained some near-earth vector measurements, Magsat will be very useful in extending previous research regarding current systems.

One reason for investigating these external current systems with Magsat is to aid in isolating their fields from the core and crustal fields. Several investigators will contribute to this effort. Regan (Phoenix Corp.) in particular will work toward removing external field effects from anomaly data.

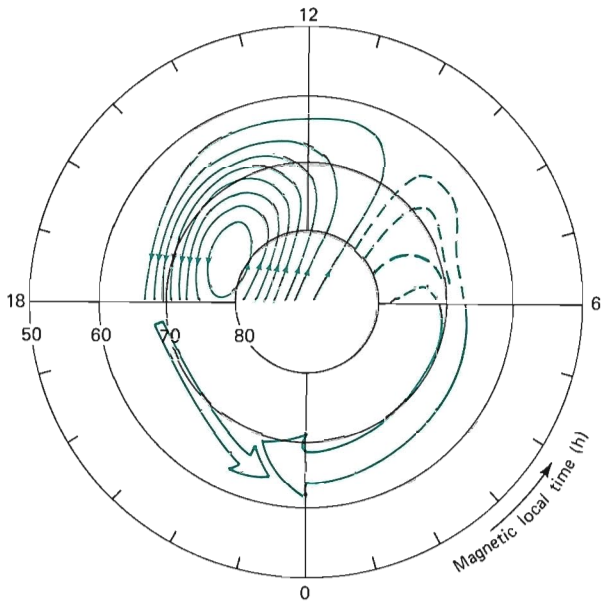

Fig. 8—Conceptual drawing of ionospheric current flow at high altitudes. Arrows indicate direction of current flow. Closure is not shown because some circuits close in the outer magnetosphere via field-aligned current.

Klumpar (University of Texas) will concentrate his effort on extending existing models for high-latitude ionospheric currents and the field-aligned currents coupling the ionospheric currents to the magnetosphere. Burrows (NRC, Canada) and Potemra (The Johns Hopkins University Applied Physics Laboratory) will investigate the field-aligned currents, also using correlative data from satellite photographs of auroral phenomena (Burrows) and with simultaneous data from the Triad satellite (Potemra).

Figure 9 shows the effects of field-aligned cur-

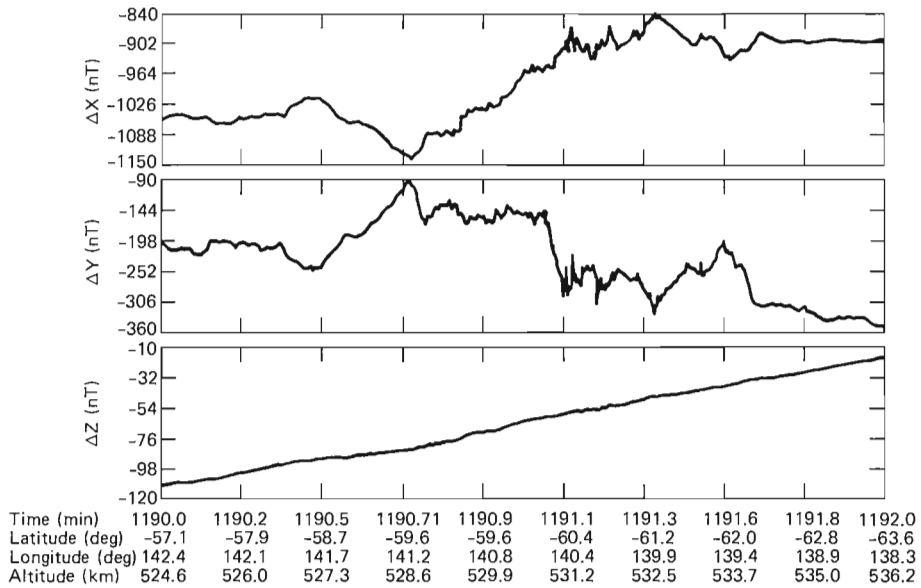

Time (min)	1190.0	1190.2	1190.5	1190.71	1190.9	1191.1	1191.3	1191.6	1191.8	1192.0
Latitude (deg)	-57.1	-57.9	-58.7	-59.6	-59.6	-60.4	-61.2	-62.0	-62.8	-63.6
Longitude (deg)	142.4	142.1	141.7	141.2	140.8	140.4	139.9	139.4	138.9	138.3
Altitude (km)	524.6	526.0	527.3	528.6	529.9	531.2	532.5	533.7	535.0	536.2

Fig. 9—Magnetic field variation caused by field-aligned current. The scale, in nT, is relative only.

rents in Magsat data. ΔX, ΔY, ΔZ are residuals from a field model in a north-, east-, and down-coordinated system. Large-amplitude, highly structured variations occur in the north and east directions but not in the vertical direction, as expected from field-aligned currents.

CONCLUSION

Satellite-based magnetic field measurements make global surveys practical for both field modeling and for the mapping of large-scale crustal anomalies. They are the only practical method of accurately modeling the global secular variation. Magsat is providing a significant contribution, both because of the timeliness of the survey and because its vector measurement capability represents an advance in the technology of such measurements.

Data from Magsat are available for any interested user through the National Space Sciences Data Center at GSFC.

With the success of Magsat, future missions should take two courses. Field modeling requires periodic surveys, but not low-altitude measurements as required for crustal studies. On the other hand, further advances in satellite crustal studies will rest on NASA's ability to orbit magnetometers at still lower altitudes; such concepts are still in the stage of discussions as to their feasibility.

REFERENCES

[1]J. C. Cain and R. A. Langel, "Geomagnetic Survey by the Polar-Orbiting Geophysical Observatories," *World Magnetic Survey 1957–1969* (A. J. Zmuda, ed.) IAGA Bulletin No. 28 (1971).

[2]R. A. Langel, "Near Earth Magnetic Disturbance in Total Field at High Latitude, 1. Summary of Data from OGO 2, 4, and 6," *J. Geophys. Res.* **79**, pp. 2363 – 2371 (1974).

[3]G. E. Backus, "Nonuniqueness of the External Geomagnetic Field Determined by Surface Intensity Measurements," *J. Geophys. Res.* **75**, pp. 6339 – 6341 (1970).

[4]L. Hurwitz and D. G. Knapp, "Inherent Vector Discrepancies in Geomagnetic Main Field Models Based on Scalar F," *J. Geophys. Res.* **74**, pp. 3009 – 3013 (1974).

[5]D. P. Stern and J. H. Bredekamp, "Error Enhancement in Geomagnetic Models Derived from Scalar Data," *J. Geophys. Res.* **80**, pp. 1776 – 1782 (1975).

[6]F. J. Lowes, "Vector Errors in Spherical Harmonic Analysis of Scalar Data," *Geophys. J. Roy Astron. Soc.* **42**, pp. 637 – 651 (1975).

[7]R. A. Langel, R. H. Estes, G. D. Mead, E. B. Fabiano, and E. R. Lancaster, "Initial Geomagnetic Field Model from Magsat Vector Data," *Geophys. Res. Lett.* (in press).

[8]R. A. Langel, R. H. Estes, G. D. Mead, and E. R. Lancaster, "A Model of the Earth's Magnetic Field, 1960 – 1980" (in preparation).

[9]J. C. Cain, S. J. Hendricks, R. A. Langel, and W. V. Hudson, "A Proposed Model for the International Geomagnetic Reference Fields – 1965," *J. Geomagn. Geoelectr.* **19**, pp. 335 – 355 (1967).

[10]R. A. Langel, R. L. Coles, and M. A. Mayhew, "Comparisons of Magnetic Anomalies of Lithospheric Origin as Measured by Satellite and by Airborne Magnetometers over Western Canada," *Can. J. Earth Sci.* **XVII**, pp. 876 – 887 (1980).

[11]IAGA Division I Study Group, "International Geomagnetic Reference Field 1975," *EOS*, **57**, pp. 120 – 121 (1976).

[12]D. R. Barraclough, J. M. Harwood, B. R. Leaton, and S. R. C. Malin, "A Model of the Geomagnetic Field at Epoch 1975" *Geophys. J. R. Astron. Soc.*, **43**, pp. 645 – 659 (1975).

[13]N. W. Peddie and E. B. Fabiano, "A Model of the Geomagnetic Field for 1975," *J. Geophys. Res.* **81**, pp. 1539 – 2542 (1976).

[14]F. S. Baker and D. R. Barraclough, "World Magnetic Chart Model for 1980," *EOS* **61**, p. 453 (1980).

[15]L. C. Pakiser and I. Zietz, "Transcontinental Crustal and Upper Mantle Structure," *Rev. Geophys.* **3**, pp. 505 – 520 (1965).

[16]I. Zietz, E. R. King, W. Geddes, and E. G. Lidiak, "Crustal Study of a Continental Strip from the Atlantic Ocean to the Rocky Mountains," *Geolog. Soc. Am. Bull.* **77**, pp. 1427 – 1448 (1966).

[17]R. T. Shuey, D. R. Schellinger, E. H. Johnson, and L. G. Alley, "Aeromagnetics and the Transition between the Colorado Plateau and the Basin Range Province," *Geology* **1**, pp. 107 – 110 (1973).

[18]D. H. Hall, "Long-Wavelength Aeromagnetic Anomalies and Deep Crustal Magnetization in Manitoba and North Western Ontario, Canada," *J. Geophys.* **40**, pp. 403 – 430 (1974).

[19]A. A. Kruithovskaya and I. K. Paskevich, "Magnetic Model for the Earth's Crust under the Ukrainian Shield," *Can. J. Earth Sci.* **14**, pp. 2718 – 2728 (1977).

[20]R. D. Regan, J. C. Cain, and W. M. Davis, "A Global Magnetic Anomaly Map," *J. Geophys. Res.* **80**, pp. 794 – 802 (1975).

[21]M. A. Mayhew, "Satellite Derived Equivalent Magnetization of the United States" (in preparation, 1979).

[22]M. A. Mayhew, B. D. Johnson, and R. A. Langel, "Magnetic Anomalies at Satellite Elevation over Australia" (submitted to *Earth Planet. Sci. Lett.*, 1980).

[23]B. K. Bhattacharyya, "Reduction and Treatment of Magnetic Anomalies of Crustal Origin in Satellite Data," *J. Geophys. Res.* **82**, pp. 3379 – 3390 (1977).

[24]R. D. Regan and B. D. Marsh, "The Bangui Anomaly: Its Geological Origin," *J. Geophys. Res.* (in press).

[25]P. J. Wasilewski, H. H. Thomas, and M. A. Mayhew, "The Moho as a Magnetic Boundary," *Geophys. Res. Lett.* **6**, pp. 541 – 544 (1979).

[26]W. J. Heikkila, "Penetration of Particles into the Polar Cap Regions of the Magnetosphere," *Critical Problems of Magnetospheric Physics* (E. R. Dyer, ed.), IUCSTP Secretariat (1972).

[27]R. A. Langel, "Near Earth Magnetic Disturbance in Total Field at High Latitude, 2. Interpretation of Data from OGO 2, 4, and 6," *J. Geophys. Res.* **79**, pp. 2373 – 2392 (1974).

ACKNOWLEDGMENTS — I wish to thank all members of the Magsat team for making possible the acquisition and analysis of these data. Although it is not feasible to name all those included, my special thanks go to Gil Ousley of GSFC and L. D. Eckard of APL for directing the effort that culminated in the successful construction, launch, and operation of Magsat; to Mario Acuna and W. H. Farthing for the design and oversight of the magnetometers; to John Berbert and Earl Beard of GSFC and Don Berman of Computer Science Corporation and their colleagues for their efforts at data preparation; and to Locke Stuart and his team at GSFC for their successful organization of and interface with the Magsat investigators. Finally, I particularly appreciate the encouragement, advice, and general support of Gil Mead, Lou Walter, and Barbara Lueders of the GSFC Geophysics Branch.

THOMAS A. POTEMRA

STUDIES OF AURORAL FIELD-ALIGNED CURRENTS WITH MAGSAT

Electric currents that flow between the outermost boundaries of the magnetosphere and the auroral zones, sometimes deliver more power to the earth than is generated in the entire United States at any given time. These field-aligned "Birkeland" currents are detected on a regular basis by Magsat.

INTRODUCTION

Following earlier suggestions by Edmund Halley and Anders Celsius that the auroral phenomena behave magnetically, Kristian Birkeland discovered in his polar expeditions of 1902-03 that large-scale currents were associated with the aurora. He was also the first to suggest that these currents originated far from the earth and that they flowed into and away from the polar atmosphere along the geomagnetic field lines. The existence of such field-aligned currents was widely disputed because it was not possible from a study of only surface magnetic field measurements to distinguish unambiguously between current systems that are field aligned[1] and those that are completely ionospheric.[2] Furthermore, theoretical calculations[3,4] predicted that the effects of field-aligned currents may be impossible to detect with ground-based magnetometers for certain models of these current systems.

The first experimental confirmation of the presence of field-aligned ("Birkeland") currents was provided by A. J. Zmuda and his colleagues[5,6] who studied magnetic disturbances in the polar regions of the earth, observed with the single-axis magnetometer used in the attitude determination system on the APL/U.S. Navy 5E-1 (1963-38C) satellite. That satellite, launched on September 28, 1963, into a nearly circular polar orbit at an altitude of 1100 km, carried an array of particle detectors and a fluxgate magnetometer.[7]

Zmuda[5,6] discovered that disturbances normal to the main geomagnetic field were often observed with 5E-1 in the same region of the earth associated with a variety of auroral phenomena. It was soon realized that the transverse disturbances could be interpreted as being caused by electric currents flowing along the geomagnetic field lines, and thus the first study of the global characteristics of Birkeland currents was begun at APL.

Recognizing the importance of sensitive satellite magnetic field measurements to the study of Birkeland currents, Armstrong and Zmuda[8] suggested a modification to the attitude magnetometer system for the APL/U.S. Navy Triad satellite. The Triad satellite was launched into a polar orbit at an altitude of 800 km on September 2, 1972, and, until the launch of Magsat on October 30, 1979, was the only satellite making continuous and high-resolution magnetic observations in the polar regions. The Triad magnetometer provides 2.25 vector samples per second with a resolution of 12 nanoteslas (1 nT = 10^{-9} weber per square meter), made possible by the 13-bit analog-to-digital converter incorporated into the system following the suggestion of Armstrong and Zmuda. The Triad magnetic field observations were used to determine for the first time the flow directions, spatial distribution, and intensities of Birkeland currents and their relationships to a variety of geophysical phenomena such as optical emissions, current-driven plasma instabilities, ionospheric currents, geomagnetic storms, and interplanetary phenomena. During its brief lifetime, the improved Magsat magnetic field observations were correlated with the Triad observations to compile more information about the important Birkeland currents and to calibrate the Triad magnetometer. Fortunately for these studies, Magsat was launched near the time of the peak solar cycle (the largest in many 11-year cycles) so that disturbances produced by the Birkeland currents were observed on almost every orbit.

The importance of Birkeland currents to the coupling between outer space and the auroral atmosphere is emphasized by their total intensity, which ranges between 10^6 and 10^7 A, and by the energy they dissipate in the upper atmosphere, which can exceed by a considerable factor the energy deposition associated with the dramatic, visual, auroral forms. The Birkeland currents are also the critical ingredient in a variety of complicated plasma phenomena that have important applications to earth (associated with substorms and the aurora), to Jupiter (associated with Io-related radio emissions),[9,10] and to the galaxy (related to comets and double radio sources).[11]

MAGNETIC DISTURBANCES AND FIELD-ALIGNED CURRENTS

The magnitude and direction of equivalent currents associated with magnetic disturbances, $\Delta\vec{B}$, are determined from the relationship $\vec{J} = (1/\mu_0)$ curl $\Delta\vec{B}$. The disturbances occur predominantly in the east-west (geomagnetic) direction so that $J = (1/\mu_0)(\partial/\partial x)\ \Delta By$, where J is the density of the field-aligned current, x is positive in the northward direction, and ΔBy is the observed disturbance in the east-west direction.[12,13] In this case, the formula is the same as that for the transverse magnetic disturbance due to current sheets of infinite longitudinal extent. At the altitude of Triad, a change in By equal to 100 nT over 1° of latitude is equivalent to a field-aligned current density of 0.64 μA/m^2. The magnitude of the current intensity, $\int Jdx$, is given directly by the amplitude of the magnetic disturbance ΔBy by $\int Jdx = (1/\mu_0)\ \Delta By$. A 100 nT disturbance corresponds to a current intensity of 0.08 A/m.

An example of a transverse magnetic disturbance often observed with Triad is shown in Fig. 1 (from Ref. 13) with the deduced field-aligned current density and intensity.

PRINCIPAL CHARACTERISTICS OF BIRKELAND CURRENTS

Large-scale Birkeland currents are concentrated in two principal areas that encircle the geomagnetic pole.[12-16] Figure 2 is a summary of the average spatial distribution in the northern high-latitude region determined from 493 Triad passes during weakly disturbed geomagnetic conditions and 366 Triad passes during an active period (from Ref. 16.) The Birkeland current flow regions have been arbitrarily designated by Iijima and Potemra [14,15] as

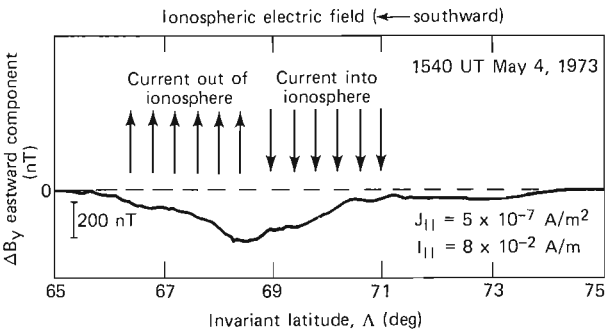

Fig. 1—An example of a magnetic disturbance transverse to the geomagnetic field measured by Triad on May 4, 1973 (from Zmuda and Armstrong[13]). The density and flow direction of the field-aligned currents producing these disturbances are determined from Maxwell's equation $\vec{J} = (1/\mu_0)$ curl $\Delta\vec{B}$ in the manner described in the text. The direction of the appropriate electric field, also shown, can produce a southward current flowing horizontally in the ionosphere to couple the upward and downward flowing field-aligned currents.

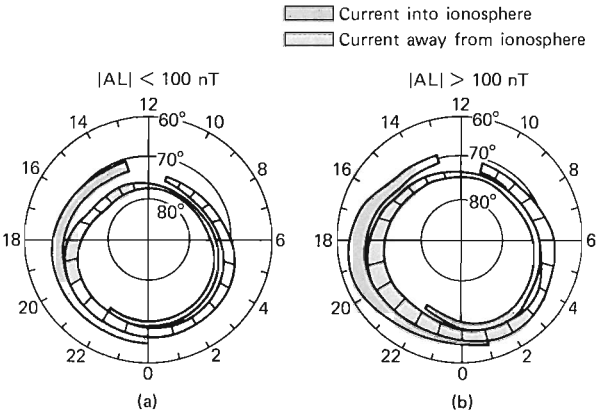

Fig. 2—Statistical distributions of the location and flow directions of large-scale Birkeland currents during weakly disturbed geomagnetic conditions (a) and during disturbed periods (b) (from Ref. 16).

Region 1 located at the poleward side and Region 2 located at the equatorward side. The Region 1 Birkeland currents flow into the ionosphere in the morning sector and away from the ionosphere in the evening sector, whereas the Region 2 currents flow in the opposite direction at any given local time. The basic flow pattern of Birkeland currents remains unchanged during geomagnetically inactive and active periods (Fig. 2), although the regions widen and shift to lower latitudes during disturbed periods (similar to optical auroral forms by Feldstein[17]).

Figure 3 (from Ref. 18) is a schematic diagram of the large-scale Birkeland currents that flow into and away from the auroral regions shown in Fig. 2 and form cone-shaped regions. The current flow reverses direction near midnight and near noon. This current system is permanent, with the total amplitude ranging between 10^6 and 10^7 A, depending on the solar-terrestrial conditions. The striking visual forms of the aurora occur only when the incoming particles are energetic enough to penetrate to low altitudes and excite the atmospheric gas.

Analyses of Triad magnetometer data acquired over the south polar regions and recorded at McMurdo, Antarctica, indicate that the basic flow pattern shown in Fig. 2 for the north pole is the same for the south pole.[19] At any given local time and invariant latitude location, the field-aligned current flow is the same.

The average values of field-aligned current density and intensity in the various regions and sectors discussed above are listed in Table 1 (from Ref. 16). The total current, estimated by integrating the observed current intensity over the local time extent of the appropriate region, is also listed in Table 1. The total amount of current flowing into the ionosphere (including Regions 1 and 2) is always equal to the total current flowing away (within 5%) for every level of magnetic activity. The fact that current continuity is always preserved is important to

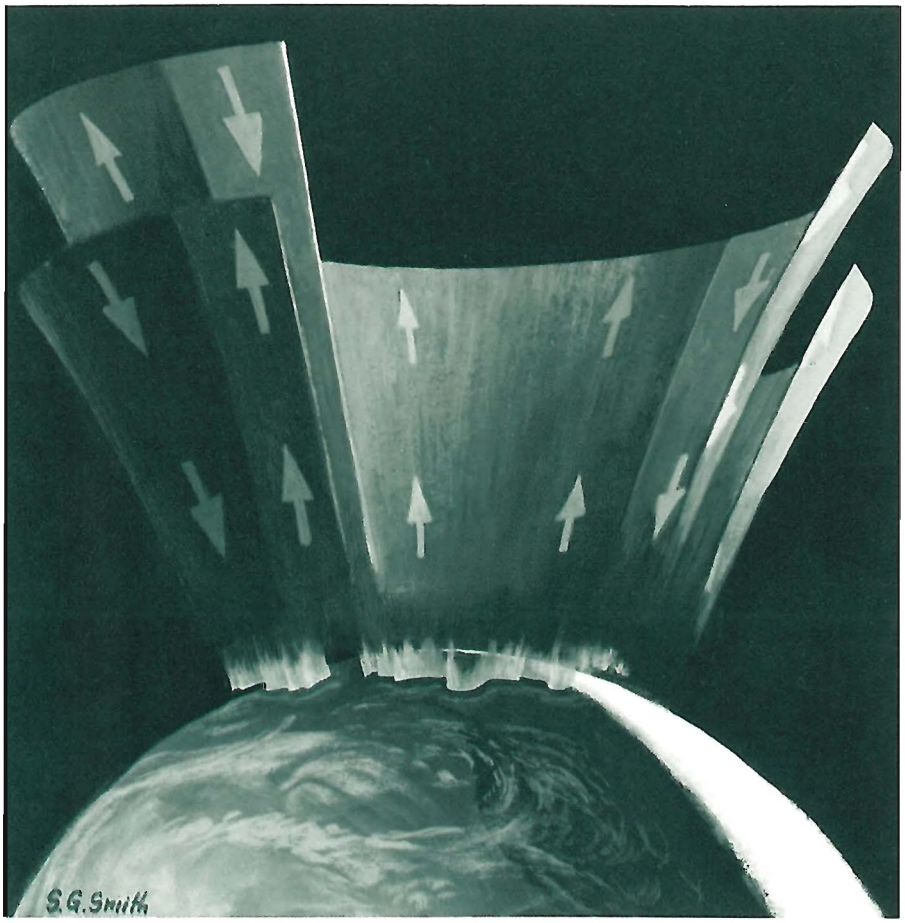

Fig. 3—Cone-shaped regions formed by Birkeland currents flowing into and away from the auroral region. The currents on a given sheet reverse direction near midnight and noon (from Ref. 18).

Table 1
AVERAGE CHARACTERISTICS OF LARGE-SCALE FIELD-ALIGNED CURRENTS

	Afternoon to Midnight		*Midnight to Forenoon*	
Parameter	*Region 1*	*Region 2*	*Region 1*	*Region 2*
Current density ($\mu A/m^2$)				
Quiet	−0.9	0.3	0.9	−0.5
Disturbed	−1.4	0.7	1.5	−1.1
Total current (10^6 A)				
Quiet	−1.3	0.8	1.5	−1.1
Disturbed	−2.8	2.6	3.2	−3.3

A positive value denotes current flow into the ionosphere.
A negative value denotes flow away from the ionosphere.
Values are averages over specified regions.

the development of the models of the three-dimensional current system that couples the magnetosphere with the lower atmosphere and ionosphere. It is also significant that the total field-aligned current in Region 1 is significantly larger than the Region 2 total current during relatively quiet conditions, while during active periods the total current flow in both regions becomes nearly equal.

MAGSAT OBSERVATIONS OF BIRKELAND CURRENTS

The Magsat spacecraft was launched into a dawn-dusk synchronous orbit, whereas Triad is in a polar orbit and appears to precess westward with respect to the earth-sun line at a rate of approximately a degree per day. The orbital planes of the two spacecraft were nearly coincident in November 1979, when magnetic field measurements were made at nearly the same point in time and space (separated only by their altitude difference and the time differential related to their orbital periods — a value that cannot exceed one-half the orbit period, or approximately 50 minutes, when they are moving in the same direction). Data were acquired by Magsat and Triad during a disturbed period on November 7, 1979 at nearly the same place in the north auroral region. Segments of their orbital tracks are shown in Fig. 4 superimposed on the statistical distribution of Birkeland currents shown in Fig. 2 determined for disturbed conditions. The Triad observations were made at 17:12:30 UT, and the Magsat observations 25.5 minutes later (at 17:38 UT). Regions of upward- and downward-flowing Birkeland currents detected by Magsat and Triad are shown by the shaded areas of Fig. 4. They are coincident and are close to the statistical distribution. The orientations of the transverse

magnetometer axes (denoted A and B) for the two spacecraft with respect to their velocity vectors are shown in the upper right corner of Fig. 4. The A and B axes for Triad are directed 135 and 45°, respectively, from the velocity vector, and for Magsat are parallel and normal, respectively, to the velocity vector.

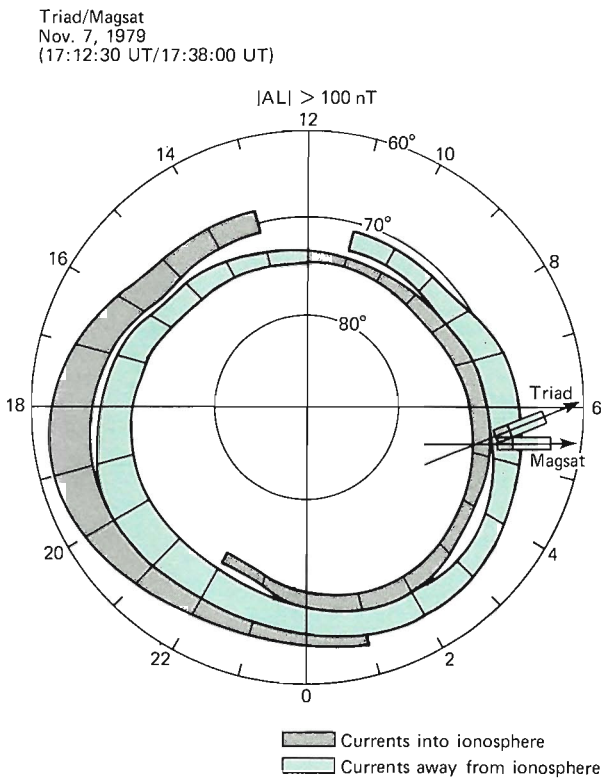

Fig. 4—Orbital tracks of Triad and Magsat superimposed on the statistical pattern of Birkeland currents shown in Fig. 2. The locations and flow directions of the Birkeland currents detected by the two satellites are shown by the shaded areas.

Theoretical magnetic field values (computed from the 1965 Model International Geomagnetic Reference Field) extrapolated to the period of observation were subtracted from the Triad and Magsat observations. The resulting disturbance vectors were rotated from the spacecraft coordinate systems to the geomagnetic reference frame. The components in the geomagnetic east-west direction (i.e., tangent to the circles in Figs. 2 and 4) from Triad and Magsat are shown in Fig. 5. These preliminary data show the amazing similarity of the details in the transverse magnetic disturbances measured by different spacecraft. The disturbances are over 1000 nT and can be interpreted as resulting from a pair of intense Birkeland currents flowing into the ionosphere between about 67 and 65° magnetic latitude and away from the ionosphere between about 65 and 61° magnetic latitude. The density of these currents is about 2 $\mu A/m^2$ and their intensity is about 0.8 A/m.

The processing of the Magsat data is in a preliminary stage and work is only beginning on the investigation of disturbances associated with Birkeland currents. The spatially separated measurements provided by Magsat and Triad will permit the determination of the spatial extent of the Birkeland currents and of the differences, if any, in the intensities of these currents over sunlit and dark portions of the polar ionosphere. The improved sensitivity of the Magsat magnetometer and its lower altitude (in comparison to Triad) will also provide data on the potential field contribution of ionospheric auroral currents that flow at an altitude of about 100 km (the magnetic effects of which have been observed on the ground on a regular basis since Birkeland's original work). The ultimate objective of these studies is to understand and define the variable high-latitude magnetic disturbances to assist in the Magsat program's goal of obtaining an accurate, up-to-date quantitative description of the earth's main geomagnetic field.

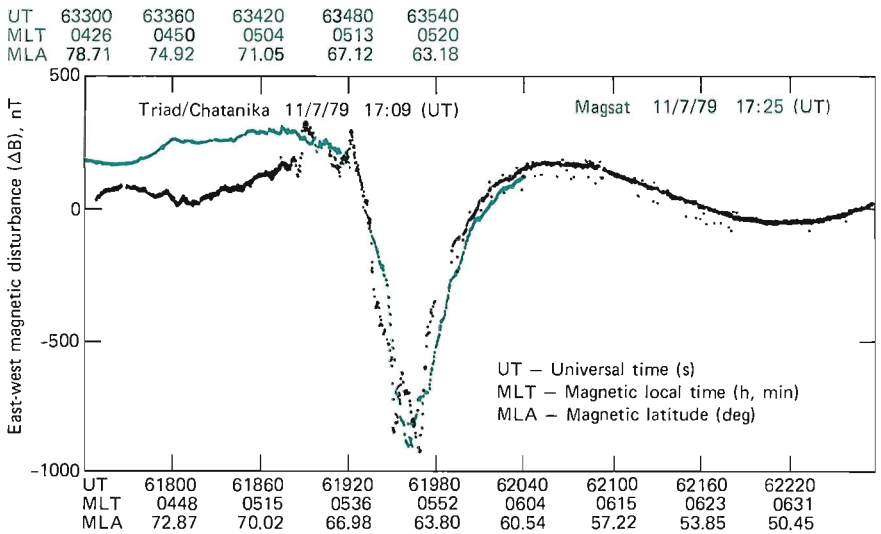

Fig. 5—The geomagnetic east-west component determined from the Magsat and Triad observations. The horizontal scale lists universal time (UT) in seconds, magnetic local time (MLT) in hours and minutes, and magnetic latitude (MLA) in degrees.

REFERENCES and NOTES

[1]K. Birkeland, The Norwegian Aurora Polaris Expedition, 1902 - 03, Aschehoug, Oslo, Norway (1908).

[2]E. H. Vestine and S. Chapman, "The Electric Current System of Geomagnetic Disturbances," *Terr. Magn. Atmos. Electr.* **43**, p. 351 (1938).

[3]N. Fukushima, "Equivalence in Ground Geomagnetic Effect of Chapman-Vestine's and Birkeland-Alfvén's Electric Current Systems for Polar Magnetic Storms," *Rep. Ionos. Space Res. Jpn.* **23**, p. 219 (1969).

[4]N. Fukushima, "Generalized Theorem for No Ground Magnetic Effect of Vertical Current Connected with Pedersen Currents in the Uniform-Conductivity Ionosphere," *Rep. Ionos. Space Res. Jpn.* **30**, p. 35 (1976).

[5]A. J. Zmuda, J. H. Martin, and F. T. Heuring, "Transverse Magnetic Disturbances at 1100 km in the Auroral Region," *J. Geophys. Res.* **71**, p. 5033 (1966).

[6]A. J. Zmuda, F. T. Heuring, and J. H. Martin, "Day Side Magnetic Disturbances at 1100 km in the Auroral Oval," *J. Geophys. Res.* **72**, p. 1115 (1967).

[7]The 5E series of satellites was designed by APL in the period 1962-64 to make scientific and engineering measurements of the environment of the Transit navigation satellites. Four were launched piggyback on Transit Type 5 satellites, and three achieved orbit. Studies of the 5E spacecraft data were carried out by scientists around the world, and 43 articles were eventually published on their findings in professional journals. The 5E-1 satellite became one of the most productive ever launched, still producing data in its eleventh year (a full solar cycle), when a symposium was held at APL on September 27, 1974, celebrating the outstanding success of the 5E program.

[8]J. C. Armstrong and A. J. Zmuda, "Triaxial Magnetic Measurements of Field-Aligned Currents at 800 km in the Auroral Region: Initial Results," *J. Geophys. Res.* **78**, p. 6802 (1973).

[9]P. A. Cloutier, R. E. Daniell, Jr., A. J. Dessler, and T. W. Hill, "A Cometary Ionosphere Model for Io," *Astrophys. Space Sci.* **55**, p. 93 (1978).

[10]A. J. Dessler and T. W. Hill, "Jovian Longitudinal Control of Io-Related Radio Emissions," *Astrophys. J.* **227**, p. 664 (1978).

[11]H. Alfvén, "Electric Currents in Cosmic Plasmas," *Rev. Geophys. Space Phys.* **15**, p. 271 (1977).

[12]A. J. Zmuda and J. C. Armstrong, "The Diurnal Variation of the Region with Vector Magnetic Field Changes Associated with Field-Aligned Currents," *J. Geophys. Res.* **79**, p. 2501 (1974).

[13]A. J. Zmuda and J. C. Armstrong, "The Diurnal Flow Pattern of Field-Aligned Currents," *J. Geophys. Res.* **79**, p. 4611 (1974).

[14]T. Iijima and T. A. Potemra, "The Amplitude Distribution of Field-Aligned Currents at Northern High Latitudes Observed by TRIAD," *J. Geophys. Res.* **81**, p. 2165 (1976).

[15]T. Iijima and T. A. Potemra, "Field-Aligned Currents in the Dayside Cusp Observed by TRIAD," *J. Geophys. Res.* **81**, p. 5971 (1976).

[16]T. Iijima and T. A. Potemra, "Large-Scale Characteristics of Field-Aligned Currents Associated with Substorms," *J. Geophys. Res.* **83**, p. 599 (1978).

[17]Y. I. Feldstein, "Peculiarities in the Auroral Distribution and Magnetic Disturbance Distribution in High Latitudes Caused by the Asymmetrical Form of the Magnetosphere," *Planet. Space Sci.* **14**, p. 121 (1966).

[18]T. A. Potemra, "Aurora Borealis: The Greatest Light Show on Earth," *Smithsonian* 7, p. 64 (1977).

[19]T. A. Potemra, S. Favin, and T. Iijima, "Field-Aligned Currents in the North and South Auroral Regions Measured with TRIAD," *EOS*, **56**, p. 617 (1975).

FREDERICK S. BILLIG

CHINA— AS VIEWED BY AN AEROSPACE ENGINEER

From November 5 through 18, 1979, a group of eight U.S. scientists and engineers (Fig. 1) visited ramjet and turbojet engine facilities in the People's Republic of China.

We took the train from Hong Kong to Canton on November 5, stayed overnight in Canton, and flew to Beijing (Peking) the next morning (Fig. 2). The next five days were spent in Beijing at the Institute of Aeronautics and Astronautics, the Institute of Mechanics of the Chinese Academy of Sciences, and the Power Plant Research Laboratory of the China Precision Machinery Corporation. On November 9, the delegation boarded the night train to Shenyang (Mukden), visited the Shenyang Aeroengine Factory and its Development Center on November 10 and 11, and returned by night train. Mr. Wilson of the Marquardt Co. and I left the delegation in Beijing to revisit the aforementioned facilities, while the remainder of the delegation went to the Sian Aeroengine Factory and the North Western Engineering University, and then to Chiang-Yu via Cheng Tu to visit the Aeronautical Research Establishment. The delegation was reunited in Beijing on November 18, flew to Canton, and left for Hong Kong the following day.

BEIJING INSTITUTE OF AERONAUTICS AND ASTRONAUTICS

Our first visit was to the Beijing Institute of Aeronautics and Astronautics, which is the principal educational institution in aeronautical engineering in China. Currently there are 3000 undergraduate and 200 graduate students. Its principal areas of study are aerodynamics, propulsion, structures, radio (electrical) engineering, and instrumentation.

After a warm greeting and a terse overview of the Institute, we were taken on a tour of the facilities. The first of two air supply systems that we saw consists of 3500 hp compressors that can pump 14 kg/s of air to 25 atm. The air storage system comprises 220 tanks with a total volume of 224 m^3. The maximum operating pressure of the facility is 8 atm. Air is heated in a combustion heater, without oxygen makeup, to a maximum temperature of 600°C and is available for compressor, combustor, and nozzle test rigs and a blowdown cold-flow wind tunnel with run times of about 2 min. The facility exhauster consists of two air-to-air ejectors that provide altitude simulation to 9 km. The wind tunnel has cross-section dimensions of 540 × 470 mm. Five contoured nozzles range in Mach from 1.5 to 2.75 and in Reynolds numbers to as high as 2×10^6. Models are mounted in a 3.8 mm diameter, six-component strain gauge balance that can provide continuously varying angles of attack of -6 to $+8°$. A minicomputer built in China (2 μs, 16K 16-bit words) is used in conjunction with a 200 sample/s data acquisition system.

Fig. 1—Delegation members and hosts in front of the Institute of Mechanics, Chinese Academy of Sciences. Left to right, first row: L. O'Brien, United Technologies Research Center; D. Wilson, The Marquardt Co.; C. Swan, Boeing Aerospace Co.; Wu Chung Hua, of the Institute; J. G. Mitchell, Arnold Air Force Station; Yao Peng, Avco Lycoming; Zhu Shouxin (the interpreter), Chinese aeronautical establishment. Staggered second/third row: Mr. Wu and Chen Nai Xing of the Institute; Dr. J. E. Bubb (delegation head), F. M. Fox and Assoc.; Tsien Shou Hua and Huang Chao Hsia of the Institute; the writer; Ko Shau Yen and S. Yue of the Institute. (E. Woll, General Electric Co., joined the delegation later.)

Beijing: Institute of Aeronautics and Astronautics
Institute of Mechanics, Chinese Academy of Sciences
Power Plant Research Laboratory, China Precision Machinery Corp.

Shenyang: Aeroengine Factory and Development Center

Sian: Sian Aeroengine Factory
North Western Engineering University

Chiang-Yu: Aeronautical Research Establishment

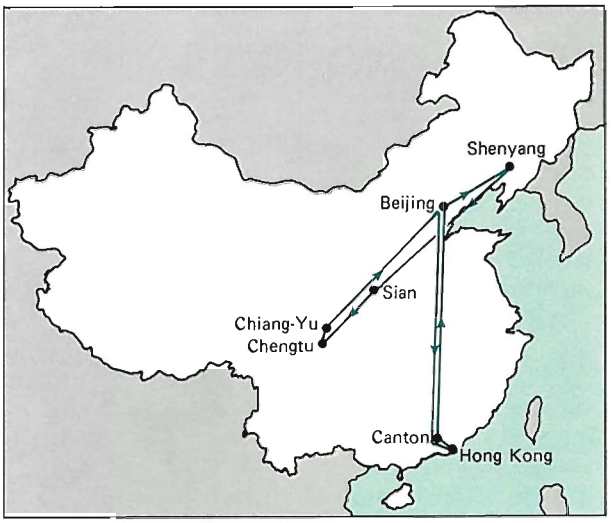

Fig. 2—Itinerary of the U.S. delegation to the People's Republic of China.

Another test rig is used to study supersonic mixing. Here we saw a 16-channel oscillograph recorder, a precisely machined spherical pressure probe about 0.8 mm in diameter containing eight separate tops, and Schlieren/shadowgraph systems, all made in China.

The second air storage system has a volume of 24 m^3 at 150 atm, 500 m^3 at 55 atm, and 1000 m^3 at 8 atm. A silica gel dryer is used in this system, and again air-to-air ejectors are used for the exhauster. Connected to the air supply is a manually controlled variable Mach number (1.5 to 3.5) wind tunnel with a 100 × 100 mm test section. Maximum total pressure in this tunnel is 8 atm and maximum run time is 5 to 8 min. A normal shock inlet about 50 mm in diameter was being tested.

Next we saw a connected pipe test setup of a ducted rocket. A rubber-based propellant with 20% aluminum and 3% magnesium was used on the gas generator. Air was brought to the secondary combustion chamber in four ducts about 50 mm in diameter each. The entrance angle was 90° and the flow rate was about 5 kg/s. The secondary combustor was about 150 mm in diameter and 760 mm in length, and the nozzle throat area was about 50% of the duct area. On our second visit, we were shown a video tape of a motor firing and were told that the air/rocket flow ratio was 3:1, the rocket pressure 70 atm, the burn time 20 s, and the average specific impulse (I_{sp}) 389 s.

We were then shown a modern large-scale computer facility that featured a 256K 32-bit word, 200,000 computations-per-second computer "Felix" built in Romania under French license. Peripherals included eight disk drives, five tape drives, two high speed card readers, and a high speed printer.

We saw a Continental jet engine with a maximum thrust of 870 kg that was used by students to measure thrust, specific fuel consumption, pressures, temperatures, etc. Quarter segments of several other engines, including the Rolls Royce HS 125, the GE J47, and engines for the MiG 15 and 17, were also in use as teaching aids.

Following our tour, each member of the delegation met with a particular group of 20 to 30 professors, graduate students, and staff for technical discussions. As it turned out, this format of "one on many" was to be typical of many subsequent sessions at this Institute and elsewhere. In some cases, an interpreter was needed, but generally the host scientist filled that role. The discussion usually focused on reports on the technical activities in the U.S., but a notable exception was a discussion by Professor J. S. Chin, a graduate of the University of Cranfield, England, on the enhancement of ignition in afterburners with the addition of small amounts of oxygen (see, e.g., Ref. 1).

Undergraduate students at the Institute are selected on the basis of nationwide examinations, which result in tuition-free university level education for only about 10% of the relevant age group in the population. A disproportionate 50% of those admitted are from urban secondary schools, whereas these students represent only 20% of the total population. The undergraduate curriculum has been extended from three years[2] to four years. Neither undergraduate nor graduate degrees are granted (graduate students spend either two or six additional years in the Institute), but the recognition that titles are important in dealing with the outside world may cause the issuance of degrees within one to two years.

INSTITUTE OF MECHANICS, CHINESE ACADEMY OF SCIENCES

On November 6, the delegation visited the Institute of Mechanics, Chinese Academy of Sciences in Beijing. I made a second visit to the Institute on November 15 to discuss catalytic combustion with Huang Chao Hsiang and his colleagues.

The Chinese Academy of Sciences, formed in 1949, is the national academic organization for research in science and technology in China. It contains four science and engineering universities, the Ministry of Education, and 112 research institutes, 36 of which are located in Beijing. The staff has grown from 300 in 1949 to 36,000 at present and includes 23,000 research scientists and engineers, 1600 research professors or associate professors, plus supporting personnel.

In 1960 the Power Laboratory was merged with several research institutes in gas dynamics that had been formed during 1956-60 into the Institute of Mechanics. At present there are 400 research scientists and engineers and 56 professors and associate professors.

The Institute has two major departments: Mechanics and Engineering Thermophysics. The Mechanics Department has five divisions: (a) High Speed Aerodynamics, (b) Solid Mechanics, (c) Explosion Mechanics, (d) Plasma Dynamics and Magnetohydrodynamics, and (e) Physical Mechanics. The Engineering Thermophysics Department also has five divisions: (a) Conversion and Transmission of Energy, (b) the 1st Research Division (Engine Thermodynamics and Aerothermodynamics of Turbomachinery), (c) the 2nd Research Division (Aerothermodynamics of Heat Engines), (d) the 3rd Research Division (Heat and Mass Transfer), and (e) the 4th Research Division (Combustion).

Professor Wu Chung Hua, Deputy Director, gave a brief description of the Institute and introduced the division heads, each of whom described his technical activities and showed us the test facilities.

The Mechanics Department

High Speed Aerodynamics — The division is involved in experimental and theoretical studies of supersonic, hypersonic, and viscous flows. Its facilities include:

1. Two supersonic blow-down wind tunnels with 200 × 200 × 300 mm test sections and Mach 1.6, 2.0, 2.5, 3.0, and 4.0 nozzles. The air supply system comprises a 7 kg/s compressor system with a maximum pressure of 9 atm and two 600 m^3 storage tanks with an 8 atm capability. The tunnels were built in 1958. Future plans call for a 30 atm, 7 kg/s air capability. The exhauster system is a single 600 m^3 vacuum tank. The run durations are 3 min at Mach 4 and continuous at Mach 1.6.
2. A Mach 6.6 to 18 shock tunnel with a test section diameter of 1.2 m (Fig. 3). The driver gas is a mixture of 6.5% oxygen and 93.5% hydrogen ignited by a 10 kV spark discharge. The driven gas is a mixture of hydrogen and nitrogen. Maximum pressure is 800 atm and the run time is 5 to 11 ms.
3. A Mach 8 to 12 shock tunnel with a test section diameter of 0.5 m. Driver and driven gas characteristics are similar to the larger tunnel.
4. A gun tunnel with a 200 × 200 mm test section and Mach 1.6 to 4 nozzles. An aluminum piston is used, and the maximum pressure is 1000 atm with run times of 20 to 30 ms.
5. An 800 kW arc-heated tunnel for ablation testing of reentry bodies.

Solid Mechanics — This division studies lightweight structures, computational methods of stress analysis, vibration fatigue, fracture mechanics, crack growth, and modeling of elastic and plastic deformations. Its laboratories are well equipped for measuring strain, crack propagation, etc., under constant and cyclical loading at ambient and elevated temperatures.

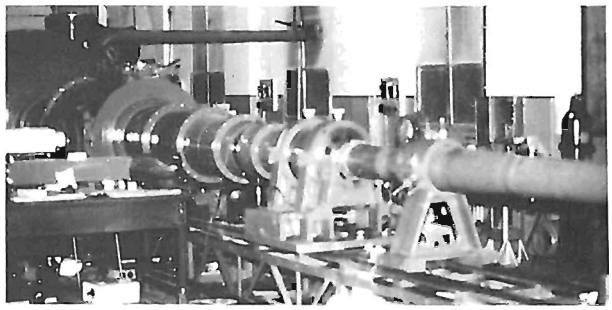

Fig. 3—Mach 6.6 to 18 shock tunnel at the Institute of Mechanics.

Explosion Mechanics — Programs include theoretical and experimental studies of the effects of explosions and high velocity.

Plasma Dynamics and Magnetohydrodynamics. — Investigations are conducted of the stability of magnetically confined high temperature plasmas and the industrial applications of low temperature plasma torches.

Physical Mechanics — Divisional studies comprise fluid mechanics, biomechanics, mechanical properties of matter, and cosmic gas dynamics.

The Engineering Thermophysics Department

Conversion and Transmission of Energy — This division studies basic academic education with particular emphasis on engineering thermodynamics, aerothermodynamics of heat engines, heat and mass transfer, and combustion.

1st Research Division (Engine Thermodynamics and Aerothermodynamics of Turbomachinery) — The division has 7 senior scientists, 18 junior scientists, and 23 engineers. Professor Chen, who speaks excellent English with a Russian accent reflecting his academic training in the Soviet Union, gave a rather detailed description of analytical work concerning an extension of Professor Wu's renowned work on turbomachinery flow theory. His work uses nonorthogonal curvilinear coordinates and nonorthogonal velocity components to provide a design procedure for axial flow turbomachine blades. Streamline extension techniques, matrix direct solution, and line relaxation methods are employed in the computer routines. By use of fictitious grid points, the storage requirement ($\approx$32K) in the matrix direct solution is reduced by about one-half.

Figure 4 shows a M $\geq$1.3 transonic cascade tunnel that has a 220 × 290 mm 5-blade cascade test section. The cylindrical tube running transverse to the tunnel axis houses the Schlieren/shadowgraph optics and provides an optical path that is free from room disturbances. Maximum airflow is 21 kg/s; maximum Reynolds number is 3 × 10^6; and

Fig. 4—Mach 1.3 cascade tunnel at the Institute of Mechanics.

maximum run time is 200 s. We were also shown a 500 kW rotating cascade driven by a 3000 kW motor at 750 rpm.

2nd Research Division (Aerothermodynamics of Heat Engines) — The division has three senior scientists, seven junior scientists, and seven engineers. The facilities include two centrifugal compressor test rigs, an axial turbine test rig, and a pressure wave supercharger engine. The compressor rigs are 250 kW and 850 kW with maximum speeds of 37,000 rpm. Under construction is a 3000 kW axial compressor test rig. The pressure wave supercharger is attached to a 150 hp rotary combustion engine.

3rd Research Division (Heat and Mass Transfer) — The division has three senior scientists, nine junior scientists, and ten engineers. Work includes experimental and theoretical studies of film cooling of turbine blades, analysis of flowfields in turbojet and ramjet combustors, tests and analysis of sodium heat pipes to 800°C for cooling electrical equipment, techniques for harnessing solar energy, and heat transfer to improve the cooling of air-and water-cooled engines. In the tour of the heat transfer laboratory, we saw film cooling tests on flat plates and blade cascades, low and high temperature heat pipes, and a rotary combustion engine. This 450 cc, 49 hp air-cooled engine had been run the equivalent of traveling 17,000 km without repair at an average specific fuel consumption of 25 gal hp-h.

4th Research Division (Combustion) — Five senior scientists, fifteen junior scientists, and four engineers comprise the division. Tasks include tests and analysis of annular gas turbine combustors and afterburners with emphasis on durability, oscillatory mixing and flow stabilization, the use of catalysts, the ignition of lean mixtures, combustion of hydrogen and air in supersonic flow, and mixing of parallel flows in a ramjet combustor. During the early 1960's, Professor Wu and his colleagues were quite interested in supersonic combustion, but at present the work in this area is minimal. Nonetheless, many of the Chinese scientists were interested in my lectures on the subject and asked many questions regarding details from the contemporary U.S. literature.

POWER PLANT RESEARCH LABORATORY, CHINA PRECISION MACHINERY CORP.

On November 7, the entire delegation visited the Power Plant Research Laboratory located at Yungang, southwest of Beijing in the Fengtai District. (En route we crossed the Yongding River on a new bridge adjacent to the old Marco Polo bridge, passing into an area of restricted access to foreigners.) The Laboratory is responsible for the development of propulsion systems, primarily ramjets, some testing of turbojets, and some research for the China Precision Machinery Corp. The Laboratory is 35 to 40 years old and the airbreathing test facilities were built in the late 1950's and early 1960's. Its activity during the Cultural Revolution (1966-69) was limited, but it is currently very busy. Most of the staff of 600 are engineers.

Mr. Shu Shen Wang, the Director, described the activities of the Laboratory and led the tour of the test facilities (shown schematically in Fig. 5). Two 3500 kW centrifugal first stage compressors and two 1500 kW second stage superchargers comprise the pumping system. The air is stored in a large number of cylindrical tanks having a total volume of 6840 m^3. Of this volume, 6600 m^3 is stored at 22 atm, the remainder at 220 atm. Air is piped to both the five test cells and two-stage air-air ejectors (Fig. 5) that are used to exhaust cells 2 through 4. In contrast to most U.S. airbreathing test facilities, which use common exhausters, each cell has its own ejector system. The maximum flow to the test cells is 230 kg/s, which can be heated directly in one of two vitiation heaters (cells 2 and 3) or indirectly in a tube-and-shell heat exchanger. For direct heating, the air is subdivided, with half of it passing into 16 kerosene-fueled turbojet can combustors and the other half bypassed for subsequent mixing. No provision is made for oxygen makeup. The vitiation heater is used for temperatures up to 350°C. The tube-and-shell heat exchanger is used for the range of 350 to 700°C, so it is possible to simulate flight Mach numbers up to 4.2 in the tropopause with unvitiated air.

Five test cells are in operation: a sea level cell, two direct-connect high altitude cells, a supersonic high altitude free-jet cell, and a ram-air-turbine test cell. A sixth cell for testing solid ducted rockets is currently under design. Test Cell 1 is approximately 2.6 m in diameter and 12 m in length, with a hydraulically actuated cell closure similar to Cell 8 at the Marquardt Co. Both ramjet and turbojet engines, with inlet diameters up to 800 mm and 1000

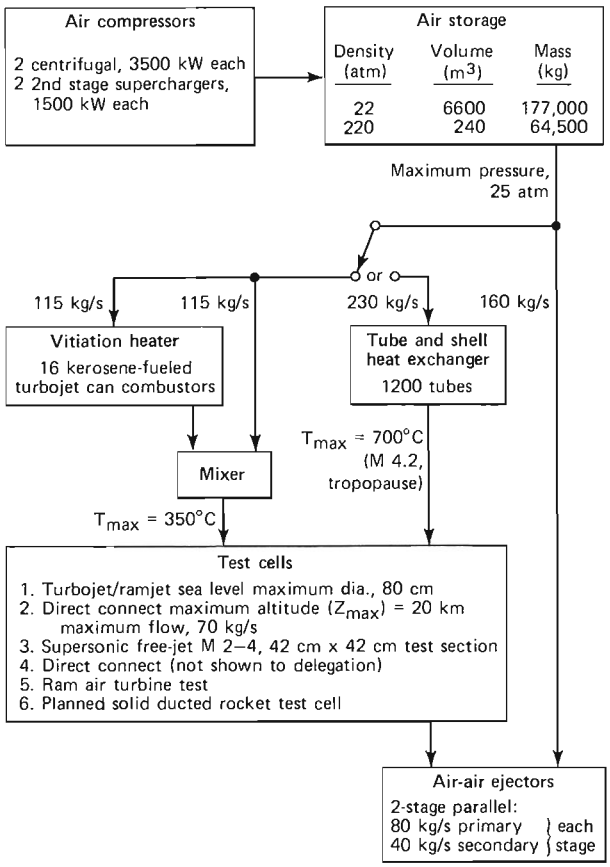

Fig. 5—Schematic diagram of the ramjet test facility at the Power Plant Research Laboratory.

mm, respectively, can be installed on a load cell balance for testing, with a maximum static thrust limit of 5700 kg.

Test Cell 2, completed in 1965, is a high altitude direct-connect facility with a maximum simulated altitude of 20 km and a maximum flow of 70 kg/s. This cell is about 1.8 m in diameter and 4.6 m in length; cell closure is accomplished by hoisting a half cylinder cap in place. Cell 3, completed in 1969, is a Mach 2 to 4 free-jet facility. Five nozzles with nominal Mach numbers of 2.0, 2.5, 3.0, 3.5, and 4.0 are used. Minor adjustments can be made in the nozzle throat blocks (not during a run) to obtain ±0.25 M change from the nominal design Mach number in the test section. The nozzle exits are square, 420 mm on a side, and the major fraction of the air not captured by a test engine inlet, generally circular in cross section, passes through a bypass diffuser to the ejector system. The cowl of the engine inlet is then centered in a cut-out of the downstream end of the test cabin, which is sized to provide a small gap that permits clearance at angles of attack. The maximum engine diameter tested to date is 300 mm, which corresponds to 40% of the nozzle discharge area. Engines are mounted on a 1000 kg maximum thrust stand that can be rotated in the horizontal plane from −2 to +10°. A long-focal-length Schlieren/shadowgraph optical system located in the vertical plane is used to view the flowfield via camera and TV coverage. Maximum flow rate to this cell was stated to be 115 kg/s, which would permit sea level testing at Mach 2 and altitude simulation of 1.3 and 2.1 km at Mach 3 and 4, respectively. Run times are typically 3 min. Instrumentation consists primarily of strain gauge pressure transducers and thermocouples connected to a 300-channel data acquisition system.

Cell 4 was not shown to the delegation. Cell 5 is a smaller test cell used for the development of ram-air turbines and pumps. Maximum airflow to this cell is 4 kg/s at pressures of 10 atm and temperatures of 600°C. We were shown a turbine/pump that produces 180 hp at 4000 rpm with a pump outlet pressure of 100 atm at a flow rate of 10 l/s. The cell is also used for testing seals and bearings.

Under development at the facility were a Mach 3.5 to 4.0 ramjet, similar in design to the Typhon that was developed in the U.S. in the early 1960's, and a solid ducted rocket. We were also shown a wind tunnel test model of an aft-inlet ramjet installed on a variable flow throttle support. The 1/4-scale model was about 88 mm in diameter, had been designed by method of characteristics, and was very precisely machined and assembled. It had been tested in a 1 × 1 m wind tunnel at the Institute of Mechanics in Beijing at angles of attack up to 6°.

Mr. Wang also described briefly other research efforts at the Laboratory, including: analysis of bridging on spike and cone inlets; evaporation of droplets; injection, mixing, and atomization; studies of atomization from centrifugal injectors by the "wax" method; low temperature ignition of kerosene and high density fuels; and catalytic ignition and combustion.

SHENYANG AEROENGINE FACTORY AND DEVELOPMENT CENTER

The U.S. delegation took the overnight train on November 9 that arrived in Shenyang the following morning. Shenyang, an industrial center of 4 million people located in Manchuria, was occupied by the Japanese from 1931 until VJ Day. Interesting was the widespread use of Pinyin (the Chinese phonetic alphabet) on street signs and buildings. The State Council has decreed that the Roman alphabet will be used to spell out Chinese names and places according to standard Beijing pronunciation beginning January 1, 1979.

On the morning of November 10, we visited the Aeroengine Factory where J6 and J7 engines for the MiG fighters are manufactured. The factory was built in the 1950's with the help of the Soviets. There are about 10,000 employees, 10% of whom are technical (500 engineers, 500 graduates — a graduate must have 6 to 7 years experience before he is designated an engineer). The factory has 2000 "precision" machine tools and turns out 1000

engines per year on a two-shift, six-day (the standard work week in China) operation. The equipment varied from 1930-vintage drop forges to computer-driven lathes for finish machining of compressor blades.

Following a visit to the manufacturing plant, we witnessed a "green run-in" of a J7 engine. With the afterburner operating, the exhaust nozzle was bright yellow and the three actuators and supports were a dull red, a most impressive sight. Normal procedure is to operate the engine for two hours at sea level conditions at various throttle settings, shut it down, disassemble and check all parts, and reassemble it for three hours of additional testing before shipment to the aircraft assembly plant. We also saw an advanced 9070 kg bypass engine about 1.15 m in diameter that was under development at the Development Center, which we visited in the afternoon.

The Development Center is a large facility used for engine development, including component testing of the compressor, combustor, turbine, afterburner, and exhaust nozzle. Power is supplied to the facility by two 18,000 kVA transformers that step down the voltage to the 6300 V compressor motors. The air supply consists of six centrifugal compressors driven by 1050 kW synchronous motors that pump 5 kg/s each to a pressure of 8 atm. This machinery was built in the Soviet Union and installed in Shenyang in the 1950's. In addition to the aforementioned bypass engine, we saw a 20,000 rpm spool test rig, several combustor test rigs emphasizing reignition capability, a set-up for bypass duct burning that was instrumented with an IR spectrometer, and a complete structural testing laboratory.

CONCLUSIONS, COMMENTS, AND TRIVIA

There is no doubt that the delegation members were truly "guests of the People's Republic of China," which is how we were treated and greeted on every occasion. The food was superb, the beer excellent, the wine sweet, and the mao tai (a liquor distilled from sorghum) strong. We entered and left China without clearing customs. We were met at each city by two or more interpreters, escorted to VIP waiting rooms, and chauffeured in vans or automobiles to guest houses or hotels, and were the guests at a banquet in each city. Our hosts could not have been more gracious.

There is no question that the principal objective of the delegation's visit was met, *viz.*, "to promote cooperation through the exchange of scientific information." The discussions were free and open. Questions in areas that would be regarded as sensitive were avoided for the most part, but when they arose, the disinclination to answer was unhesitatingly accepted. The Chinese were appreciative of the technical advice they were given and want further exchanges. We were impressed by both their technical capability and their strong commitment to the training of aerospace engineers and to the development of facilities for testing and manufacturing advanced jet engines. Our hosts were very familiar with U.S. technical literature; it was not uncommon to be asked very detailed questions regarding derivations of one's equations or methods of solution, or explanations of a particular figure where the questioner had a photostatic copy of the material in hand. On many occasions, the Chinese described their own equipment as inferior and their technology as primitive. The delegation felt quite differently. We were impressed by both their technical capability and their ability to manufacture complex equipment. Obviously, although their resources at present are limited, they are focused on specific goals. There is little doubt that their national commitment to "The Great Goal of Four Modernizations," *viz.*, achieving modernization of agriculture, industry, national defense, and science and technology by the end of this century, will result in world prominence in aerospace sciences and technology.[3]

We were quite impressed by the apparent adequacy, if not abundance, of food. The fields of South China were lush, interwoven with myriad irrigation channels. In North China it was harvest time for bok toi, the white cabbage, which was stacked like cordwood on many of the sidewalks of Beijing and Shenyang. It sells for about four cents a kilogram and can be used during the entire winter. Wages range from $40 to $70 per month. All able-bodied adults work a six-day, 48-hour week, with five public holidays and one week vacation each year. Housing is very modest, being assigned by the state and consisting of one to two rooms per family at a cost of $2 to $5 per month. Most people live within walking or bicycling distance of their work. Private ownership of automobiles is nonexistent, but higher officials are assigned vehicles with drivers. Most of the automobiles are made in China and are eastern European in appearance. Both city and rural roads are crowded with buses (many imported), automobiles, trucks, vans, mechanized or animal-drawn farm vehicles, bicycles, and pedestrians.

Primary and secondary education for all is provided by the government but university admission is limited and very competitive. Nationwide entrance examinations are the basis for admittance. University life has returned to normal following the acute disruptions of the Cultural Revolution, which created a large void in the population of those with advanced education. Many people with technical inclinations had to be trained on the job during that period; they represent a significant part of the technical staff at the Power Plant Research Laboratory and similar facilities. Such people, who are anxious for opportunities to study abroad, inundated the writer with résumés and requests for the

names of people to contact in the U.S. Similarly, there were many expressions by university people for establishing programs to exchange graduate students.

Manufactured goods of all types were available in stores with prices comparable to the United States, e.g., good quality bicycles selling for $120 and color television sets for $500. However, not only does such a purchase represent many months of saving, but for many goods a ration coupon issued by the state is a prerequisite for purchase. The state-run television system broadcasts only a few hours a day, with heavy emphasis on education. In Beijing there is a daily program teaching English and one on computer programming (in English). We were also told that English is taught by radio throughout the nation.

Finally, although our sightseeing was limited, the places we visited — the Forbidden City, the Great Wall, the Ming Tombs, the Summer Palace, Beihai Park, and others — were magnificent.

REFERENCES

[1]J. S. Chin, "The Effect of Oxygen Addition on the Minimum Ignition Energy in a Homogeneous Combustible Mixture," Report H-B429, Beijing Institute of Aeronautics and Astronautics, p. 3 (1979).

[2]G. Corning, "An Aeronautical Visit to China," *Aeronaut. Astronaut.*, pp. 16-19 (1974).

[3]*Economic Reporter*, English Supplement, July-September 1979, Economic Information & Agency, Hong Kong.

PUBLICATIONS

F. J. Adrian, "Principles of the Radical Pair Mechanism of Chemically Induced Nuclear and Electron Spin Polarization," *Rev. Chem. Intermed.* **3**, No. 3, pp. 3 – 43 (1979).

F. J. Adrian and L. Monchick, "Analytic Formula for Chemically Induced Magnetic Polarization by S-$T_{\pm 1}$ Mixing in a Strong Magnetic Field," *J. Chem. Phys.* **72**, No. 10, pp. 5786 – 5787 (1980).

W. H. Avery, "Ocean Thermal Energy Conversion Contribution to the Energy Needs of the United States," *Johns Hopkins APL Tech. Dig.* **1**, No. 2, pp. 101 – 107 (1980).

C. B. Bargeron, "High Vacuum Scanning Electron Microscopy as a Tool in Surface Analysis," *Johns Hopkins APL Tech. Dig.* **1**, No. 1, pp. 38 – 44 (1980).

R. C. Beal, "The Potential of Spaceborne Synthetic Aperture Radar for Oceanography," *Johns Hopkins APL Tech. Dig.* **1**, No. 2, pp. 148 – 156 (1980).

R. C. Beal, "Spaceborne Imaging Radar: Monitoring of Ocean Waves," *Science* **208**, No. 4450, pp. 1373 – 1375 (1980).

W. G. Berl, "Albert Einstein - A Moral Visionary in a Distraught World," *J. Wash. Acad. Sci.* **69**, No. 3, pp. 101 – 108 (1979).

W. G. Berl and B. M. Halpin, "Human Fatalities from Unwanted Fires," *Johns Hopkins APL Tech. Dig.* **1**, No. 2, pp. 129 – 134 (1980).

F. S. Billig, P. J. Waltrup, and R. D. Stockbridge, "The Integral-Rocket, Dual-Combustion Ramjet: A New Propulsion Concept," *J. Spacecr. Rockets* **17**, No. 5, pp. 416 – 424 (1980).

J. F. Bird, "Sonomagnetic Pulses from Underwater Explosions and Implosions," *J. Acoust. Soc. Am.* **67**, No. 2, pp. 491 – 495 (1980).

J. F. Bird, R. W. Flower, and G. H. Mowbray, "Analysis of the Retina via Suprafusion Electroretinography," *Biophys. J.* **29**, pp. 379 – 396 (1980).

H. D. Black, "The Transit System, 1977: Performance, Plans, and Potential," *Philos. Trans. R. Soc. London* **A294**, pp. 217 – 236 (1980).

R. W. Blevins, H. L. Donnelly, J. T. Stadter, R. O. Weiss (APL), and L. Perez y Perez (DOE), "At-Sea Test of a Large Diameter Steel, Cold Water Pipe," *Ocean Engineering for OTEC* **OED-9**, ASME, pp. 47 – 65 (1980).

B. I. Blum (APL) and C. J. Johns, E. E. McColligan, C. R. Smith, and D. M. Steinwachs (JHMI), "A Low Cost Ambulatory Medical Information System," *J. Clinical Eng.* **4**, No. 4, pp. 372 – 378 (1979).

B. I. Blum (APL) and R. E. Lenhard, Jr. (JHMI), "An Oncology Clinical Information System," *Comput. Mag.*, pp. 42 – 50 (Nov 1979).

D. W. Bockemeier (MDAC/St. Louis), W. C. Caywood, P. J. Waltrup, R. D. Stockbridge, and F. S. Billig (APL), and R. S. Burford (Hercules/ABL), "Conceptual Design of the Hypersonic Wide Area Defense Missile," CPIA Pub. 315, Vol. II, pp. 387 – 449.

J. Bohandy and B. F. Kim, "A Normal Mode Analysis of Free Base Porphyrin," *Spectrochim. Acta* **36A**, pp. 463 – 466 (1980).

H. Bouver (APL) and R. E. Bargmann (Univ. Georgia), "Comparison of Computational Algorithms for the Evaluation of the Univariate and Bivariate Normal Distribution," *Computer Science and Statistics: 12th Ann. Symp. on the Interface*, pp. 344 – 348 (1979).

N. J. Brown (Univ. California) and D. M. Silver (APL), "Comparison of Reactive and Inelastic Scattering of $H_2 + D_2$ Using Four Semiempirical Potential Energy Surfaces," *J. Chem. Phys.* **72**, No. 7, pp. 3869 – 3879 (1980).

J. L. Calkins (JHMI) and B. F. Hochheimer (APL), "Retinal Light Exposure from Operation Microscopes," *Arch. Ophthalmol.* **97**, pp. 2363 – 2367 (1979).

J. F. Carbary, "Periodicities in the Jovian Magnetosphere: Magnetodisc Models after Voyager," *Geophys. Res. Lett.* **7**, No. 1, pp. 29 – 32 (1980).

J. F. Carbary and S. M. Krimigis, "Energetic Particle Activity at 5-min and 10-s Time Resolution in the Magnetotail and Its Relation to Auroral Activity," *J. Geophys. Res.* **84**, No. A12, pp. 7123-7137 (1979).

L. L. Cronvich and H. P. Liepman, "Advanced Missile Technology – A Review of Technology Improvement Areas for Cruise Missiles," NASA CR 3187 (1979).

O. J. Deters and C. B. Bargeron (APL), G. M. Hutchins (JHMI), and F. F. Mark and M. H. Friedman (APL), "Velocities in Unsteady Flow through Casts of Human Arteries (Abstract)", *Proc. 32nd Annual Conf. on Engineering in Medicine and Biology* (1979).

O. J. Deters and M. H. Friedman, "Simple Directionally Sensitive Two-Component Laser Doppler Anemometer," *Appl. Opt.* **19**, No. 8, p. 1221 (1980).

G. L. Dugger, "Is There a Chance for OTEC?" *Astronaut. Aeronaut.* **17**, No. 11, pp. 36-42 (1979).

G. L. Dugger, E. J. Francis, and W. H. Avery, "Comparisons of Estimates, Sharing Potentials, Subsidies, and Uses for OTEC Facilities and Plantships," *Expanded Abstracts, Proc. 7th Ocean Energy Conf.*, paper IIIC/1 (1980).

G. L. Dugger and F. K. Hill, "Use of Satellite-Derived Sea Surface Temperatures by Cruising OTEC Plants," *Proc. 6th OTEC Conf.*, Vol. II (1980).

G. L. Dugger, F. E. Naef, and J. E. Snyder III, "Ocean Thermal Energy Conversion," Chap. 19, *Solar Energy Handbook*, J. Kreider and F. Kreith (eds.), McGraw-Hill (1980).

C. Feldman, C. H. Arrington III, F. G. Satkiewicz, and N. A. Blum, "Vacuum Deposited Polycrystalline Silicon Films for Solar Cell Applications," Solar Research Institute Quarterly Report, 15 Sep – 31 Dec 1979, SERI/XS9/82781-1 (Mar 1980).

S. N. Foner and R. W. Hart, "The Milton S. Eisenhower Research Center: Its Objectives and Activities," *Johns Hopkins APL Tech. Dig.* **1**, No. 1, pp. 8-33 (1980).

E. J. Francis and G. L. Dugger, "Promising Applications of OTEC," *Proc. 7th Energy Technology Conf.*, pp. 1272 – 1286 (1980).

A. B. Fraser, R. E. Walker, and F. C. Jurgens, "Spatial and Temporal Correlation of Underwater Sunlight Fluctuations in the Sea," *IEEE J. Oceanic Eng.* **OE-5**, No. 3, pp. 195 – 198 (1980).

R. K. Frazer, "Duplication of Radome Aerodynamic Heating Using the Central Receiver Test Facility Solar Furnace," *Proc. 15th Symp. on Electromagnetic Windows* (1980).

M. H. Friedman, C. B. Bargeron, O. J. Deters, and F. F. Mark (APL) and G. M. Hutchins (JHMI), "Hemodynamic Measurements in Human Arterial Casts: Geometric Effects and Morphological Correlates," *Proc. 31st ASME Biomech. Symp.* (1979); also in *Proc. XII Int. Conf. on Medical and Biological Engineering* (1979).

R. M. Fristrom, "Report of the Task Force on the Flammability of Solid Polymer Cable Dielectrics, Final Report," National Research Council EL-1263, pp. 2-1/2-27 (Nov 1979).

J. Goldhirsh, "A Review on the Application of Nonattenuating Frequency Radars for Estimating Rain Attenuation and Space-Diversity Performance," *IEEE Trans. Geosci. Electron.* **GE-17**, No. 4, pp. 218 – 239 (1979).

J. Goldhirsh, "Comparison of Radar Derived Slant Path Rain Attenuations with the COMSTAR Beacon Fades at 28.56 GHz for Summer and Winter Periods," *IEEE Trans. Antennas Propag.* **AP-28**, No. 4, pp. 577 – 580 (1980).

J. Goldhirsh, "The Use of Radar at Nonattenuating Wavelengths as a Tool for the Estimation of Rain Attenuation at Frequencies above 10 GHz," *EASCON '79 Record* **AES 1**, pp. 48-55 (1979).

B. L. Gotwols and G. B. Irani, "Optical Determination of the Phase Velocity of Short Gravity Waves," *J. Geophys. Res.* **85**, No. C7, pp. 3964-3970 (1980).

W. M. Gray and R. W. Witte, "Guidance System Evaluation Laboratory," *Johns Hopkins APL Tech. Dig.* **1**, No. 2, pp. 144 – 147 (1980).

R. A. Greenwald (Max-Planck Inst. Aeronomie), T. A. Potemra (APL), and N. A. Saflekos (Boston College), "Stare and Triad Observations of Field-Aligned Current Closure and Joule Heating in the Vicinity of the Harang Discontinuity," *J. Geophys. Res.* **85**, No. A2, pp. 563 – 568 (1980).

G. Gücer (JHMI) and L. J. Viernstein (APL), "Clinical Evaluation of Long – Term Epidural Monitoring of Intracranial Pressure," *Surg. Neurol.* **12**, pp. 373 – 377 (1979).

G. Gücer (JHMI) and L. J. Viernstein (APL), "Continuous Recording of ICP in the Normal Monkey," *Intracranial Pressure IV*, (K. Shulman et. al., eds.), Springer – Verlag, Berlin (1980).

G. Gücer (JHMI) and L. J. Viernstein (APL), "Intracranial Pressure in the Normal Monkey while Awake and Asleep," *J. Neurosurg.* **51**, pp. 206 – 210 (1979).

G. Gücer (JHMI), L. J. Viernstein and J. G. Chubbuck (APL), and A. E. Walker (JHMI), "Clinical Evaluation of Long Term Epidural Monitoring of Intracranial Pressure," *Surg. Neurol.* **12**, pp. 373 – 377 (1979).

G. Gücer (JHMI), L. J. Viernstein and W. H. Guier (APL), "A Hemodynamic Model for Relating Phasic Pressure and Flow in the Large Arteries," *IEEE Trans. Biomed. Eng.* **BME-27**, No. 8, pp. 479 – 482 (1980).

G. Gücer (JHMI), L. J. Viernstein (APL), and A. E. Walker (JHMI), "Continuous Intracranial Pressure Recording in Adult Hydrocephalus, *Surg. Neurol.*, **13**, pp. 323 – 328 (1980).

M. E. Hawley, W. A. Bryden, A. N. Bloch, and D. O. Cowan (JHU), T. O. Poehler (APL), and J. P. Stokes (JHU), "Mott Transition and Magnetic Properties of HMTSF $(TCNQ)_x(TCNQF_4)_{1-x}$," *Bull. Am. Phys. Soc.* **24**, No. 3, p. 232 (1979).

B. F. Hochheimer (APL) and S. A. D'Anna and J. L. Calkins (JHMI), "Retinal Damage from Light," *Am. J. Ophthalmol.* **88**, pp. 1039 – 1044 (1979).

H. Hopfield, "Improvements in the Tropospheric Refraction Correction for Range Measurement," *Philos. Trans. R. Soc. London* **A294**, pp. 341 – 352 (1980).

A. N. Jette and J. G. Parker, "Excitation of an Elastic Half-Space by a Buried Line Source of Conical Waves," *J. Sound Vib.* **67**, No. 4, pp. 523 – 531 (1979).

A. N. Jette and J. G. Parker, "Surface Displacements Accompanying the Propagation of Acoustic Waves within an Underground Pipe," *J. Sound Vib.* **69**, No. 2, pp. 265 – 274 (1980).

S. M. Krimigis, "Observations of Particle Acceleration in the Earth's Magnetotail," *AIP Conf. Proc.*, No. 56, pp. 179 – 197 (1979).

S. M. Krimigis (APL), T. P. Armstrong (Univ. Kansas), W. I. Axford (Max-Planck Inst. Aeronomie), C. O. Bostrom (APL), C. Y. Fan (Univ. Arizona), G. Gloeckler (Univ. Maryland), L. J. Lanzerotti (Bell Labs), D. C. Hamilton (Univ. Maryland), and R. D. Zwickl (Los Alamos Scientific Lab.), "Energetic ($\approx$100keV) Tailward Directed Ion Beam Outside the Jovian Plasma Boundary," *Geophys. Res. Lett.* 7, No. 1, pp. 13 – 16 (1980).

S. M. Krimigis (APL) and E. T. Sarris (Democritos Univ. Thrace), "Energetic Particle Bursts in the Earth's Environment," in *Dynamics of the Magnetosphere*, D. Reidel, pp. 599 – 630 (1979).

J. R. Kuttler and V. G. Sigillito, "Upper and Lower Bounds for Frequencies of Clamped Rhombical Plates," *J. Sound Vib.* **68**, No. 4, pp. 597 – 607 (1980).

A. T. Y. Lui, "Observations on Plasma Sheet Dynamics during Magnetospheric Substorms," in *Dynamics of the Magnetosphere*, D. Reidel, pp. 563 – 597 (1979).

M. M. Labes, M. Jones, H. Kao, L. Nichols, and C. Hsu (Temple Univ.) and T. O. Poehler (APL), "Conductivity and Optical Properties of a Polyiodine Canal Complex (Benzophenone)$_9$ $(KI)_2I_7CHCl_3$," *Mol. Cryst. Liq. Cryst.* **52**, p. 115 (1979).

M. Maxfield, D. O. Cowan, and A. N. Bloch (JHU) and T. O. Poehler (APL), "Synthesis of 13,13,14,14-Tetracyano-4,5,9,10-Tetrahydropyrenoquinodimethane, an Electron Acceptor for Organic Metals," *Nouv. J. Chimie* **3**, No. 11, p. 647 (1979).

C.-I. Meng, "Polar Cap Variations and the Interplanetary Magnetic Field," in *Dynamics of the Magnetosphere*, D. Reidel, pp. 23 – 46 (1979).

R. A. Meyer, M. E. Zaruba, and G. M. McKhann, "Flow Cytometry of Isolated Cells from the Brain," *Anal. Quant. Cytol. J.* **2**, No. 1, pp. 66 – 74 (1980).

L. Monchick, "Surface Diffusion and Spin Polarization: Two Dimensional CIDEP," *J. Chem. Phys.* **72**, No. 11, pp. 6258 – 6264 (1980).

L. Monchick, J. G. Parker, and T. A. Potemra, "The Role of Vibrationally Excited Oxygen in Auroral Excitation of O_2 ($^1\Delta_g$)," *J. Geophys. Res.* **85**, No. A4, pp. 1792 – 1794 (1980).

M. L. Moon, "Environmental Impact of Salt Drift from a Natural Draft Cooling Tower," *Johns Hopkins APL Tech. Dig.* **1**, No. 2, pp. 120 – 128 (1980).

R. R. Newton, "On the Fractions of Degrees in an Ancient Star Catalogue," *Q. J. R. Astron. Soc.* **20**, pp. 383 – 394 (1979).

V. O'Brien, "Fully Developed Forced Convection in Rectangular Ducts and Illustrations of Some General Inequalities," *J. Appl. Math. Phys. (ZAMP)* **30**, pp. 913 – 928 (1979).

V. O'Brien, "Pulsatile Flow through a Constricted Artery," *Bull. Am. Phys. Soc.* **24**, No. 8, p. 1130 (1979).

V. O'Brien and L. W. Ehrlich, "Pulsatile Flow through a Constricted Artery," *Proc. 2nd Mid-Atlantic Conf. on Bio-Fluid Mechanisms*, pp. 497 – 516 (1980).

F. C. Paddison and K. Yu, "Use of Geothermal Energy in the Eastern United States," *Johns Hopkins APL Tech. Dig.* **1**, No. 2, pp. 88 – 100 (1980).

D. A. Payne, "Bäcklund Transformations in Several Variables," *J. Math. Phys.* **21**, No. 7, pp. 1593 – 1602 (1980).

T. E. Phillips (APL) and B. M. Hoffman, C. J. Schramm, and S. K. Wright (Northwestern Univ.), "Conductive Molecular Crystals: Metallic Behavior in Partially Oxidized Porphyrin, Tetrabenzporphyrin, and Phthalocyanine," *Molecular Metals*, Plenum Press, p. 393 (1979).

T. O. Poehler (APL) and M. E. Hawley, W. A. Bryden, J. P. Stokes, A. N. Bloch, and D. O. Cowan (JHU), "Charge Transfer Salts of Fluorinated TCNQ: Mott Insulators Isostructural with Organic Conductors," *Proc. Conf. Organic Conductors and Semiconductors*, Springer-Verlag, Berlin (1979).

T. O. Poehler and R. S. Potember (APL) and D. O. Cowan and A. N. Bloch (JHU), "Switching and Memory Phenomena in Semiconducting Charge-transfer Complexes, *Proc. Electrochem. Soc.* **80 – 1**, pp. 189-190 (1980).

I. P. Pollack (JHMI), L. J. Viernstein (APL), and R. L. Radius (JHMI), "An Instrument for Constant-Pressure Tonography," *Exp. Eye Res.* **29**, pp. 579 – 585 (1979).

R. S. Potember and T. O. Poehler (APL) and A. Rappa, D. O. Cowan, and A. N. Bloch (JHU), "A Reversible Field Induced Phase Transition in Semiconducting Films of Silver and Copper TNAP Radical-Ion Salts," *J. Am.*

Chem. Soc. **102**, Vol. 10, pp. 3659 – 3660 (1980).

T. A. Potemra, "Current Systems in the Earth's Magnetosphere," *Rev. Geophys. Space Phys.* **17**, No. 4, pp. 640 – 656 (1979).

T. A. Potemra (APL), T. Iijima (Univ. Tokyo), and N. A. Saflekos (Boston College), "Large-Scale Characteristics of Birkeland Currents," in *Dynamics of the Magnetosphere*, D. Riedel, pp. 165 – 199 (1979).

W. R. Powell, "Community Annual Storage Energy System," *Johns Hopkins APL Tech. Dig.* **1**, No. 2, pp. 108 – 113 (1980).

D. W. Rabenhorst, "Demonstration of a Low Cost Flywheel in an Energy Storage System," *Proc. 1979 Mechanical and Magnetic Energy Storage Contractors' Review Meeting*, pp. 408 – 414 (1979).

D. W. Rabenhorst, "Energy Conservation with Flywheels," *Johns Hopkins APL Tech. Dig.* **1**, No. 2, pp. 114 – 119 (1980).

R. P. Rich, "Mechanical Proof Testing," *Comput. Lang.* **5**, pp. 1 – 28 (1980).

C. H. Ronnenburg and R. L. Trapp, "Automated Antenna Tests Save Time and Cut Costs, *Microwaves* **19**, No. 1, pp. 66 – 72 (1980).

L. J. Rueger and A. G. Bates, "Nova Satellite Time Experiment," *Radio Sci.* **14**, No. 4, pp. 707 – 714 (1979).

N. A. Saflekos and T. A. Potemra, "The Orientation of Birkeland Current Sheets in the Dayside Polar Region and Its Relationship to the IMF," *J. Geophys. Res.* **85**, No. A5, pp. 1987-1994 (1980).

F. G. Satkiewicz, "Secondary Ion Mass Spectrometry for the Study of Solids," *Johns Hopkins APL Tech. Dig.* **1**, No. 1, pp. 45 – 48 (1980).

J. A. Schetz, F. S. Billig, and S. Favin, "Approximate Analysis of Axisymmetric Supersonic Base Flows with Injection," *AIAA J.* **18**, No. 8, pp. 867 – 868 (1980).

G. Schmeisser (JHMI) and W. Seamone (APL), "An Assistive Equipment Controller for Quadriplegics," *Johns Hopkins Med. J.* **145**, No. 3, pp. 84 – 88 (1979).

G. Schmeisser (JHMI) and W. Seamone (APL), "Low Cost Assistive Device Systems for a High Spinal Cord Injured Person in the Home Environment," *Bull. Prosthetics Res.* **BPR 10 – 32**, pp. 212 – 223 (1979).

D. M. Silver, "Interaction Energy between Two Ground-State Helium Atoms Using Many-Body Perturbation Theory," *Phys. Rev. A* **21**, No. 4, pp. 1106 – 1117 (1980).

D. M. Silver, "Rotationally Inelastic Collisions of LiH with He. I. *Ab Initio* Potential Energy Surface," *J. Chem. Phys.* **72**, No. 12, pp. 6445 – 6451 (1980).

D. M. Silver (APL) and N. J. Brown (Univ. California), "Valence Bond Model Potential Energy Surface for H_4," *J. Chem. Phys.* **72**, No. 7, pp. 3859 – 3868 (1980).

W. D. Stanbro and D. A. Pyrck, "Stability of Rhodamine WT in Saline Waters," *Water Resour. Res.* **15**, No. 6, pp. 1631 – 1632 (1979).

J. P. Stokes, A. N. Bloch, W. A. Bryden, D. O. Cowan, and M. E. Hawley (JHU) and T. O. Poehler (APL), "Mott Transition and Conductivity in the Organic Solid Solutions HMTSF $(TCNQ)_x$ $(TCNQF_4)_{1-x}$," *Bull. Am. Phys. Soc.* **24**, No. 3, p. 232 (1979).

A. M. Stone, "Geothermal Energy – An Overview," *Johns Hopkins APL Tech. Dig.* **1**, No. 2, pp. 78 – 87 (1980).

H. Sulzbacher and W. Baumjohann (Univ. Münster, FRG) and T. A. Potemra (APL), "Coordinated Magnetic Observations of Morning Sector Auroral Zone Currents with Triad and the Scandinavian Magnetometer Array: A Case Study," *J. Geophys. Res.* **48**, pp. 7 – 17 (1980).

L. J. Viernstein, "Intracranial Pressure Monitoring," *Johns Hopkins APL Tech. Dig.* **1**, No. 2, pp. 135 – 143 (1980).

L. J. Viernstein (APL) and I. P. Pollack (JHMI), "Validity of the Imbert-Fick Law for Constant-Pressure Tonography," *Exp. Eye Res.* **29**, pp. 587 – 594 (1979).

J. L. Wagner (APL) and J. D. Anderson, Jr. (Univ. Maryland), "Laser Radiation – Gasdynamic Coupling in the SF_6-Air Laminar Boundary Layer," *AIAA J.* **18**, No. 3, pp. 333 – 334 (1980).

L. T. Watson (Michigan State Univ.) and D. Fenner (APL), "Algorithm 555: Chow-Yorke Algorithm for Fixed Points or Zeros of C^2 Maps [C5]," *ACM Trans. Math. Software* **6**, No. 2, pp. 252 – 259 (1980).

R. O. Weiss, R. W. Blevins, H. L. Donnelly, J. T. Stadter (APL), and L. Perez y Perez (DOT), "At-Sea Test of a Large Diameter Steel, Cold Water Pipe," *Ocean Engineering for OTEC, Proc. 1980 Energy-Sources Technology Conf.*, pp. 47 – 67 (1980).

R. O. Weiss and J. T. Stadter, "Analysis of Contact through Finite Element Gaps," *Comput. Struct.* **10**, pp. 867 – 873 (1979).

S. Wilson (Science Research Council, UK) and D. M. Silver (APL), "On the Contribution of Higher-Order Excitations to Correlation Energies: The Ground State of the Water Molecule," *Theoret. Chim. Acta* **54**, pp. 83 – 91 (1979).

S. Wilson (Science Research Council, UK) and D. M. Silver (APL), "Diagrammatic Perturbation Theory: An Application to the Nitrogen, Carbon Monoxide, and Boron Fluoride Molecules Using a Universal Even-Tempered Basis Set," *J. Chem. Phys.* **72**, No. 3, pp. 2159 – 2165 (1980).

S. K. Wright and C. J. Schramm (Northwestern Univ.), T. E. Phillips (APL), and D. M. Scholler and B. M. Hoffman (Northwestern Univ.), "Conductive Molecular Solids: Partial Iodine Oxidation of Octaethylporphyrins," *Synth. Metals* **1**, No. 1, p. 43 (1979).

PRESENTATIONS

F. J. Adrian, "Nature of the Three-Electron Bond in Noble Gas Monohalides as Revealed by ESR Spectroscopy," Meeting, Greater Washington ESR Discussion Group, Georgetown Univ., 22 Feb 1980.

F. J. Adrian, "Radical Pair Mechanism of Chemically Induced Magnetic Polarization," Seminar, Princeton Univ., 23 Oct 1979.

R. H. Andreo, "Stochastic Variational Principles for Electromagnetic Wave Scattering from Random Systems," Meeting on Recent Developments in Classical Wave Scattering: Focus on the T-Matrix Approach, Ohio State Univ., 25 – 27 Jun 1979.

R. H. Andreo and J. A. Krill, "Vector Stochastic Variational Expressions for Electromagnetic Wave Scattering from Random Magnetic Objects," Workshop on Wave Propagation in Random Media, VPI&SU, 25 Mar 1980.

R. H. Andreo and J. A. Krill, "Vector Stochastic Variational Principles: Generalizations and Computational Features," 1980 CSL Scientific Conference on Obscuration and Aerosol Research, Aberdeen Proving Ground, 22 Jul 1980.

W. H. Avery, "The OTEC Contribution to Energy Needs of All Regions of the U.S.," IEEE 1980 Region 6 Conf., San Diego, 21 Feb 1980.

C. B. Bargeron, "Precursive Blistering in the Localized Corrosion of Aluminum," Corrosion Seminar, NSWC, White Oak, Md., 15 Jan 1980; also presented at Washington, D.C. Chapter, Electrochemical Society, 3 Apr 1980.

J. L. Calkins (JHMI), B. F. Hochheimer (APL), and S. A. D'Anna (JHMI), "Potential Hazards from Specific Ophthalmic Devices," Conference on Intense Light Hazards in Ophthalmic Diagnosis and Treatment, Houston, 25 Nov 1979.

L. L. Cronvich, "Aerodynamics of Air-Breathing Missiles for U.S. Navy Surface-to-Air Application," Workshop

on Aerodynamics of Missiles with Air-breathing Propulsion, London, 8 – 9 May 1980.

G. L. Dugger, "Ocean Thermal Energy Conversion," First International Symp. on Non-Conventional Energy, Trieste, 27 Aug – 21 Sep 1979, AEO-79-41, Sep 1979.

G. L. Dugger, E. J. Francis, and W. H. Avery, "Projected Costs for Electricity and Products from OTEC Facilities and Plantships," IECEC '80, 15th Intersociety Energy Conversion Engineering Conf., "Energy to the 21st Century," Seattle, 18 – 22 Aug 1980.

W. L. Ebert, "Multiple Marker Bi-Plane Cineventriculogrammetry," Interdepartmental Seminars on Cardiovascular Research, The Johns Hopkins Univ., 25 Oct 1979.

A. Eisner and S. M. Yionoulis, "Neutral Density Variations in the 900-1200 km Region of the Upper Atmosphere," International Symp. on Space Geodesy and Its Applications, Cannes, 18 – 21 Nov 1979.

C. Feldman, "Vacuum Deposited Polycrystalline Silicon Films for Solar Cell Applications," 14th IEEE Photovoltaic Conf., San Diego, 7 – 10 Jan 1980.

D. W. Fox, "Bounds for Eigenfrequencies of Reinforced Elastic Plates," Seminar, Dept. Mathematical Sciences, The Johns Hopkins Univ., 10 Apr 1980.

J. W. Giles and H. A. Kues, "Photographic Dye Studies of Underwater Wakes," Ocean Optics VI, Naval Postgraduate School, 25 Nov 1979.

J. F. George and D. Richards, "Design and Integration of a 40 MW_e Floating OTEC Pilot Plant," 7th Ocean Energy Conf., Washington, D.C., 2 – 4 Jun 1980.

J. F. George and D. Richards, "Preliminary Design of a Cruising OTEC Modular Experiment," 14th Intersociety Energy Conversion Engineering Conf., Boston, 10 Aug 1979.

G. Gücer (JHMI) and L. J. Viernstein (APL), "Continuous Recording of ICP in the Normal Monkey," American Association of Neurological Surgeons, Los Angeles, Apr 1979; also presented at the 4th International Symp. on Intracranial Pressure, Williamsburg, Va., Jun 1979.

A. N. Jette, "Interpretation of Hyperfine Interaction and Structure of Defect Centers Using a Spin-Correlated Valence Bond Theory," Seminar, Univ. Antwerp, 4 Mar 1980; also presented at Seminar, Gesamthochschule Paderborn, FRG, 22 Apr 1980.

A. N. Jette, "Valence Bond Study of Hyperfine Interactions and Structure of Hypervalent Radicals," Zentrum Interdisziplinäre Forschung, Univ. Bielefeld, FRG, 11 Mar 1980.

H. A. Kues, "Retinal Nerve Fiber Enhancement Techniques," Wilmer Research Institute Meeting, Baltimore, 27 Sep 1979.

J. R. Kuttler, "Estimating Characteristic Frequencies of Orthotropic Clamped Plates," Meeting, American Mathematical Society, San Antonio, 6 Jan 1980.

L. Monchick, "Anisotropic Forces and Molecular Collisions," Zentrum Interdisziplinäre Forschung, Univ. Bielefeld, FRG, 20 Nov 1979; also presented at Inst. Theoretical Physics, Univ. Erlangen-Nürnberg, 3 Dec 1979.

K. Moorjani, "Disordered Magnets," Physics Dept. Seminar, Univ. Maryland, College Park, 27 Feb 1980.

K. Moorjani, "Magnetic Glasses," Groupe de Transition des Phases, C.N.R.S., Grenoble, France, 23 Jul 1979; also presented at 7th AIRAPT International Conf., Le Creusot, France, 30 Jul – 3 Aug 1979.

K. Moorjani (APL) and S. K. Ghatak (Indian Inst. of Tech., Khargpur), "Competing Exchange Interactions in Random Magnets," American Physical Society Meeting, Chicago, 20 – 21 Jan 1980.

J. C. Murphy, "Time Dependent Processes in Photoacoustic Spectroscopy," Topical Meeting on Photoacoustic Spectroscopy, Univ. Iowa, 1 – 3 Aug 1979.

V. O'Brien, "Pulsatile Blood Flow," Bioengineering Seminar, The Johns Hopkins Univ., 22 Oct 1979.

V. O'Brien, "Pulsatile Flow in Arteries," Fluid Dynamics Reviews, Univ. Maryland, College Park, 2 May 1980.

V. O'Brien and L. Ehrlich, "Planar Entry Flow of Viscoelastic Fluid," Workshop of VE Flow, Brown Univ., 2 Nov 1979.

T. O. Poehler, "Infrared Extinction in Organic Compounds and Polymers," CSL Scientific Conf. on Obscuration and Aerosol Research, Aberdeen Proving Ground, Md., 17 – 21 Sep 1979.

T. O. Poehler, "Switching and Memory Effects in Organic Semiconducting Charge-Transfer Complexes," Chemistry Div. Symp., Naval Res. Lab., Washington, D.C., 13 Feb 1980.

R. S. Potember and T. O. Poehler, "Switching Phenomena and Memory in Organic Semiconductors," Chemistry Dept. Colloq., Univ. Pennsylvania, 29 Jan 1980.

R. S. Potember and T. O. Poehler (APL) and A. Rappa, D. O. Cowan, and A. N. Bloch (JHU), "Electrical Switching and Memory Phenomena in Semiconducting Organic Charge-Transfer Complexes," NATO Advanced Study Inst. on Physics and Chemistry of Low Dimensional Solids, Tomar, Portugal, 27 Aug – 7 Sep 1979.

R. S. Potember and T. O. Poehler (APL) and D. O. Cowan (JHU), "Switching and Memory Phenomena in Semiconducting Charge-Transfer Complexes," Meeting, American Chemical Society, Washington, D.C., 10 – 13 Sep 1979.

J. C. W. Rogers, "Numerical Solution of Systems of Conservation Laws," Colloq., Dept. Mathematics, Univ. Wisconsin, Madison, 1 Apr 1980.

J. C. W. Rogers, "The Stefan Problem," Analysis Seminar, Univ. Minnesota, 31 Mar 1980.

J. A. Schetz, F. S. Billig, and S. Favin, "Analysis of Mixing and Combustion in a Scramjet Combustor with Co-Axial Fuel Jet," 16th AIAA/SAE/ASME Joint Propulsion Conf., Hartford, Jun 1980.

J. A. Schetz, F. S. Billig, and S. Favin, "Approximate Analysis of Base Drag Reduction by Base and/or External Burning for Axisymmetric Supersonic Bodies," 16th AIAA/SAE/ASME Joint Propulsion Conf., Hartford, Jun 1980.

D. M. Silver, "Electron Correlation in Simple Chemical Systems," Univ. of Electro-Communications, Chofu-shi, Tokyo, 16 Nov 1979.

D. M. Silver, "Rotational Energy Transfer in LiH-He Collisions: A Comparison between Theory and Experiment," Hebrew Univ., Jerusalem, 23 Dec 1979.

J. E. Tillman, "Differentiation of Mesozoic Fractures by Fluid Inclusion Analysis," U.S. Geological Survey Seminar, Reston, Va., 7 Feb 1980.

J. E. Tillman, "Hydrothermal and Uplift Histories of the Northern Appalachian Basin," Eastern Section Meeting, Assoc. of Petroleum Geologists, Morgantown, W. Va., 1 – 4 Oct 1979.

J. E. Tillman, "Unraveling the Cenozoic Tectonic History of the Eastern U.S.," Nuclear Regulatory Commission Seminar, Bethesda, Md., 19 Feb 1980.

P. J. Waltrup, "Observed Pressure Oscillations in Full-Scale Subsonic Dump Combustors," and "Overview of NAVSEA Air Breathing Propulsion Programs," 1979 JANNAF Workshop on Pressure Oscillations in Ramjets, Monterey, 7 – 8 Sep 1979.

P. J. Waltrup, F. S. Billig, and M. C. Evans, "Critical Considerations in the Design of Supersonic Combustion Ramjet (Scramjet) Engines," 16th AIAA/SAE/ASME Joint Propulsion Conf., Hartford, 30 Jun – 2 Jul 1980.

G. P. Warman, J. C. Murphy, and L. C. Aamodt, "Surface Area Effects in Photoacoustic Spectroscopy," Topical Meeting on Photoacoustic Spectroscopy, Univ. Iowa, 1 – 3 Aug 1979.

L. B. Weckesser, "DC93-104 Thermal Modeling Efforts," JANNAF Ramjet Combustor Insulator Thermal Modeling Workshop, Monterey, 14 Mar 1980.

L. B. Weckesser, "Radome Aerodynamic Heating Effects on Boresight Error," 15th Symp. on Electromagnetic Windows, Atlanta, 18 – 20 Jun 1980.

L. B. Weckesser and L. L. Perini, "Thermal Modeling of Combustor Insulation DC93-104," JANNAF 1980 Propulsion Meeting, Monterey, 11 – 13 Mar 1980.

R. O. Weiss (APL), R. Barr (Hydronautics), J. Gianotti (Giannotti and Assoc.), W. Deuchler (Gibbs and Cox), R. Scotti (NOAA), J. Stadter (APL), and J. Walsh (VSE), "Report of the Ad Hoc OTEC CWP Committee: An Assessment of Existing Analytical Tools for Predicting CWP Stresses," 7th Ocean Energy Conf., Washington, D.C., 2 – 4 Jun 1980.

APL COLLOQUIA

Jan. 4, 1980 – "The Riddle of Tektites," by J. A. O'Keefe, NASA/Goddard Space Flight Center.

Jan. 11 – "Technical – Congressional Interaction on Synthetic Fuel Production," by H. C. Hottel, Massachusetts Inst. of Technology.

Jan. 18 – "An Overview of Our Energy Future," by O. M. Phillips, The Johns Hopkins Univ.

Jan. 25 – "The Acid Rain," by J. N. Galloway, Univ. of Virginia.

Feb. 1 – "Fireplaces and Woodburning Stoves," by R. D. Thulman, Thulman Eastern Corp.

Feb. 8 – "The Physics of Violins," by N. Pickering, Southampton Hospital.

Feb. 15 – "Designing a Global Future: Some Reflections on the New Social Paradigm," by D. Pirages, Univ. of Maryland.

Feb. 22 – "Quarks, Gluons, ... A Walk Through the Garden of Elementary Particles," by A. Pevsner, The Johns Hopkins Univ.

Feb. 29 – "Gas Industry Perspective on Future Energy Resources," by A. C. Eberle, Columbia Gas System Service Corp.

Mar. 7 – "Particle-Beam Weapons," by K. Tsipis, Massachusetts Inst. of Technology.

Mar. 14 – "Electrochemistry of Solid State Batteries," by A. Schneider, Catalyst Research Corp.

Mar. 21 – "Photoacoustics – Principles and Recent Developments," by A. Rosencwaig, Lawrence Livermore Laboratory.

Mar. 28 – "The New Genetics," by D. Nathans, The Johns Hopkins Univ.

Apr. 4 – "Impressions of Soviet Science and Technology," by A. S. Greenberg, U.S. Dept. of State.

Apr. 11 – "A Visit to China," by F. S. Billig, APL.

Apr. 18 – "Godel, Escher, Bach: An Eternal Golden Braid," by D. R. Hofstadter, Univ. of Indiana.

Apr. 25 – "National Laboratories: What Are They? What Do They Do? Who Cares?," by W. E. Massey, Argonne National Lab.

May 2 – "The Automatic Implantable Defibrillator from Inception to Clinical Application," by M. Mirowski, Sinai Hospital and The Johns Hopkins Univ.

May 9 – "The Piltdown Man Hoax: Whodunit?," by J. Weiner, Univ. of London.

May 16 – "The Role of the Oceans in the Earth's Heat Balance," by A. H. Oort, Princeton Univ.

May 30 – "The Role of Oxygen in Retinopathy: A 14-Year APL – Wilmer Institute Cooperative Study," by R. W. Flower, APL.

THE AUTHORS

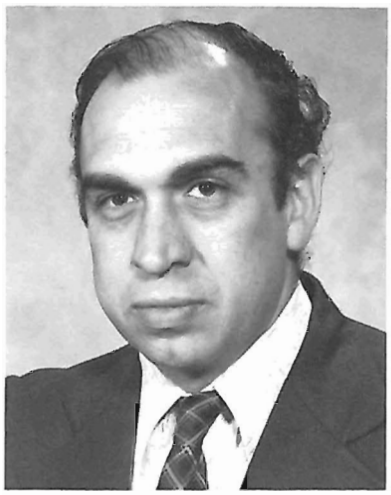

MARIO H. ACUNA was born in 1940 in Cordoba, Argentina, where he received his undergraduate degree from the University. He earned the M.S.E.E. degree from the University of Tucuman (1967) and the Ph.D. in space science from The Catholic University of America (1974). In 1969, he joined the Goddard Space Flight Center, where his research interests have centered around instrumentation for geophysical and space research as well as studies of magnetic fields and plasmas in interplanetary space and in magnetospheres. Dr. Acuna has been involved with Explorers 47 and 50, Mariner 10, Pioneer 11, Voyagers 1 and 2, Magsat, the International Solar Polar Mission, Project Firewheel, and Ampte as instrument engineer, principal investigator or engineer, or project scientist. He has received many awards in recognition of his contributions to NASA programs.

WALTER E. ALLEN was born in New York City in 1932. He attended Queens College, Indiana Technical College, and The Polytechnic Institute of Brooklyn where he obtained the B.S.M.E. degree in 1954. He was an engineering instructor at the U.S. Naval Academy for three years prior to joining the Space Department of APL in 1960. He is a power systems specialist and has been responsible for the design and development of both solar and nuclear power systems for many spacecraft, including Transit, Geos, Triad, Transit Improvement Program, and Magsat. Mr. Allen is supervisor of the Space Power Systems Section and assistant supervisor of the Spacecraft Systems Group.

FREDERICK S. BILLIG was born in Pittsburgh in 1933. He did his undergraduate work at The Johns Hopkins University and earned the M.S. (1957) and Ph.D. (1964) degrees in mechanical engineering from the University of Mary-

land. He joined APL in 1955 where he participated in experimental programs involving hypersonic wind tunnels and external burning, and developed theoretical/experimental techniques for analyzing supersonic combustion. Subsequently Dr. Billig studied hypersonic propulsion ramjets, hydrogen and storable liquid fuels, the SCRAM combustor, ignition and combustion of fuels, and the penetration of liquid jets into supersonic streams. Since 1977, he has been assistant supervisor of the Aeronautics Division.

He received the Distinguished Young Scientist Award of the Maryland Academy of Sciences in 1966 and the Silver Combustion Medal of The Combustion Institute in 1970. He is presently a director of the AIAA.

RONALD K. BUREK was born in Detroit in 1940. He received the B.E.E. degree from the University of Detroit

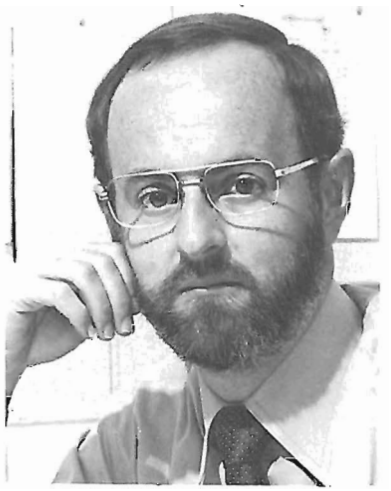

(1964) and has done graduate work at The Johns Hopkins University. In 1964 he joined APL where he has been involved primarily in hardware and software design for digital electronic systems associated with space, shipboard, and ground applications. In particular he contributed to the design of the Seasat radar altimeter and the Transim satellite navigation processor. Mr. Burek designed and programmed the LORAN-C navigation software used in the Hydro and Aries ocean experiments, and has been responsible for the data storage subsystems for several recent spacecraft. He is working on a microprocessor-based data handling system for the Ampte spacecraft and is exploring the potential use of magnetic bubble memories for space applications.

THOMAS B COUGHLIN was born in Baltimore in 1941. He studied mechanical engineering at the University of Maryland (B.S., 1964) and at Drexel

University (M.S., 1967). He worked in missile dynamics at the Martin Co. during 1964-67 and in the mechanical design and structural analysis of the ATS-6 and Sert spacecraft at Fairchild Industries during 1967-72.

Since joining APL in 1972, Mr. Coughlin participated in the analysis and testing of spacecraft mechanical systems. He is now supervisor of the Structural Analysis and Test Section of the Space Electromechanical Design Group.

JOHN R. DOZSA was born in Alpha, N.J. He received a B.S.E.E. from Lafayette College in 1963 and has done graduate work at the University of Maryland. Upon joining APL in 1963, he assisted in the installation of the Typhon Radar System aboard the USS *Norton Sound*. From 1964 to 1973 he was involved in the design of electronic flight and ground equipment for space satellite systems including portions of the Dodge satellite TV cameras and

other imaging camera systems, scan converters, and displays. During 1973-78, Mr. Dozsa designed shipboard hardware units for the SEATIPS and AN/SYS-1 automatic detection and tracking radars. In 1978 he became the cognizant engineer for the Magsat standard s-band transponder. At present, he is a design engineer in the Ocean Engineering Program Sensor Evaluation Laboratory of the Strategic Systems Department

LEWIS D. ECKARD, JR. was born in Philadelphia in 1923. He received the B.S.M.E. degree (aeronautical option) in 1949 from the University of Maryland, and has done graduate work in aeronautical engineering at the University of Maryland and in engineering administration at George Washington University.

In 1952 Mr. Eckard started working for the Engineering Research Corporation, where he performed analyses in support of the development of electronic flight simulators. In 1957 he joined APL

where he specialized in thermal analysis of spacecraft. During 1961-63 he served as a branch manager in the Environmental Test Division at the Goddard Space Flight Center. Returning to APL in 1963 as a project engineer, he has been supervisor of the Space Systems Branch since 1967. During 1977-79, he also acted as program manager for the Magsat spacecraft. On January 1, 1981, he will become Assistant Head of the Space Department and Programs Manager.

WINFIELD H. FARTHING was born in North Carolina in 1934. He received his undergraduate education at North Carolina State University, and the Ph.D. from The Catholic University of America. He was employed by the National

Security Agency before transferring to the Goddard Space Flight Center (GSFC) in 1962.

He now is an electronics engineer with GSFC, where he has participated in the design and implementation of a variety of scientific instruments for spaceflight. He was project engineer of the scalar magnetometers flown on the Pogo satellites and participated in the early efforts to bring a follow-on mission such as Magsat into being. In addition to being technical officer for the Magsat scalar magnetometer, Dr. Farthing is a co-investigator for the magnetic fields experiments on Dynamics Explorer, and is science manager for the Space Environment Monitor onboard Geos.

GLEN H. FOUNTAIN was born in Hutchinson, Kans. in 1942 and received the B.S.E.E. and M.S.E.E. degrees from Kansas State University in 1965 and 1966. Since 1966 he has been employed by APL in the area of satellite attitude control and detection and system instrumentation. He has participated in the design of control systems for a number of satellites including the Small

Astronomy Satellites. Appointed assistant project scientist for Magsat in 1977, Mr. Fountain has been principally concerned with the design of the attitude control and determination subsystems. Other professional interests have included biomedical engineering and the study of coherence of the earth's magnetic noise field.

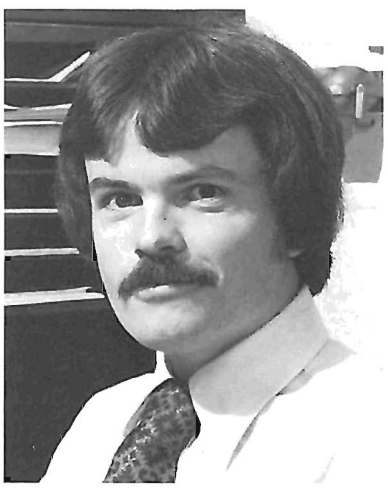

KEVIN J. HEFFERNAN was born in Bryn Mawr, Pa. in 1952 and received his B.S.E.E. from Drexel University and his M.S.E.E. from The Johns Hopkins Uni-

versity in 1975 and 1980 . Specializing in control theory and electronic design, he joined APL's Attitude Control Systems Group in 1977. His principle responsibilities on Magsat were as program sponsor of the IR scanner reaction wheel, co-designer of the microprocessor-based attitude signal processor, and participant in the simulation and analysis of the various pitch control modes for stability purposes.

Mr. Heffernan is currently designing another microprocessor-based system — a magnetometer signal processor — for the Air Force Defense Meteorological Satellite Program.

ROBERT A. LANGEL was born in Pittsburgh in 1937 but spent most of his youth in Ohio. His undergraduate degree was earned at Wheaton College (1959) and his Ph.D. in physics was received from the University of Maryland in 1973. After undergraduate school he worked for three years at the Naval Research Laboratory before going to Goddard Space Flight Center (GSFC) where he is presently a member of the Geophysics Branch. While at GSFC he has participated in the magnetic field experiments on the Ogo and Pogo satellites, including pioneering studies of magnetic disturbances at high latitudes. During his professional career Dr. Langel has authored or co-authored 30 papers and is recognized as an authority in geomagnetism. He is presently project scientist for the Magsat project and a leader in GSFC's research in the area of the earth's main magnetic field and crustal magnetic anomalies.

ARK L. LEW was born in Canton, China, in 1941. He received the B.S.E.E. degree from Case Institute of Technology (1963) and the M.S.E. degree from The Johns Hopkins University in 1968. Since joining APL in 1963, he has worked in the areas of spacecraft systems and electronics design. He has designed electronics for the Explorer,

Geos, and Small Astronomy Satellite vehicles. Mr. Lew has been the command system leader for the Triad, Transit Improvement Program, and Magsat spacecraft. Currently, he is working on another microprocessor-based design — the data system for the LAN experiment of the Solar Polar spacecraft. Mr. Lew is supervisor of the Systems Analysis and Development Section of the Space Instrumentation Systems Group.

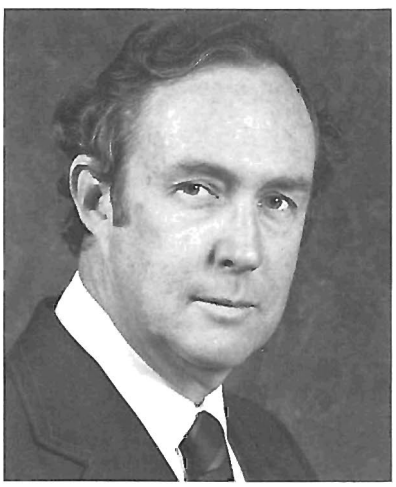

FREDERICK F. MOBLEY was born in Atlanta in 1932. He received a B.S. degree from the University of Illinois in 1953 and an M.S. in aeronautical engineering from the Massachusetts Institute of Technology in 1958. He came to APL in 1955. Since 1960 Mr. Mobley has worked on satellite attitude control, including gravity-gradient stabilization of the Transit satellites and the use of magnetic control systems in the Small Astronomy Satellites and Magsat. He was the APL project scientist on Magsat and participated in the overall satellite design and its implementation. Mr. Mobley is supervisor of the Space Attitude Control Systems Group.

BRUCE C. MOORE was born in Hackensack, N.J., in 1943. He received the B.E.E. from Rensselaer Polytechnic Institute in 1965 and the M.S.E.E. from The Johns Hopkins University in 1978. Prior to joining APL in 1975, he was employed as an engineer by RCA Astro Electronics Division where he worked on such space programs as Tiros, Apollo, and Atmosphere Explorer. At APL he has been involved in the design of command and telemetry hardware on the Transit, Transit Improvement Program, and Magsat satellites. Mr. Moore is a member of the Space Instrumentation Systems Group and is providing technical support to the Fleet Systems Department for telemetry pertaining to the Standard Missile program.

GILBERT W. OUSLEY received his B.S.M.E. (1954) and M.S.M.E. (1958) from the University of Maryland. In 1959 he joined the NASA Goddard Space Flight Center (GSFC) where he has held several line, staff, and project manager positions . He spent two years in Paris in the mid-1960's as the first representative in Europe of NASA Headquarters. He has been the Magsat project manager from project initiation

through in-orbit mission operations. He is now manager of NASA's Ampte project.

Mr. Ousley is the recipient of the DoD Meritorious Civilian Service Award, the NASA Exceptional Service Medal, the Medaille de Vermeil du CNES, the Bundesverdienstkreuz, as well as GSFC performance and achievement awards.

THOMAS A. POTEMRA was born in Cleveland in 1938. He did both his undergraduate and graduate work in

electrical engineering, receiving the B.S. from Case Institute of Technology (1966), the M.E.E. from New York University (1962) and the Ph.D. from Stanford University (1966).

Since joining APL in 1965 Dr. Potemra has engaged in research in ionosphere and space physics. He was principal investigator for the Triad magnetometer experiment and co-investigator for the Atmospheric Explorer photoelectron spectrometer experiment. He is presently assistant group supervisor of the Space Physics and Instrumentation Group. Among his many activities outside the Laboratory, he is associate editor of the *Journal of Geophysical Research* and secretary of the Aeronomy Section of the American Geophysical Union.

FREDERICK W. SCHENKEL was born in Jersey City in 1932. He earned a B.S.E.E. degree at Fairleigh Dickinson University in 1958, and has done graduate work at Johns Hopkins and the University of Maryland. During 1955-63 he was engaged in physical electronics R&D and engineering with the Allen B. DuMont and CBS Laboratories.

Mr. Schenkel joined APL in 1963 as section supervisor in the Microelectronics Group. Since 1965 he has been with the Space Department, where he has been involved in electro-optic systems design and analysis, including the Dodge satellite's color TV camera system, which secured the first color pictures of the full earth. He was also responsible

for the Small Astronomy Satellite star mappers built at APL and was heavily involved in the development of the Attitude Transfer System and optical metrology for Magsat. He is a senior member of the IEEE.

JAMES F. SMOLA was born in Chicago in 1928 and obtained a B.S.M.E. at the Illinois Institute of Technology in

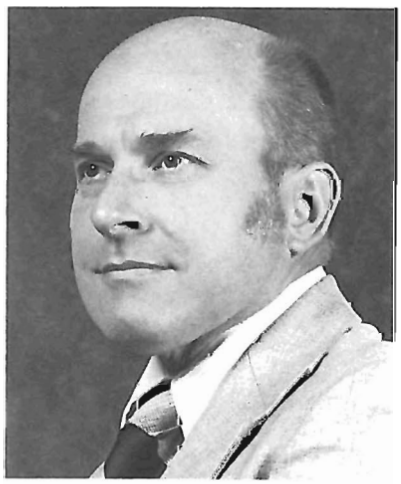

1951 and an M.S. in numerical science from The Johns Hopkins University in 1969. During 1955-58 he was directly involved in the integration of the Terrier, Tartar, and Talos surface-to-air missiles aboard vessels of the U.S. Navy's surface fleet. During that period he was employed by the Vitro Corp. and the Washington Technological Associates.

In 1958 Mr. Smola joined APL where he has been involved in the design, fabrication and testing of mechanical, electromechanical, and attitude control systems for spacecraft. At present he is an assistant group supervisor and section supervisor in the Space Attitude Systems Group.

BARRY E. TOSSMAN was born in Baltimore in 1940 and received his B.S.M.E. and M.S.M.E. degrees from the University of Maryland in 1961 and 1964. He is currently enrolled in the M.S. program in technical management of the Johns Hopkins Evening College. Since joining APL in 1961, he has spent most of his time in the Space Department where he has been responsible for mechanical and attitude control system design, control system simulations, electronic and electromechanical hardware development, and post-launch operations and analysis. Mr. Tossman has also been responsible for state-of-the-art systems development of magnetic instrumentation for the Strategic Systems Department. He is currently program

manager for the Galileo Energetic Particles Detector Project and the LAN project of the Solar Polar spacecraft.

CLARENCE A. WINGATE was born in 1930 in Charlotte, N.C. He received a B.S.M.E. (1952) and an M.S.M.E. (1958) from North Carolina State University and did graduate work in physics during 1960-64 at the University of Maryland. Upon joining APL in 1958 he worked on ramjet performance analysis until 1967, when he became supervisor of the Thermal Systems Design Section of the Spacecraft Systems Group. Since then he has been directly involved in the design analysis and testing of 12 spacecraft and five spacecraft instruments.

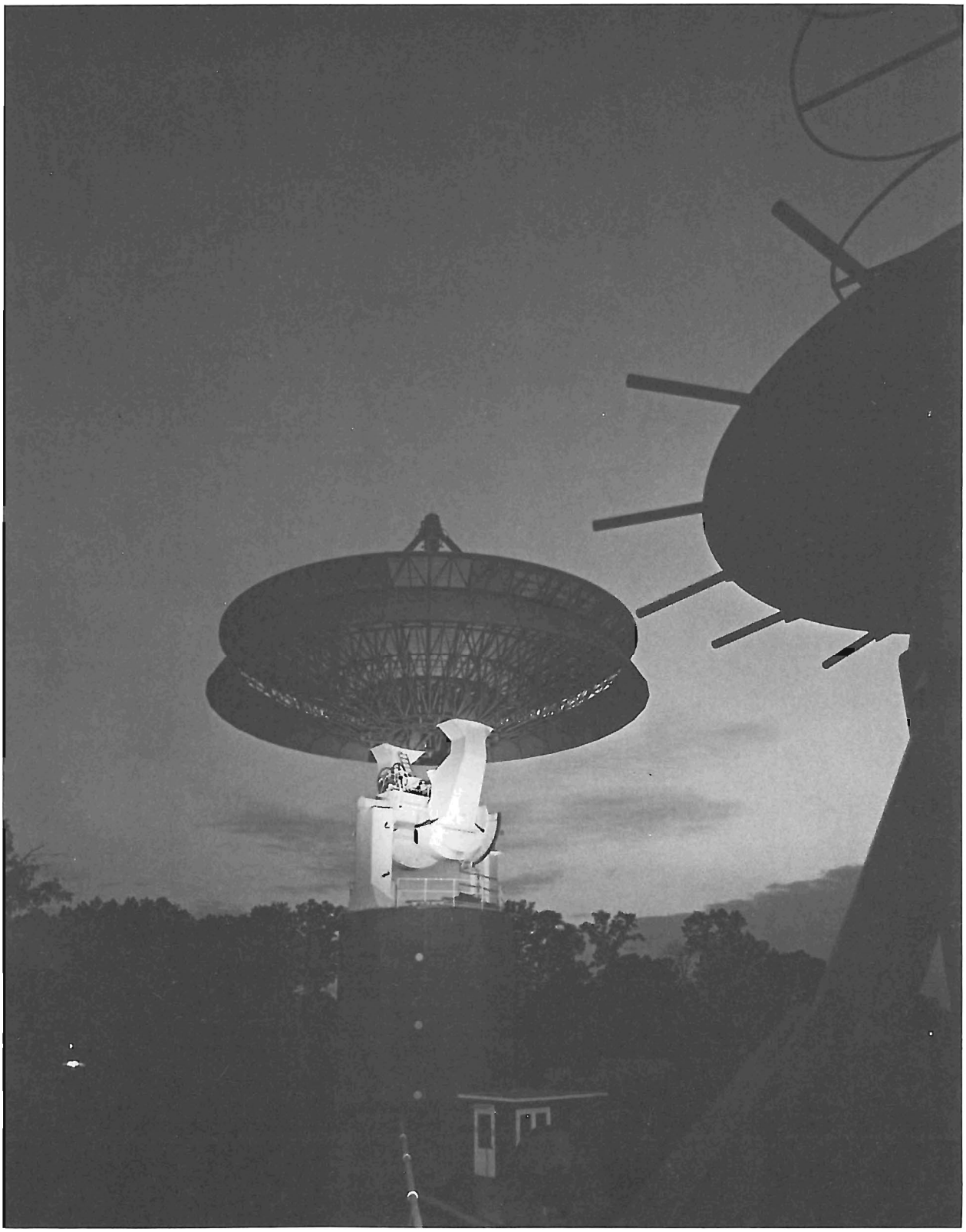

The APL 60-foot-diameter parabolic antenna for transmitting commands to and receiving telemetry from some orbiting satellites.